Theoretical studies of bright solitons in trapped atomic Bose-Einstein condensates

Martin, Andrew David

Theoretical Studies of Bright Solitons in Trapped Atomic Bose-Einstein Condensates

Andrew David Martin

A thesis submitted in partial fulfilment
of the requirements for the degree of
Doctor of Philosophy

Department of Physics
University of Durham
March 2008

Theoretical Studies of Bright Solitons in Trapped Atomic Bose-Einstein Condensates

Andrew David Martin

Abstract

Bright solitary-waves may be created in dilute Bose-Einstein condensates of attractively interacting atoms in one dimensional regimes. In integrable systems, such solitary waves are particle-like objects called solitons. We investigate the consequences of non-integrability on the solitary waves in trapped Bose-Einstein condensates caused by an axial harmonic trap, and non-integrability caused by three dimensional effects.

To analyse the soliton-like nature of the solitary-waves in an axial harmonic trap, a particle analogy for the solitary-waves is formulated. Exact soliton solutions exist in the absence of an external trapping potential, which behave in a particle-like manner, and we find the particle analogy we employ to be a good model also when a harmonic trapping potential is present up to a gradual shift in the trajectories when the harmonic trap period is short compared with the collision time of the solitons. We find that the collision time of the solitons is dependent on the relative phase of the solitons as they collide. In the case of two solitons, the particle model is integrable, and the dynamics are completely regular. In the case of a system of two solitary waves of equal norm, the solitons are shown to retain their phase difference for repeated collisions. The extension to three particles supports both regular and chaotic regimes. The trajectory shift observed for two solitons carries over to the case of three solitons. This shift aside, the agreement between the particle model and the wave dynamics remains good, even in chaotic regimes. We predict that these chaotic regimes will be an indicator of rapid depletion of the condensate due to quantum transitions of the condensate particles into non-condensate modes.

To analyse the residual effects of the three dimensional nature of the solitary waves, we use a nonlinear Schrödinger equation with an additional quintic term. We perform variational calculations, and confirm the collapse of a soliton when the number of particles contained therein is increased past a critical number. We investigate the effects of varying the axial trap frequency and scattering length on the critical number. We propose a method to model particle exchange between solitons by extending the variational treatment to two solitons.

Declaration

I confirm that no part of the material offered has previously been submitted by myself for a degree in this or any other University. Where material has been generated through joint work, the work of others has been indicated.

Andrew Martin
Durham, 31st March 2008

Preface

The structure of this thesis is as follows:
Part I contains introductory information. Some of the content of part I appears in Ref. [1].
Part II contains work on harmonically-trapped 1D solitons. This work was done in cooperation with my supervisors Simon Gardiner and Charles Adams. Most of this work has been published in Refs. [1,2].
Part III contains work on 3D effects in cylindrically-shaped condensates. Some of this work was done under the supervision of James Anglin (University of Kaiserslautern), as well as Simon Gardiner and Charles Adams.

Acknowledgements

I'm very grateful to Simon Gardiner for his able supervision, support, useful suggestions and the benefit of his mathematical experience. I am also grateful to Charles Adams, for his supervision, intuitive ideas and presentational tips. Many thanks to Nick Parker for interesting discussions and help with numerical methods. Thanks also to James Anglin for his hospitality and helpful suggestions. I wish to thank J. Brand, S. L. Cornish, K.-P. Marzlin, T. S. Monteiro, and N. R. Walet for useful discussions. I acknowledge support from the UK EPSRC and from the European Science Foundation (ESF) for the activity entitled 'Quantum Degenerate Dilute Systems'.
Thanks to all the members of AtMol for stimulating conversations. Thanks in particular to Antoine, Meltem and Steve for their company on our voyage around the physics department. I also thank Steve for useful/entertaining discussions and for his extreme helpfulness whenever it was required.
Finally, thanks to all the Martin family for their love and support.

Contents

List of Figures

Part I

Introductory material

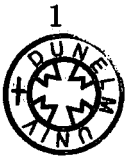

Chapter 1

Introduction

"I believe that I shall best introduce this phenomenon by describing the circumstances of my own first acquaintance with it. I was observing the motion of a boat which was rapidly drawn along a narrow channel by a pair of horses, when the boat suddenly stopped - not so the mass of water in the channel which it had put into motion; it accumulated round the prow of the vessel in a state of agitation, then suddenly leaving it behind, rolled forward with great velocity, assuming the form of a large solitary elevation, a rounded, smooth and well-defined heap of water, which continued its course along the channel apparently without change of form or diminution of speed. I followed it on horseback, and overtook it still rolling on at a rate of some eight or nine miles an hour, preserving its original feature some thirty feet long and a foot to a foot and a half in height. Its height gradually diminished, and after a chase of one or two miles I lost it in the windings of the channel. Such in the month of August 1834, was my first chance interview with that singular and beautiful phenomenon which I have called the Wave of Translation, a name which it now very generally bears."

-John Scott Russell,
"Report on Waves": (Report of the fourteenth meeting of the British Association for the Advancement of Science, September, 1844)

1.1 Solitons in shallow water

The first observation of a solitary wave was made by John Scott Russell on the Union Canal, six miles from the centre of Edinburgh. Scott Russell was so intrigued by his discovery, which he named the wave of translation, that he constructed a reservoir in his garden to study such phenomena. He noticed that "the great primary waves of translation cross each other without change of any kind." [3]

The following linear partial differential equation is called the "classical wave equation":

$$u_{tt} - c^2 u_{xx} = 0, \tag{1.1}$$

where the subscript denotes the partial derivative. The general solution to Eq. (1.1) is given by:

$$u = f(x - ct) + g(x + ct), \tag{1.2}$$

where f and g can be any twice differentiable functions. It is clear that f and g are impulses travelling at speed $\pm c$ whilst retaining their profiles. Moreover, f and g cross each other without change. At first, Eq. (1.1) may seem a good candidate for modelling solitary waves. However, in real systems, there are at least some dispersive and/or dissipative effects and waves do not usually retain their form for any considerable time. It is for this reason that solitary waves are so surprising.

In 1895, Korteweg and de Vries showed that shallow water waves are modelled by the Korteweg-de Vries equation (KdV) [4]:

$$u_t + (1 + u)u_x + u_{xxx} = 0. \tag{1.3}$$

Note that without the nonlinear term, the Fourier components, $\exp i(k_i x - \omega_i t)$, of a wave packet would spread out with phase velocities $1/k_i^2$. However, since Eq. (1.3) is nonlinear, the superposition principle doesn't hold, and it cannot be solved by Fourier transform, i.e., the Fourier components of a wave packet cannot be treated individually. We will see in chapter 2 that a nonlinear analogue of the Fourier transform - the inverse scattering transform (IST) - can be used to solve equations such as Eq. (1.3). Gardner *et al.* first used this method to solve the KdV [5]. Equations amenable to this method of solution are called Lax integrable. This method produces solutions including those which

retain their form as they propagate. These solutions are now commonly called solitary waves, rather than waves of translation.

Since superpositions of solutions of Eq. (1.3) are not generally themselves solutions, the ability of Russell's waves of translation to emerge from collisions unscathed is rather interesting. We will see in chapter 2 that there is an analogue of the superposition principle for certain solutions to Lax integrable equations in the limit that $t \to \pm\infty$. Solutions exist that take the form of distinct wavepackets which come together and collide and then reform up to phase shifts; in the case of the KdV equation these are shifts in the position of the outgoing wavepackets relative to where they would have been had there been no interaction (see figure 1.1). By coming together, interacting as though through some force, and moving apart, these solutions have a clear particle-like character, and were thus given the particle-inspired name solitons by Zabusky and Kruskal [6], who first simulated solitons numerically before the advent of the IST.

We mention in passing topological solitons (or topological defects). Whereas 'true' solitons (found in Lax integrable systems) are constrained to retain their form because of conserved quantities associated with the wave equation, topological solitons are constrained to retain their form due to the existence of some topological charge (e.g., the phase winding in a vortex). We will not consider topological solitons further in this thesis.

1.2 Bose Einstein condensates

Bose Einstein condensation is the process of inducing a system of bosons to occupy the same single-particle state. The first atomic Bose Einstein condensates (BECs) were produced in 1995 in gases of rubidium [7] and sodium [8]. The process of condensation was achieved by cooling the gases to fractions of microkelvins by laser and evaporative cooling such that the 'ground' state became macroscopically occupied. (This ground state is really a metastable state, but decay processes to the solid state are negligible over the timescale of experiments [9]). The signature of BEC in experiments is the sudden appearance of a peak in the atom-number distribution, inferred from time-of-flight measurements on releasing the condensate. Subsequently, many BEC experiments have

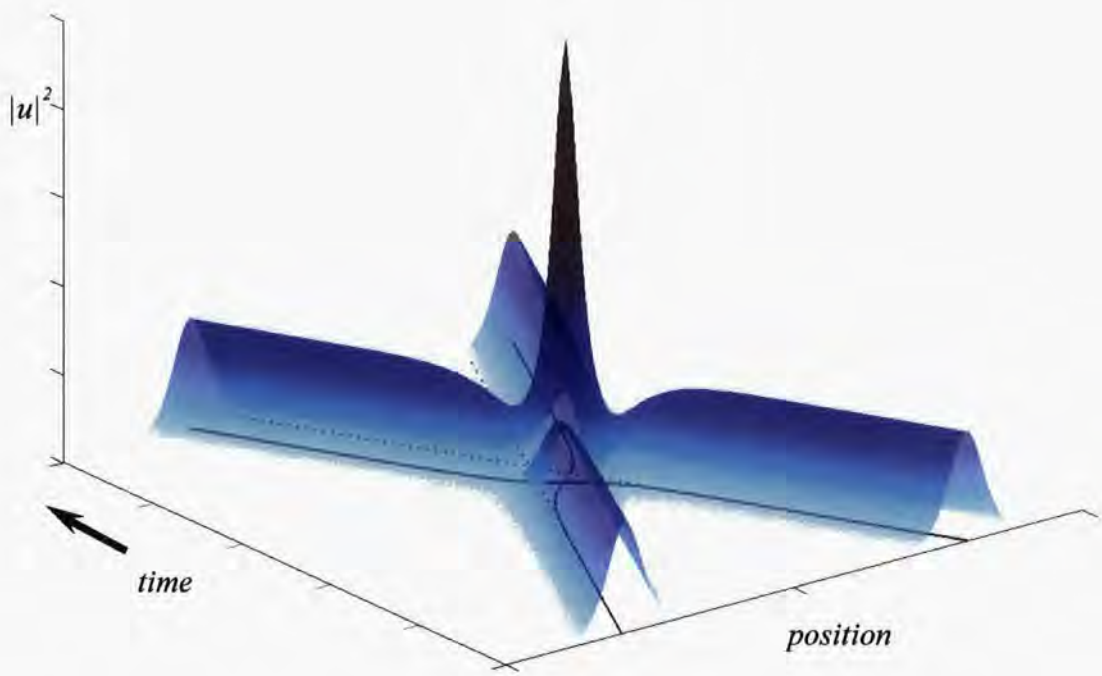

Figure 1.1: A graphical representation of a soliton collision. In this case, u is the wavefunction of the NLS. The solitons approach one another, a "nonlinear interaction" takes place and the solitons emerge with a position shift. The paths of the solitons are given by the full lines, and the paths of the solitons had they not undergone position shifts are given by the dotted lines.

been performed, and currently BECs are a subject of intense interest [9].

1.3 Solitons in Bose Einstein condensates

The linear Schrödinger equation, which describes the probability density of a single quantum particle in one dimension, is linear and dispersive:

$$iu_t + \frac{1}{2}u_{xx} = 0. \tag{1.4}$$

By adding a nonlinear term, we obtain a nonlinear Schrödinger equation (NLS):

$$iu_t + \frac{1}{2}u_{xx} \pm |u|^2 u = 0. \tag{1.5}$$

Unlike those of the linear Schrödinger equation, the solutions of the NLS are not generally additive; but, like the KdV, the NLS can be solved by the IST and has soliton solutions. Happily, the NLS has many physical interpretations. We show in chapter 4 that the particle density of a quasi one-dimensional BEC may be modelled to first approximation by the nonlinear NLS, known in the BEC community as the 1D homogeneous Gross-Pitaevskii equation (GPE). Equation (4.34) is the 1D GPE with interpretation and units appropriate for BEC, i.e., the modulus of the wave function squared is interpreted as atomic density in units indicated by Eq. (4.36) and x and t are position and time coordinates in units given by Eqs. (4.32) and (4.33). Equation (4.34) contains an additional external harmonic trapping potential, which is provided in BEC experiments by a magnetic trap [9].

The NLS also describes the envelope of a light wave-packet in a Kerr medium, and has been studied widely by the nonlinear optics community [10, 11]. When the nonlinearity in Eq. (1.5) is focussing (i.e. the positive sign is taken), the solitons are a nonzero-valued wavepacket in an otherwise zero-valued medium. In a nonlinear optics context these solitons represent a pulse of light, and for this reason are known as bright solitons. This name has been carried over into the BEC context, and these solitons are the starting point for this thesis.

1.4 Solitons in harmonically trapped Bose-Einstein condensates

In this thesis, we will investigate models of BECs in cylindrical trapping potentials. These are interesting for a number of reasons:

Solitons in non-integrable systems

Cylindrically trapped BECs are a weakly non-integrable system for two main reasons. The condensate is governed by a 3D GPE with tight radial and loose

axial trapping potentials. The 3D GPE is not integrable, even when it is homogeneous. The tight radial potential reduces the dynamics to 1D; however, residual 3D effects break the integrability, especially when the radial trap is weak compared to the radial kinetic energy of the condensate. Moreover, even when neglecting 3D effects completely, i.e., when the system is described by the 1D GPE with harmonic potential (the axial trapping potential), the system is thought not to be integrable - indeed, in chapter 8 we find evidence that it is not.

Systems of solitary waves in non-integrable systems cannot be true solitons in the sense defined by the inverse scattering transform. We investigate the extent to which the soliton nature of the solution is robust against the breaking of integrability of the equations of motion.

Chaos in wave mechanics

In the classical mechanics of particles, chaos is well defined by considering the system's trajectory in phase space. Chaos in wave mechanical systems is harder to grasp, since trajectories in infinite dimensional phase space are, at best, hard to visualise. Since soliton-like solutions have a particle character, chaos in wave dynamical systems may be defined (and easily visualised) when the corresponding particle dynamics are chaotic.

Quantum chaos

Classical mechanics emerges from quantum mechanics in classical limit, although the exact nature of that limit is not yet well established and a topic of great interest. Chaos is well defined in classical systems through the chaotic solutions to Hamilton's equations (see chapter 2), but a definition of quantum chaos is harder to formulate [12]. It is often claimed that since the Schrödinger equation is linear, chaotic dynamics are not possible in quantum systems; but to exist in classical mechanics, chaos must arise from quantum mechanics somehow. This apparent paradox is misconceived since Heisenberg's equations of motion can be nonlinear and it is *these* equations that correspond to Hamilton's equations. The GPE is a classical wave equation which arises from an approximation to the Heisenberg equations of motion. By finding chaotic solu-

tions to the GPE we have one example of how chaotic dynamics can arise from quantum systems. We look for (and find) such trajectories in chapter 8 when we consider systems of three harmonically trapped solitons.

Instabilities and depletion

Bose-Einstein condensates are a macroscopic population of a single particle state. This state may be depleted by quantum and thermal transitions. We discuss in chapter 4 that linear instabilities in the GPE may be an indication of depletion of the condensate, as suggested in Refs. [13, 14]. Regimes in which the soliton trajectories are chaotic are likely indicators of such instabilities.

Probe of quantum mechanics

Solitons in BECs can be used to investigate general problems in quantum mechanics. For example, the theory of decoherence draws an arbitrary distinction between the variables of the system and those of the surroundings. Since solitons can be described by a finite number of variables among the infinity of possible variables, they may be a useful model to probe the problem of decoherence [15].

Solitons are usually described as classical objects with well defined positions and momenta, even though they are composed of quantum particles. In reality, the positions and momenta must obey uncertainty relations. The positions and momenta of the solitons can be gradually inferred by measurements of the component particles. This might give a Bayesian interpretation of the uncertainty relations [15].

Applications

As well as their intrinsic interest, matter-wave solitons have many potential applications. Solitons may have applications in nonlinear interferometry [16]. A soliton laser has been proposed for use in precision measurements and interferometry by Strecker *et al.* [17]. Chen and Malomed [18], Carpentier *et al.* [19] and Carr and Brand [20] also propose a matter-wave soliton laser.

Solitons may also have a use in quantum information. Schemes for a quantum switch and quantum memory have been proposed using lattice solitons. Lattice

solitons are a slightly different type of soliton from that which we consider, where the effect of the band structure permits the existence of bright solitons in a lattice even when the inter-atomic interactions are repulsive [21].

Chapter 1 Summary

- Solitons are wave packets that pass through each other and emerge unscathed up to phase-shifts.
- The nonlinear Schrödinger equation has soliton solutions.
- The nonlinear Schrödinger equation is useful for modelling Bose-Einstein condensates of dilute quantum gases.
- This thesis concerns soliton-like objects in cylindrically-shaped Bose-Einstein condensates.
- These objects are interesting since they let us study soliton-like objects in non-integrable system, chaos in wave mechanics, quantum chaos, instabilities and depletion in Bose-Einstein condensates and general problems in quantum mechanics.
- Solitons have potential applications in interferometry, matter-wave lasers and quantum information.

Chapter 2

Classical mechanics of particles and fields

2.1 Overview

As mentioned in the introduction, solitons are particle-like solutions to field equations. In this chapter we attempt to clarify this statement. In order to explain what we mean by particle-like, we give an overview of the classical mechanics of systems of particles. This also enables us to introduce the concepts of chaos and regularity, which will become important later in this thesis. We then overview the classical theory of fields and, in particular, the inverse scattering transform (IST). The IST puts the concept of solitons on a more secure footing by allowing us a precise definition of solitons and a method of finding soliton solutions to nonlinear partial differential equations. We will illustrate the IST by using it to solve the nonlinear Schrödinger equation (NLS), which has an interpretation in the description of Bose-Einstein condensates (see chapter 4).

2.2 Classical theory of particles

2.2.1 Lagrangian mechanics

The equations of motion of a system of N dynamical variables q_i may be obtained by requiring that the action

$$S = \int L(\dot{q}_i, q_i)dt \tag{2.1}$$

be stationary for all variations in q_i with fixed endpoints. Here, $L(\dot{q}_i, q_i)$ is the so-called Lagrangian, which describes the difference between the kinetic and potential energy of the system.

The equations of motion are given by N partial differential equations:

$$\frac{\partial L}{\partial q_i} = \frac{d}{dt}\frac{\partial L}{\partial \dot{q}_i}, \tag{2.2}$$

known as the Euler-Lagrange equations. For a clear, reasonably full account of Lagrangian mechanics see the book by Goldstein [22].

2.2.2 Hamiltonian mechanics

While it is sometimes convenient to consider the Lagrangian formulation, Hamiltonian mechanics compose an extremely elegant alternative formulation of the equations of motion of a classical system with its own advantages. The dynamics of N degrees of freedom with positions q_i and momenta p_i are described by $2N$ first order differential equations, known as Hamilton's equations:

$$\dot{p}_i = -\frac{\partial H}{\partial q_i}, \tag{2.3}$$

$$\dot{q}_i = \frac{\partial H}{\partial p_i}, \tag{2.4}$$

where H is the total energy of the system. The trajectory of the system inhabits a $2N$ dimensional "phase-space". A transformation $\{p_i, q_i\} \mapsto \{P_i, Q_i\}$, such that the new co-ordinates $\{P_i, Q_i\}$ also obey Hamilton's equations, is called a canonical transformation. The new coordinates might not be canonical in the same Hamiltonian as the original coordinates.

We define the Poisson bracket of two physical quantities, $f(q_i, p_i, t)$ and $g(q_i, p_i, t)$ as:

$$\{f, g\} := \sum_i^N \left[\frac{\partial f}{\partial q_i}\frac{\partial g}{\partial p_i} - \frac{\partial f}{\partial p_i}\frac{\partial g}{\partial q_i}\right]. \tag{2.5}$$

The time evolution of a physical quantity, $f(q_i, p_i, t)$, follows from Hamilton's equations and the definition of the Poisson bracket:

$$\frac{d}{dt}f = \frac{\partial f}{\partial t} - \{H, f\}. \tag{2.6}$$

Therefore, if f has no explicit time dependence, it is a constant of the motion if its Poisson bracket with the Hamiltonian is zero. Isolating constants of the motion are associated with symmetries of the system (which may be hidden [12]). If a constant of the motion exists, it constrains the trajectory of the system to a subset of phase space with dimension $2N - 1$. This geometrical picture is key to understanding the qualitative dynamics of the system as we will see in the next section and is sometimes a sufficient tool for solving the equations of motion.

2.2.3 Integrability and chaos

In systems with N degrees of freedom ($2N$-dimensional phase space) the total energy, H, is conserved if it is has no explicit time dependence. This restricts the trajectories to a $(2N - 1)$-dimensional surface of constant energy in phase-space. If there are more functionally-independent isolating constants of the motion in addition to the energy, the allowed trajectories are restricted to lower dimensional surfaces. Constants of the motion are said to be in involution if they have mutually vanishing Poisson brackets. If there are N functionally-independent isolating constants of the motion in involution then the motion is constrained to N-dimensional tori which form a regular structure in phase-space, and the system is said to be integrable (see figure 2.1). There is no formula for finding the constants of the motion for a given Hamiltonian, so it is not always straightforward to determine whether or not a system is integrable. If a system is suspected not to be integrable, this can often be confirmed if trajectories are found which do not lie on tori in phase space.

In integrable systems, if a canonical transform can be made to the so-called action-angle variables $\{p_i, q_i\} \mapsto \{J_i, \theta_i\}$ (named after their dimensions) [22],

the Hamiltonian is a function of the J_i only. The radii of the invariant tori are functions of the action variables $\{J_i\}$, which are constant in time, and the angular position of the trajectories on the tori are described by the angle variables $\{\theta_i\}$, which change linearly in time. Because of this simple behaviour, the trajectories of an integrable system are said to be regular.

Figure 2.1: Two invariant tori in the phase space of an integrable system. The trajectories of the system wind around the tori at constant frequency.

Roughly speaking, a Hamiltonian has a resonance if there are frequencies such that there is rapid energy exchange between degrees of freedom. In non-integrable systems, multiple resonances may occur. Resonances are characterised by the appearence of both elliptic fixed points (stable fixed points in the middle of some torus) and hyperbolic fixed points (unstable fixed points between abutting tori) in the phase space. If these overlap, then the tori in phase space may be broken up. A theorem by Kolmogorov, Arnold and Moser shows that if the system is nearly integrable (i.e., the Hamiltonian is a slightly perturbed version of a Hamiltonian of an integrable system) then almost all of the invariant tori in phase space are preserved [23]. However, when the perturbation is increased, resonances appear in the phase space, breaking up the tori. Regions of ergodic behaviour emerge between the remaining tori in the phase space. By ergodic behaviour, we mean that given enough time, any trajectory originating in that region of phase space will come arbitrarily close to every point in that region. In such "ergodic seas", trajectories become mixed with each other. As the system becomes increasingly far from an integrable system, the ergodic sea spreads to cover an increasingly large proportion of the available phase-space of the system. The trajectories in such ergodic seas are called chaotic.

In the popular perception, a dynamical system is chaotic if trajectories that are

initially close diverge exponentially in time. This is commonly illustrated by the example of the butterfly effect, where a butterfly flapping its wings in Brazil causes a tornado in Texas [24]. Trajectories in a regular region of phase space obviously cannot mutually diverge. Trajectories in an ergodic region of phase space *do* mutually diverge; this divergence is characterised by the so-called Lyapunov exponents:

$$\lambda_i = \lim_{t\to\infty} \frac{1}{t} \ln \frac{|\delta \mathbf{z}_i(t)|}{|\delta \mathbf{z}_{0i}|}, \tag{2.7}$$

where $|\delta \mathbf{z}_i(t)|$ is the difference between the trajectories for an initial displacement $\delta \mathbf{z}_{0i}$. There are $2N$ exponents for each trajectory; each exponent accompanies an initial displacement in a different orthogonal direction in phase-space. If the trajectory is chaotic, at least one of these will be positive. In practice, the ergodic regions of phase-space fill up after some critical time, and the trajectories will reach a maximum divergence, so the limit in the Lyapunov exponents must be taken as t tends to this critical value rather than infinity.

Clearly chaotic trajectories cannot be obtained analytically, and the dynamics must be obtained by numerical means. To illustrate the trajectories (chaotic or otherwise) in a $2N$-dimensional phase-space when $N > 1$, it is common practice to take a section through the phase space. This is particularly suited to conservative systems where $N = 2$. In this case the energy will be conserved

$$H = \frac{1}{2}p_1^2 + \frac{1}{2}p_2^2 + V(q_1, q_2) = E, \tag{2.8}$$

constraining the trajectories to the 3D volumes of constant E. Consider the intersection of this volume with the volume $q_2 = 0$, this is a 2D surface which we may parameterise with the coordinates p_1 and q_1. For a trajectory with some initial conditions, Hamilton's equations will define uniquely the first point p_1, q_1 in which the trajectory crosses the plane $q_2 = 0$. Inverting Eq. (2.8), for the value of p_2 at this point will give us two solutions. Thus each point on the surface of section defines two sets of initial conditions for the equations of motion which could be integrated to find the next point. However, if we only consider points such that $p_2 < 0$, each point on the surface uniquely defines the next point. This choice of conditions defines a Poincaré surface of section (or Poincaré section) that we will make use of later in the thesis. This is not a unique choice of section - other sections may be taken depending on the region of phase space that is to be sampled. The appropriate choice may depend on

the symmetry of the potential. Clearly, the points lie on the surface:

$$\frac{1}{2}p_1^2 + V(q_1, 0) \leq E. \tag{2.9}$$

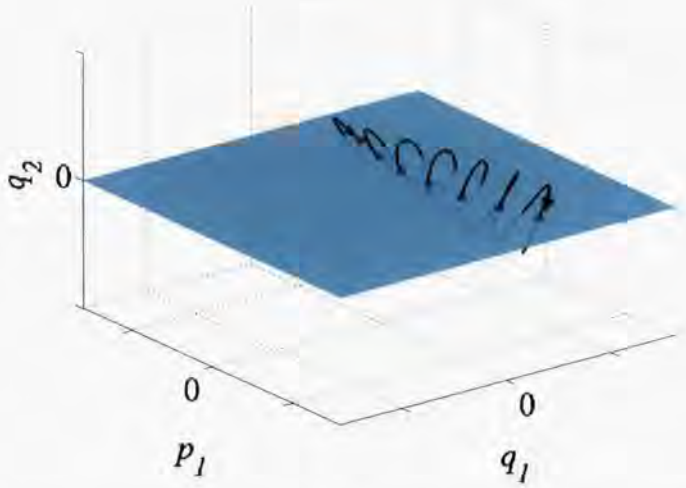

Figure 2.2: A trajectory cutting the surface $q_2 = 0$. Points are plotted when the trajectory cuts the surface with $p_2 < 0$. A Poincaré section is generated when multiple trajectories of some given energy, E, cut the surface.

If there is a second integral of the motion, $I(p_1, p_2, q_1, q_2)$, in involution with the Hamiltonian, the trajectories will be constrained to lines of intersection of the surface defined by Eq. (2.9) with surfaces of constant I. These will be 1D curves in the Poincaré section. If the system is not integrable, regular regions of the phase space will look the same as in integrable systems (1D curves), and Ergodic regions of phase space may be easily observed because these regions in the Poincaré section will 'fill up' as the trajectories come arbitrarily close to all possible points in the region.

2.3 Classical theory of fields

If the number of degrees of freedom in a Hamiltonian system is taken to be infinite and can be described by a continuous set of indices, the system is described by a partial differential equation (PDE), usually interpreted as a wave or field equation. Many of the concepts from the classical theory of particles carry over

to this limit, but sums over degrees of freedom are replaced by integrals (usually over space).

2.3.1 Lagrangian system

We may generalise Lagrangian mechanics to a theory of fields. In this case, the Lagrangian is an integral:

$$L = \int_{-\infty}^{\infty} \mathcal{L} dx. \tag{2.10}$$

The action principle requires that the action is stationary with respect to variations in any of the infinity of degrees of freedom of the system. We will make use of this useful result in part III of this thesis.

The Euler-Lagrange equations are now functions of the Lagrange density $\mathcal{L}$:

$$\frac{\partial \mathcal{L}}{\partial q_i} = \partial_j \frac{\partial \mathcal{L}}{\partial \partial_j q_i}. \tag{2.11}$$

For an introduction to classical Lagrangian field theory, we refer the reader to Goldstein's book [22].

2.3.2 Hamiltonian system

The Hamiltonian approach also admits an integral formulation:

$$H = \int_{-\infty}^{\infty} \mathcal{H}\left[p(x,t), q(x,t)\right] dx. \tag{2.12}$$

Hamilton's equations in a continuum are

$$\frac{\partial q}{\partial t} = \frac{\delta H}{\delta p}, \tag{2.13}$$

$$\frac{\partial p}{\partial t} = -\frac{\delta H}{\delta q}, \tag{2.14}$$

where the functional derivatives are defined by:

$$\begin{aligned} \frac{\delta F\left[p(x), q(x)\right]}{\delta p(y)} &:= \lim_{\epsilon \to 0} \frac{F\left[p(x) - \epsilon \delta(x-y), q(x)\right]}{\epsilon}, \\ \frac{\delta F\left[p(x), q(x)\right]}{\delta q(y)} &:= \lim_{\epsilon \to 0} \frac{F\left[p(x), q(x) - \epsilon \delta(x-y)\right]}{\epsilon}. \end{aligned} \tag{2.15}$$

Poisson brackets may be defined analogously to those in finite dimensional systems:

$$\{F, G\} = \int_{-\infty}^{\infty} \left(\frac{\delta F}{\delta q} \frac{\delta G}{\delta p} - \frac{\delta F}{\delta p} \frac{\delta G}{\delta q} \right) dx. \tag{2.16}$$

2.3.3 Inverse scattering, solitons and integrability

The concept of integrability in wave equations is interesting, and is connected with the existence of solitons, and the method of obtaining such solutions, the inverse scattering transform (IST).

The IST was first used by Gardner, Green, Kruskal and Miura to solve the Korteweg- de Vries equation [5], and later generalised to solve other equations including the nonlinear Schrödinger equation (NLS) [25] and the sine Gordon equation [26].

The IST is rather involved, so what follows is a brief outline of its principles, followed by a sketch of the solution of the NLS using this method. (We are interested in the NLS due to its interpretation in the physics of Bose-Eintein condensates, as we will see in chapter 4.) We omit all gory details, and refer readers to Ref. [27] for a clear pedagogical outline of the method, and Refs. [25, 28, 29], for a more rigorous treatment of the problem with discussion of some more interesting details. Our discussion will follow closely the method and notation in Refs. [25, 28].

Sketch of the inverse scattering transform

The IST can be thought of as a nonlinear analogue of the Fourier transform method for solving linear equations. The Fourier Transform method is well known, and involves three steps (illustrated by Figure 2.3):

- Fourier transform the initial condition.
- Evolve the Fourier transform in accordance with the dispersion relation.
- Inverse transform the time-evolved Fourier transform.

Similarly, the IST can be broken up into three steps (illustrated by figure 2.4):

- Given an initial condition $u(x,0)$ (the initial condition for the nonlinear PDE), construct a linear scattering problem $L_{\text{Lax}}\psi = \lambda\psi$, where L_{Lax} is a specially chosen operator with functional dependence on $u(x,t)$. $u(x,t)$ is the solution to the PDE we are trying to find, and it acts as a scattering

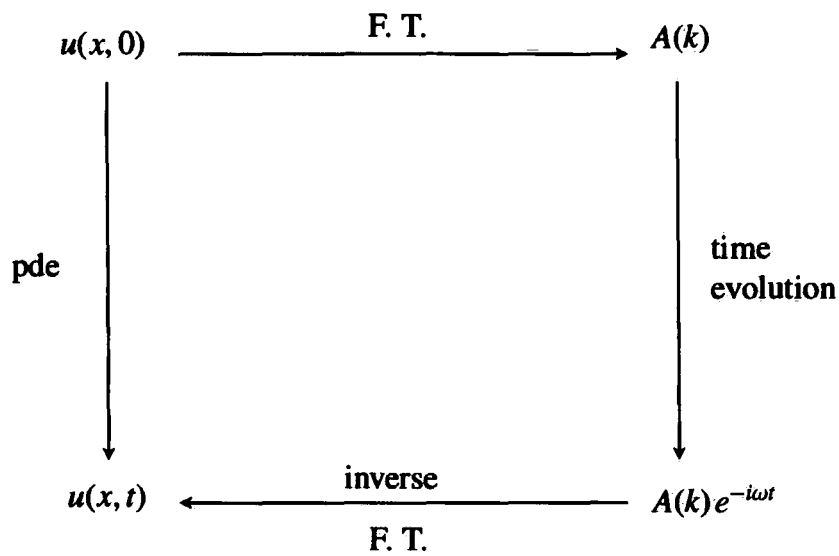

Figure 2.3: The Fourier transform method of solving linear PDEs.

potential in the linear scattering problem. Solve this scattering problem at $t = 0$ to obtain scattering data (the asymptotic behaviour of ψ as $|x| \to \infty$).

- Find an operator, M (which is, in general, a function of $u(x,t)$) such that

$$\frac{dL_{\text{Lax}}}{dt} + i[L_{\text{Lax}}, M] = 0 \tag{2.17}$$

guarantees the PDE. $\{L_{\text{Lax}}, M\}$ is called a Lax pair. Hence, evolve the scattering data in time, requiring that $\psi(t)$ is an eigenstate of $L_{\text{Lax}}(t)$ with constant eigenvalue λ, i.e.,

$$i\psi_t = M\psi. \tag{2.18}$$

Clearly, at time t, M depends on $u(x,t)$, and hence $\psi(t)$ contains the information needed to reconstruct $u(x,t)$.

- Solve the inverse scattering problem with the time-evolved scattering data to obtain $u(x,t)$. This involves solving linear integral equations called Marchenko equations. If the scattering data is wholly transmitted, then the solution of the PDE has an interpretation as solitons, otherwise the solution describes, in general, solitons plus radiation (which often has an interpretation as sound waves).

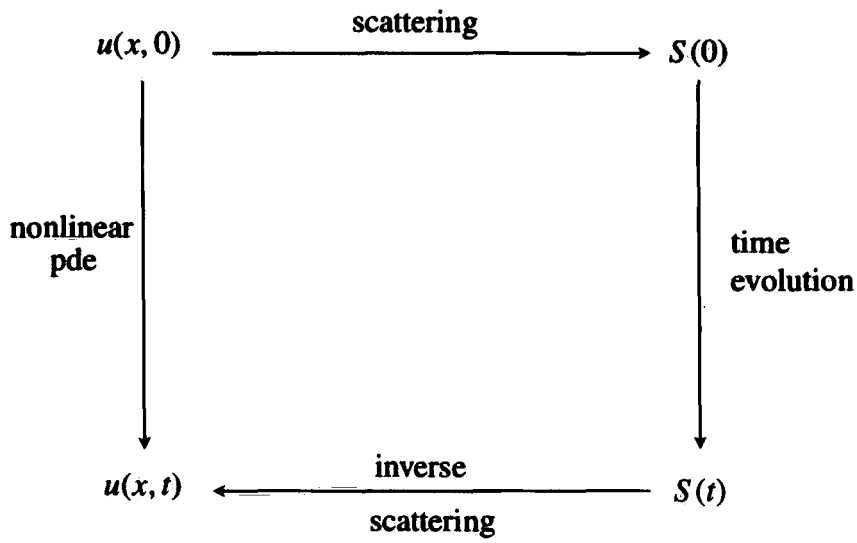

Figure 2.4: The inverse scattering transform method of solving Lax integrable nonlinear PDEs.

Link with integrability

If the problem can be formulated in terms of a Lax pair, the system is called Lax integrable and can be solved by considering only linear equations. Additionally, when the system is considered as a Hamiltonian system, the existence of a Lax pair implies an infinite number of independent constants of the motion exist in involution, which provides a satisfying link with finite dimensional Hamiltonian systems. Moreover, the IST can be interpreted as a conversion to action angle variables followed by time evolution of these variables before implementation of the inverse conversion.

2.3.4 Nonlinear Schrödinger equation

Consider the self-focussing NLS:

$$iu_t + u_{xx} + k|u|^2 u = 0, \tag{2.19}$$

for $k > 0$. In order to perform the inverse scattering transform more easily, we choose some parameters K and m such that $k = 2K/(1-m^2)$ and $0 < m < 1$, and scale the solution $\tilde{u} := \sqrt{K}u$. The rescaled solution $\tilde{u}$ now satisfies the

equation:

$$i\tilde{u}_t + \tilde{u}_{xx} + \frac{2}{1-m^2}|\tilde{u}|^2\tilde{u} = 0, \tag{2.20}$$

Furthermore, let us assume that $\tilde{u}$ and its derivatives decay to zero rapidly as $x \to \pm\infty$.

Then we define the Lax pair, $\{L_{\text{Lax}}, M\}$; we impose that these obey Eq. (2.17), which then implies Eq. (2.20) for the choice:

$$L_{\text{Lax}} = i\begin{pmatrix} 1+m & 0 \\ 0 & 1-m \end{pmatrix}\frac{\partial}{\partial x} + \begin{pmatrix} 0 & \tilde{u}^* \\ \tilde{u} & 0 \end{pmatrix}; \tag{2.21}$$

$$M = -m\begin{pmatrix} 1 & 0 \\ 0 & 1 \end{pmatrix}\frac{\partial^2}{\partial x^2} + i\begin{pmatrix} |\tilde{u}|^2/(1+m) & i\tilde{u}_x \\ -i\tilde{u}_x & -|\tilde{u}|^2/(1-m) \end{pmatrix}. \tag{2.22}$$

Now the vector, which we write in terms of its components: $\psi = (\psi_1, \psi_2)^T$ is a solution of the scattering problem, i.e., an eigenvalue of L_{Lax}. In order to obtain a manageable scattering problem, we make a useful change of variables:

$$v_1 := \frac{\psi_2}{\sqrt{1+m}}\exp\left(i\frac{\lambda x}{1-m^2}\right), \tag{2.23}$$

$$v_2 := \frac{\psi_1}{\sqrt{1-m}}\exp\left(i\frac{\lambda x}{1-m^2}\right), \tag{2.24}$$

yielding the new scattering problem:

$$\begin{aligned} v_{1x} + i\zeta v_1 &= qv_2, \\ v_{2x} - i\zeta v_2 &= -q^* v_1, \end{aligned} \tag{2.25}$$

where $q = i\tilde{u}/\sqrt{1-m^2}$ and $\zeta = \lambda m/(1-m^2)$. Note that in this problem $q(x,t)$ and $-q(x,t)^*$ may be interpreted as potentials, and ζ as a time independent eigenvalue. We write the eigenvalues in the form $\zeta = \xi + i\eta$, where ξ and η are real. Henceforth in this chapter we consider the solution $q(x,t)$ since it obeys a rescaled NLS, and is trivially related to u by $q = iu\sqrt{k/2}$.

We initially consider the scattering problem at $t = 0$. Eq. (2.25) will have a continuous spectrum of real eigenvalues ξ, with eigenstates given by the Jost solutions [28], defined in terms of their asymptotic behaviour:

$$\begin{aligned} \varphi_- &\to \begin{pmatrix} 1 \\ 0 \end{pmatrix} e^{-i\xi x} \quad \text{as } x \to -\infty, \\ \varphi_+ &\to \begin{pmatrix} 0 \\ 1 \end{pmatrix} e^{i\xi x} \quad \text{as } x \to \infty. \end{aligned} \tag{2.26}$$

We also define:

$$\bar{\varphi}_+ := \begin{pmatrix} \varphi^*_{+2} \\ -\varphi^*_{+1} \end{pmatrix}, \tag{2.27}$$

where φ^*_{+i} is the complex conjugate of the ith component of φ_+. $\bar{\varphi}_+$ is clearly also an eigenstate of Eq. (2.25) with eigenvalue $\xi^* = \xi$. Since φ_+ and $\bar{\varphi}_+$ form a basis, we may write:

$$\varphi_- = a(\xi)\bar{\varphi}_+ + b(\xi)\varphi_+. \tag{2.28}$$

By dividing Eq. (2.28) by $a(\xi)$, it is clear that $1/a(\xi)$ and $b(\xi)/a(\xi)$ have interpretation as the transmission and reflection coefficients of the scattering potential. The Jost solutions and the function $a(\xi)$ may be extended by analytic continuation into the upper half-plane. As well as scattered states, Eq. (2.25) may have bound eigenstates corresponding to the points ζ_j in the upper half-plane where $a(\zeta) = 0$. These bound states may be written:

$$\varphi_- = a'(\zeta_j)c_j\varphi_+, \tag{2.29}$$

where the prime denotes the derivative of a with respect to ζ_j. The coefficients $\{a(\xi), b(\xi), c_j\}$ and elements of the discrete spectrum $\{\zeta_j\}$ are called the scattering data [28].

By considering Eq. (2.18) in the limit $x \to \pm\infty$, the time dependence of the scattering data may be inferred:

$$\begin{aligned} a(\xi, t) &= a(\xi, 0), \\ b(\xi, t) &= b(\xi, 0)e^{4i\xi^2 t}, \\ c_j(t) &= c_j(0)e^{4i\zeta_j^2 t}. \end{aligned} \tag{2.30}$$

The time-evolved potential, $q(x,t)$, may be reconstructed from the time-evolved scattering data by using standard methods for solving inverse scattering problems [25, 27, 28]. It turns out that c_k correspond to the existence of solitons, and $b(\xi)$ corresponds to radiation.

By defining

$$F(x) = \frac{1}{2\pi}\int_{-\infty}^{\infty} \frac{b(\xi)}{a(\xi)} e^{i\xi x} d\xi + \sum_{k=1}^{N} c_k e^{i\xi_k x}, \tag{2.31}$$

the Marchenko equations

$$\begin{aligned} K_1(x,y) &= F(x+y) + \int_x^{\infty} K_2(x,s)F(s+y)ds, \\ K_2^*(x,y) &= -\int_x^{\infty} K_1(x,s)F(s+y)ds, \end{aligned} \tag{2.32}$$

allow us to express $q(x,t)$ in terms of the solutions K_1 and K_2:

$$q(x) = -2K_1(x,x), \tag{2.33}$$

$$\int_x^\infty |q(s)|^2 ds = -2K_2(x,x). \tag{2.34}$$

N-soliton solution

When $b(\xi,t) \equiv 0$, i.e., the scattering problem is reflectionless, we may express Eqs. (2.32) as coupled summations (see Ref. [25]):

$$\begin{aligned} \psi_{1j}(x,\zeta_j)\exp(-i\zeta_j x) + \sum_{k=1}^{N} \frac{\exp(-i\zeta_k^* x)}{\zeta_j - \zeta_k^*} c_k^* \psi_2^*(x,\zeta_k) = 0, \\ \psi_{2j}^*(x,\zeta_j)\exp(i\zeta^* x) = 1 + \sum_{k=1}^{N} \frac{\exp(i\zeta_k^* x)}{\zeta_j^* - \zeta_k} c_k \psi_1(x,\zeta_k). \end{aligned} \tag{2.35}$$

The solution can then be written

$$q(x) = -2i \sum_{k=1}^{N} c_k^* \exp(-i\zeta_k x)\psi_2^*(x,\zeta_k), \tag{2.36}$$

$$\int_x^\infty |q(s)|^2 ds = -2i \sum_{k=1}^{N} c_k \exp(i\zeta_k)\psi_1(x,\zeta_k). \tag{2.37}$$

When $N = 1$, i.e., $a(\zeta)$ has only one zero in the upper half plane at $\zeta = \xi + i\eta$, Eq. (2.36) may be written:

$$q(x,t) = i\eta \mathrm{sech}(2\eta(x - x_0 + 8\eta\xi t)\exp\left[-4i(\xi^2 - \eta^2)t - 2i\xi x + i\phi_0\right], \tag{2.38}$$

where $x_0 = \log(|c|/2\eta)/2\eta$ and $\phi_0 = -2\arg\sqrt{c}$. This is clearly a solitary wave solution, i.e., it retains its profile which moves at a constant speed, since its profile is a function of $(x - x_0 + 8\eta\xi t)$.

For $N > 1$, we consider the system in the limit $t \to \infty$, holding $x - 4\xi_j t$ constant for some $1 \le j \le N$. We find [25]:

$$\begin{aligned} \psi_{1j} + \frac{|\lambda_j^+|^2}{2i\eta_j}\psi_{2j} = 0, \\ \frac{|\lambda_j^+|^2}{2i\eta_j}\psi_{1j} + \psi_{2j}^* = \lambda_j^{+*}, \end{aligned} \tag{2.39}$$

where

$$\lambda_j^+ := \sqrt{c_j} e^{i\xi_j x} \prod_{k=j+1}^{N} \frac{\xi_j - \xi_k}{\xi_j - \xi_k^*}, \tag{2.40}$$

for $j = 1...N$. By comparison with Eq. (2.35) with $N = 1$, we see that in this limit, the solution takes the form of a sum of N distinct solitons with displaced centres and phases:

$$x_{0j}^+ - x_{0j} = \frac{1}{\eta_j} \sum_{k=j+1}^{N} \log \left| \frac{\xi_j - \xi_k}{\xi_j - \xi_k^*} \right|, \tag{2.41}$$

where x_{0j} is the displacement of the jth soliton in the limit $t \to -\infty$, and $x_{0j}^+ + x_{0j}$ is the displacement of the jth soliton in the limit $t \to +\infty$, and

$$\phi_{0j}^+ - \phi_{0j} = -2 \sum_{k=j+1}^{N} \arg \left(\frac{\xi_j - \xi_k}{\xi_j - \xi_k^*} \right), \tag{2.42}$$

where ϕ_{0j} is the displacement of phase of the jth soliton in the limit $t \to -\infty$, and $\phi_{0j}^+ + \phi_{0j}$ is the displacement of the phase of the jth soliton in the limit $t \to +\infty$.

Similarly, in the limit $t \to -\infty$, holding $x - 4\xi_j t$ constant, we find the same behaviour, but with

$$\lambda_j^- := \sqrt{c_j} e^{i\xi_j x} \prod_{k=1}^{j-1} \frac{\xi_j - \xi_k}{\xi_j - \xi_k^*}, \tag{2.43}$$

etc.

Taking the limits $t \to \pm\infty$, holding $x - 4\xi t$, where ξ doesn't coincide with any ξ_j, the solution tends asymptotically to zero. Hence the complete solution as $t \to \pm\infty$ represents a sum of N distinct solitons.

NLS as a classical dynamical system

The NLS [Eq. (2.20)] is a classical field equation, and may be derived from the following Lagrange density:

$$\mathcal{L} = \frac{i}{2}(uu_t^* - u^* u_t) + \frac{1}{2}|u_x|^2 - \frac{k}{2}|u|^4. \tag{2.44}$$

The NLS is also a Hamiltonian system, and by defining the momentum $p(x,t) = -q^*(x,t)$, the following Hamiltonian produces the equation of motion for q:

$$H = -i \int_{-\infty}^{\infty} \left[q_x p_x + (qp)^2 \right] dx \tag{2.45}$$

Note that this choice of Hamiltonian is different from the conventional energy functional by a factor of i. These can be made to be equal by redefining Hamilton's equations to include the factor of i on the right-hand side, as is sometimes done [29].

It is shown in Ref. [28] that the existence of a Lax pair implies that the NLS has the following constants of the motion in involution:

$$C_n = \int_{-\infty}^{\infty} \mu_n dx, \tag{2.46}$$

where $\mu_0 = -qp$, $\mu_1 = -qp_x$, and

$$\mu_{n+1} = q\left(\frac{\mu_n}{q}\right)_x + \sum_{k=0}^{n-1} \mu_k \mu_{n-k-1} \quad \text{for } n \geq 1. \tag{2.47}$$

The first three constants have the physical interpretation as conservation of norm (mass), momentum and energy, and are associated with the symmetries of the system with respect to phase, displacement and time respectively.

Interestingly, the Hamiltonian may be expressed in terms of the scattering data:

$$H = \frac{2}{\pi}\int_{-\infty}^{\infty} \log\left[|a(\xi)|^2\right] A_-(\xi)d\xi + 4i\sum_{m=1}^{N}\int_{\zeta_m^*}^{\zeta_m} A_-(\zeta)d\zeta, \tag{2.48}$$

where $A_-(\zeta) := 2i\zeta^2$. The second integral in Eq. (2.48) is an anti-derivative, and is formally computed as if ζ were a real variable and ζ_m^* and ζ_m were real limits.

The scattering data compose the following action-angle variables:

$$P(\xi) = \log\left[|a(\xi)|^2\right], \tag{2.49}$$

$$Q(\xi) = -\frac{1}{\pi}\log b(\xi), \tag{2.50}$$

$$P_m = \zeta_m, \tag{2.51}$$

$$Q_m = -2i\log c_m, \tag{2.52}$$

such that Hamilton's equations are equivalent to Eqs. (2.30).

Chapter 2 Summary

- Lagrangian dynamics may be derived from an action principle.
- The Hamiltonian dynamics in $2N$ dimensional phase-space is a useful alternative picture of classical mechanics.
- Isolating constants of the motion confine the dynamics to $2N-1$ dimensions.
- A system is integrable if it has N functionally-independent isolating constants of the motion in involution.
- Trajectories in an integrable system are confined to regular tori in phase-space, can be described by action-angle variables, and are hence completely regular.
- Systems which are not integrable may support chaotic regimes.
- A region of phase space is chaotic if its trajectories are sensitive to small changes in initial conditions and display topological mixing, and if it has a dense subset of regular trajectories.
- Field equations can be represented by a trajectory in an infinite dimensional phase-space.
- Some important field equations may be solved by the inverse scattering transform.
- Soliton solutions to such equations correspond to initial conditions where the corresponding scattering problem has zero reflection coefficient.
- Systems soluble by the inverse scattering transform are completely integrable and have an infinite number of contants of the motion in involution. The inverse scattering transform is a conversion to action angle variables.

Chapter 3

Solitons as classical particles

3.1 Overview

We stated in chapter 1 that solitons have a particle nature in the sense that they approach each other, collide and reemerge with shifts in position as if they have interacted through some force. In this chapter, we further this analogy by formulating a model treating nonlinear Schrödinger (NLS) solitons as classical particles interacting through an explicit force. We first recap the N-soliton solution to the NLS before deducing an "inter-soliton potential" that reproduces the shifts in position in a particle model.

3.2 N-soliton solution to the nonlinear Schrödinger equation

We recast Eq. (2.20) as:

$$iu_t + \frac{1}{2}u_{xx} + |u|^2 u = 0. \tag{3.1}$$

In chapter 4 we will find that this is a useful rescaling for the purposes of modelling Bose-Einstein condensates. We showed in chapter 2 that there exists an N-soliton solution to Eq. (3.1). Equations (2.39) to (2.43) suggest a straightforward interpretation of the solution in terms of a scattering problem [29]: In the limit $t \to -\infty$, the solutions take the form of an arbitrary number of well

separated (incoming) solitons, which are given, using our rescaling, by:

$$\psi_j(x,t) = 2\eta_j \mathrm{sech}\left[2\eta_j(x-q_j)\right] e^{iv_j(x-q_j)} e^{i(2\eta_j^2+v_j^2/2)t} e^{i\alpha_{0j}}. \tag{3.2}$$

Here $q_j = v_j t + x_{0j}$ is the position of the peak of the jth soliton; x_{0j} is the peak position at $t = 0$; $\alpha_{0j} - v_j x_{0j}$ is the phase for a single soliton (i.e., in the absence of collisions with other solitons) at $x = 0$, $t = 0$; v_j is the soliton velocity and η_j gives the relative size of the soliton. We normalise the solution such that $\sum_j^{N_s} 4\eta_j = 1$, where N_s is the number of solitons present.

The solitons come together and collide, during which time the form of the solution is complicated and solitons are not individually defined. However, as $t \to \infty$, the outgoing solitons re-emerge from the collisions unscathed, taking the same asymptotic form [Eq. (3.2)], up to shifts in position and phase: $q_j \mapsto q_j + \delta x_j$ and $\alpha_{0j} \mapsto \alpha_{0j} + \delta\phi_j$, where the position shift δx_j and phase-shift $\delta\phi_j$ of the jth soliton are given by [29,30]:

$$2\eta_j \delta x_j + i\delta\phi_j = \sum_{j\neq k} \pm 2 \ln\left[\frac{v_j - v_k + i2(\eta_j + \eta_k)}{v_j - v_k + i2(\eta_j - \eta_k)}\right]. \tag{3.3}$$

The positive sign applies if the soliton is on the left prior to the collision with the kth soliton ($v_j > v_k$), otherwise the negative sign applies. Note that these shifts are dependent on the solitons' initial speeds v_j, and effective masses η_j only, not on their relative phase.

3.3 Particle model for 1D solitons

The trajectories of solitons emerging from collisions with each other are independent of the relative phase of the incoming solitons. The only effect of the relative phase of the solitons is on the form of the wavefunction (peak or trough) during the collision. This is illustrated in figure 3.1. The phase-independence of the solitons' incoming and outgoing trajectories allows a model to be formulated that treats the solitons as classical particles, each with only the positional degree of freedom (rather than position and phase degrees of freedom used, for example, in [31]). This model was introduced by Scharf and Bishop in the context of nonlinear optics [32–34], which we have adapted for the purpose of modeling a quasi-1D harmonically trapped BEC [1,2] by using a potential and units appropriate for modeling BEC (see part II of this thesis).

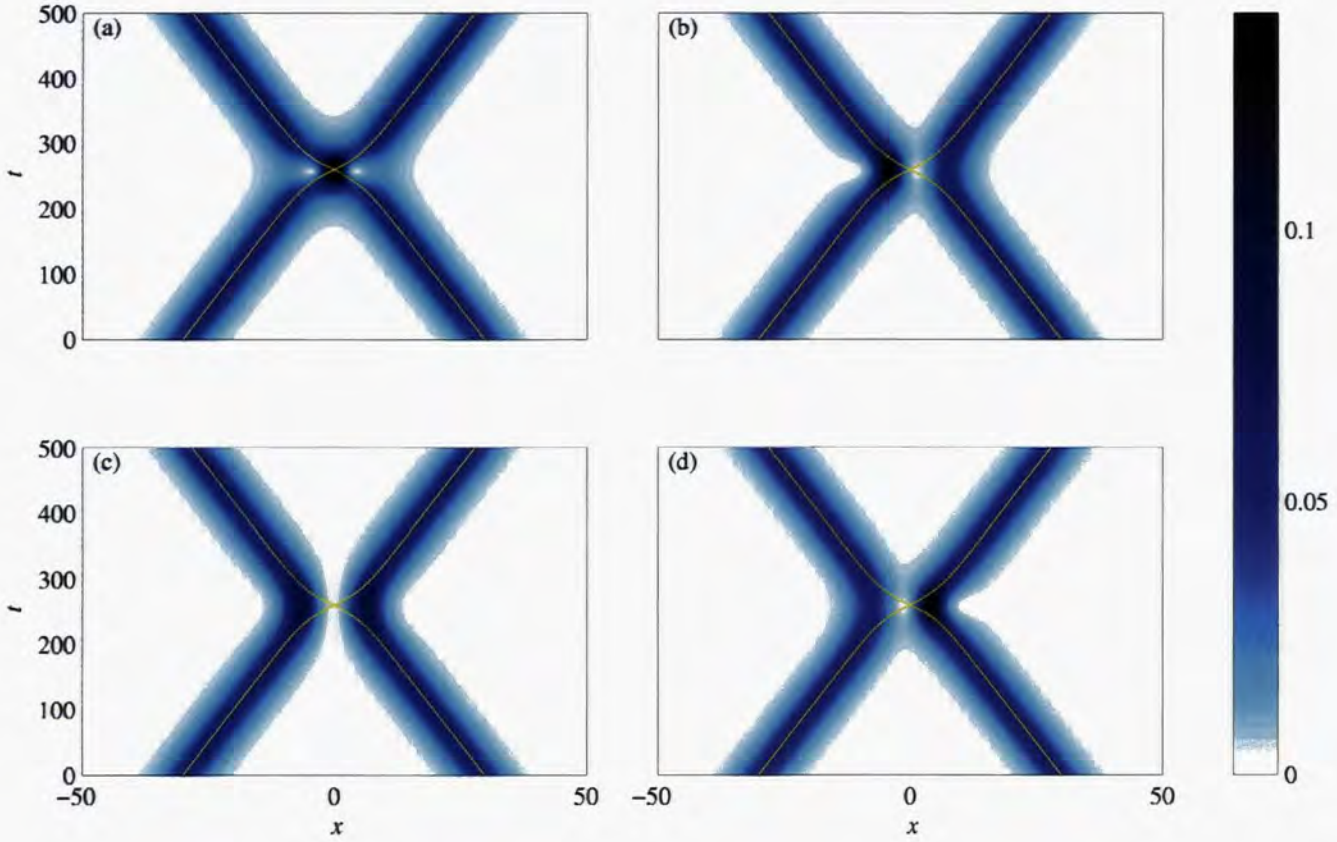

Figure 3.1: Two soliton collision taking place when (a) $\Delta\phi_{\text{col}} = 0$, (b) $\Delta\phi_{\text{col}} = \pi/2$, (c) $\Delta\phi_{\text{col}} = \pi$ and (d) $\Delta\phi_{\text{col}} = 3\pi/2$. The total wavefunction is normalised to one, and the value of density is indicated by the colorbar.

To construct the particle model, we first consider the homogeneous solution before introducing the effects of the harmonic trap. Following the approach in [35], one can derive an effective inter-soliton potential:

$$V(q_j - q_k) = -2\eta_j\eta_k(\eta_j + \eta_k)\mathrm{sech}^2\left[\frac{2\eta_j\eta_k}{\eta_j + \eta_k}(q_j - q_k)\right], \tag{3.4}$$

which treats the solitons as particles of position q_j and effective mass η_j, the parameters used to describe the bright soliton solutions of Eq. (3.2). This potential reproduces the asymptotic position shifts [Eq. (3.3)] in the homogeneous GPE for the outgoing particle trajectories, i.e., the position shifts as the solitons become infinitely far apart. It yields accurate results when $2|\eta_1 - \eta_2| \ll |v_1 - v_2|$, where v_1 and v_2 are the soliton velocities, which gives a lower limit for the relative velocity for which the particle model is applicable.

The position-shifts given by Eq. (3.3) are equivalent to the asymptotic time-shifts for two solitons of initial speeds v_1 and v_2, and effective masses η_1 and η_2, given by

$$\Delta t = -\frac{1}{2(v_1 - v_2)}\left(\frac{1}{\eta_1} + \frac{1}{\eta_2}\right)\ln\left[\frac{(v_1 - v_2)^2 + 4(\eta_1 + \eta_2)^2}{(v_1 - v_2)^2 + 4(\eta_1 - \eta_2)^2}\right]. \tag{3.5}$$

We will show that when the $(\eta_1 - \eta_2)$ term is omitted from the denominator of the logarithm in Eq. (3.5), we can produce the same shifts with a classical scattering potential. This is the origin of the constraint $2|\eta_1 - \eta_2| \ll |v_1 - v_2|$.

We wish to produce the position shifts in a system of two classical particles described by the Hamiltonian:

$$H := \frac{p^2}{2\mu_r} + V(q) \tag{3.6}$$

where $q := q_1 - q_2$ is the relative coordinate, $\mu_r := \eta_1\eta_2/(\eta_1 + \eta_2)$ is the reduced effective mass, $p = (\eta_1 p_2 - \eta_2 p_1)/(\eta_1 + \eta_2)$ is the relative momentum, and the centre of mass has been separated from the problem. For particles initially separated at infinity, and noting that $p^2/2\mu_r = \mu_r\dot{q}^2/2$, this Hamiltonian takes the asymptotic form

$$H = \frac{\mu_r}{2}(v_1 - v_2)^2 := E_\infty, \tag{3.7}$$

i.e., we assume the potential must vanish asymptotically.

By rearranging Eq. (3.6), we may write the infinitesimal

$$dq = \sqrt{\frac{2\left[E_\infty - V(q)\right]}{\mu_r}}dt, \tag{3.8}$$

since energy is conserved over the whole trajectory. Integrating the time difference between trajectories with and without the inter-particle potential, we determine the asymptotic timeshift to be

$$\Delta t = \left(\frac{\mu}{2}\right)^{1/2} \int_{-\infty}^{\infty} dq \frac{1}{E_\infty^{1/2}} \left[\left(1 - \frac{V(q)}{E_\infty}\right)^{-1/2} - 1\right]. \tag{3.9}$$

Now, expanding Eqs. (3.5) and (3.9) in terms of powers of $1/E_\infty$, and equating equal powers, we obtain

$$\begin{aligned}\int_{-\infty}^{\infty} dq V(q)^n =& \frac{1}{2}\left(\frac{1}{\eta_1} + \frac{1}{\eta_2}\right) \\ &\times \left\{\left[4\eta_1\eta_2\left(\eta_1 + \eta_2\right)\right]^n - \left[\frac{4\eta_1\eta_2\left(\eta_1 - \eta_2\right)^2}{\eta_1 + \eta_2}\right]^n\right\} \\ &\times \frac{(-1)^n 2^{n-1}\left[(n-1)!\right]^2}{(2n-1)!}\end{aligned} \tag{3.10}$$

for all positive integers n. We now evaluate the integral of a candidate potential:

$$\begin{aligned}\int_{-\infty}^{\infty} dq V(q)^n &= \int_{-\infty}^{\infty} dq \left[-2(\eta_1 + \eta_2)\eta_1\eta_2 \mathrm{sech}^2\left(\frac{2\eta_1\eta_2}{\eta_1 + \eta_2} q\right)\right]^n \\ &= \frac{1}{2}\left(\frac{1}{\eta_1} + \frac{1}{\eta_2}\right)\left[4\eta_1\eta_2\left(\eta_1 + \eta_2\right)\right]^n \\ &\quad \times \frac{(-1)^n 2^{n-1}\left[(n-1)!\right]^2}{(2n-1)!}\end{aligned} \tag{3.11}$$

Comparing the expressions (3.10) and (3.11) we see that the potential

$$V(q) = -2(\eta_1 + \eta_2)\eta_1\eta_2 \mathrm{sech}^2\left(\frac{2\eta_1\eta_2}{\eta_1 + \eta_2} q\right) \tag{3.12}$$

gives the correct time shift in the limit $2|\eta_1 - \eta_2| \ll |v_1 - v_2|$.

Figure 3.1 shows the particle trajectories predicted by our model interaction potential [Eq. (3.4)] superimposed on the density profile dynamics predicted by solution of the NLS. In this figure, $\eta_1 = \eta_2$, so that the particle model gives the exact position shift.

Since the phase-shifts of a soliton given by Eq. (3.3) is a sum of phase shifts from interactions with the other solitons, we can extend our particle model to treat N_s solitons simply by summing the inter-particle potentials. Hence the Hamiltonian for N_s solitons in the homogeneous GPE is given by

$$H = \sum_{j=1}^{N_s} \frac{p_j^2}{2\eta_j} - \sum_{1\leq j<k\leq N_s} 2\eta_j\eta_k(\eta_j+\eta_k)\mathrm{sech}^2\left[\frac{2\eta_j\eta_k}{\eta_j+\eta_k}(q_j-q_k)\right]. \tag{3.13}$$

Chapter 3 Summary

- Approaching solitons in the nonlinear Schrödinger equation that are initially well separated collide and re-emerge unscathed up to shifts in position and phase.
- A classical scattering potential produces the same position shifts for initially well-separated approaching particles. The agreement is exact for solitons of the same size.
- The solitons in the nonlinear Schrödinger equation can be modelled as classical particles interacting via this classical scattering potential.

Chapter 4

Dilute Bose-Einstein condensates of attractively interacting atoms

4.1 Overview

In this chapter we review the theoretical description of a dilute Bose-Einstein condensate (BEC). We do not describe the details of the process of condensation, but details of this process, and other background information on BEC physics, may be found in Refs. [9, 36, 37].

The atomic number-density of a dilute BEC is frequently described theoretically by a classical field equation known as the Gross-Pitaevskii equation (GPE) [9, 36, 37]. This equation reduces to an effective 1D field equation when a tight radial potential is applied. When the atoms interact attractively, the nonlinear term in the GPE becomes self-focussing. This 1D system supports bright soliton solutions, as we will see in chapter 5. The GPE generally gives very good agreement with experimental results, but is by no means a complete theoretical description of dilute atomic BECs. The GPE describes the dynamics of the condensate mode (to first order), but does not capture the physics of thermal or quantum transitions between the condensate mode and other modes of the system. For BECs with temperatures higher than zero Kelvin, or with linear instabilities in the dynamics, we expect such transitions to become significant.

This is relevant to the work in this thesis, for in chapter 8 we encounter chaotic dynamics of bright solitons described by the GPE, which we expect to coincide with linear instabilities in the field equations.

In this chapter we outline the theoretical treatment of a dilute gas of attractively interacting Bosonic atoms, following the methods in [13,38]. To first order, this treatment produces the GPE, but higher order considerations reveal corrections to the GPE and equations for the non-condensate mode. We then outline the reduction of the GPE from a 3D to a 1D classical field equation in the regime of tight radial confinement.

4.2 Bose-Einstein condensates of a dilute cold atomic gas

In this section we recap the quantum description of a gas of identical Bose particles, using the formalism commonly known as second-quantisation, and discuss what it means for a condensate to be present. We then briefly sketch the results of the number conserving treatment of the system's dynamics, which was developed by Gardiner [38] and Castin and Dum [13] (see also [39]); from which we arrive at the well-known Gross-Pitaevski equation, which describes the dynamics of the condensate to lowest order. This approach also produces higher order corrections to the condensate dynamics along with equations for the non-condensate atoms (these are essentially modified Bogoliubov-de Gennes equations) [40–42].

The number-conserving treatment is different from the conventional (symmetry-breaking) treatment, which partitions the field operator into an expectation value and a fluctuation part [36,37]. These parts are not, in general, spatially orthogonal and the total number of particles is not conserved. At the level of the GPE (used for the results generated in this thesis) both treatments are identical, and at the level of the Bogoliubov-de Gennes equations the treatments are equivalent up to a projection of the non-condensate modes. At higher orders than the Bogoliubov-de Gennes equations, more significant differences occur between the treatments [39]. Calculations using higher orders than the GPE are beyond the scope of this thesis, but we outline the theory as a guide to

further study.

4.2.1 Bose gas

A system of identical Bose particles is described by a state vector that is symmetric under exchange of any two particles. A Fock state is a symmetrised state vector $|n_1, n_2...\rangle\rangle$, where n_i is the number of particles in the single particle state corresponding to $|\Phi_i\rangle$, a member of some othonormal basis of single particle states $\{|\Phi_i\rangle\}_i$. (We denote the bras and kets of a Fock state with a double bracket, to provide a distinction from the bras and kets of the single particle states, which we denote with a single bracket.) The vectors $\{|n_1, n_2...\rangle\rangle\}_{n_1,n_2...}$ form an orthonormal basis for the symmetric subspace of the tensor product of the individual particle Hilbert spaces, known as the Fock space; hence, the state of a general system of identical Bose particles is described by a superposition of Fock states.

In order to constuct general operators for the many-particle system, we define the following so-called creation and annihilation operators:

$$\hat{a}_i^\dagger |n_1, n_2, n_i...\rangle\rangle = \sqrt{n_i + 1}|n_1, n_2, n_i + 1...\rangle\rangle \tag{4.1}$$

$$\hat{a}_i |n_1, n_2, n_i...\rangle\rangle = \sqrt{n_i}|n_1, n_2, n_i - 1...\rangle\rangle. \tag{4.2}$$

From the symmetry of the state vectors, we may infer the following commutation relations:

$$\left[\hat{a}_i, \hat{a}_j^\dagger\right] = \delta_{jk} \tag{4.3}$$

$$[\hat{a}_i, \hat{a}_j] = 0 \tag{4.4}$$

$$\left[\hat{a}_i^\dagger, \hat{a}_j^\dagger\right] = 0. \tag{4.5}$$

We introduce the so-called field operators:

$$\hat{\Psi}^\dagger(\mathbf{r}) = \sum_i \hat{a}_i^\dagger \Phi_i^*(\mathbf{r}) \tag{4.6}$$

$$\hat{\Psi}(\mathbf{r}) = \sum_i \hat{a}_i \Phi_i(\mathbf{r}). \tag{4.7}$$

The field operators are useful in describing the atomic ensemble, and can be interpreted as creation and annihilation operators for a particle in the position state $|\mathbf{r}\rangle$. We will evaluate the time evolution of these operators (using the

Heisenberg picture) in order to find the dynamics of the condensate and non-condensate.

4.2.2 Many-body Hamiltonian

In terms of field operators, the many-body Hamiltonian for interacting particles takes the form:

$$\hat{H} = \int_{-\infty}^{\infty} d\mathbf{r}\hat{\Psi}^\dagger(\mathbf{r})\mathcal{H}\hat{\Psi}(\mathbf{r}) + \frac{1}{2}\int_{-\infty}^{\infty}\int_{-\infty}^{\infty} d\mathbf{r}d\mathbf{r}'\hat{\Psi}^\dagger(\mathbf{r}')\hat{\Psi}^\dagger(\mathbf{r})V_{\text{int}}(\mathbf{r},\mathbf{r}')\hat{\Psi}(\mathbf{r})\hat{\Psi}(\mathbf{r}'), \tag{4.8}$$

where $V_{\text{int}}(\mathbf{r},\mathbf{r}')$ is the inter-particle potential, and

$$\mathcal{H} = -\frac{\hbar^2\nabla^2}{2m} + V_{\text{ext}}(\mathbf{r}) \tag{4.9}$$

is the Hamiltonian for a single particle in the external trapping potential $V_{\text{ext}}(\mathbf{r})$.

At the temperatures typically encountered in atomic BEC experiments (nK), for sufficiently dilute Bose gases, atomic interactions are dominated by low energy two-body collisions [9, 36, 37]. In this case, the atom-atom interactions are characterised by one parameter: the s-wave scattering length, a. Moreover, we may generally replace the true interaction potential by an effective contact interaction, subject to an appropriate renormalization procedure [43–45]. Hence, we let $V_{\text{int}}(\mathbf{r},\mathbf{r}') = g_{3\text{D}}\delta(\mathbf{r}-\mathbf{r}')$ where $g_{3\text{D}} = 4\pi\hbar^2 a/m$ and m is the particle mass of the species. Depending on the species, a may be positive or negative, corresponding to an effective repulsive or attractive interaction. By exploiting a Feshbach resonance, it may also be tuned using an external magnetic field [46, 47].

The many-body Hamiltonian [Eq. (4.8)] then takes the form:

$$\hat{H} = \int d\mathbf{r}\hat{\Psi}^\dagger(\mathbf{r})\left[\mathcal{H} + \frac{g_{3\text{D}}}{2}\hat{\Psi}^\dagger(\mathbf{r})\hat{\Psi}(\mathbf{r})\right]\hat{\Psi}(\mathbf{r}). \tag{4.10}$$

4.2.3 Existence of a condensate

In order to define a BEC, it is useful to define a single particle density operator in terms of its matrix elements in the position representation:

$$\langle\mathbf{r}'|\rho|\mathbf{r}\rangle := \langle\hat{\Psi}^\dagger(\mathbf{r})\hat{\Psi}(\mathbf{r}')\rangle = \langle\langle\Psi_{\text{sys}}|\hat{\Psi}^\dagger(\mathbf{r})\hat{\Psi}(\mathbf{r}')|\Psi_{\text{sys}}\rangle\rangle \tag{4.11}$$

when the system is in the state $|\Psi_{\rm sys}\rangle\rangle$.

When we diagonalise the density operator

$$\rho = \sum_i N_i |\Phi_i\rangle\langle\Phi_i|, \tag{4.12}$$

the eigenvectors, $|\Phi_i\rangle$, are single particle eigenstates, with eigenvalues N_i. This is similar in form to a density operator in its usual statistical quantum mechanics setting, except $\mathrm{Tr}\rho = N$ (the total number of particles) rather than 1. Our definition of the presence of a condensate implies that ρ has one eigenvector $|\Phi_{\rm ex}\rangle$ (which we call the exact condensate mode) with eigenvalue $N_{\rm ex}$ much bigger than the others. If the state of the system can be written as $|\Psi_{\rm sys}\rangle\rangle = |n_1, n_2 ...\rangle\rangle$ in this basis, then the density matrix's eigenvectors are $N_i = n_i$, although, in general, the eigenvectors correspond to mean occupation number.

4.2.4 Expansion of quantum field equations

Following the formalism of Castin and Dum [13,38] we are now free to partition the field operator into condensate and non-condensate parts [48]:

$$\hat{\Psi}(\mathbf{r}) = \sum_i \hat{a}_i \Phi_i(\mathbf{r}) = \hat{a}_{\rm ex}\Phi_{\rm ex}(\mathbf{r}) + \delta\hat{\Psi}, \tag{4.13}$$

where $\delta\hat{\Psi} = \sum_{i\neq \rm ex} \hat{a}_i\Phi_i(\mathbf{r})$ is the field operator for the non-condensed particles. We wish to expand our dynamical variables in terms of some small quantity. We have assumed that the non-condensate occupation number:

$$\int_{-\infty}^{\infty} d\mathbf{r}\langle\delta\Psi^\dagger(\mathbf{r})\delta\Psi(\mathbf{r})\rangle = \langle\delta\hat{N}\rangle \tag{4.14}$$

is much smaller than N, so a natural small parameter to consider is $\sqrt{\langle\delta\hat{N}\rangle}/N$. By analysing the dynamics of the operator:

$$\hat{\Lambda}_{\rm ex}(\mathbf{r}) := \frac{1}{\sqrt{\hat{N}}}\hat{a}^\dagger_{\rm ex}\delta\hat{\Psi}(\mathbf{r}) \tag{4.15}$$

we can extract the dynamics of both condensate and non-condensate parts of the system. Here, $\hat{N}$ is the total particle number operator, which we may freely replace by N since the total particle number is conserved. $\hat{\Lambda}_{\rm ex}(\mathbf{r})$ has elements of the order $\sqrt{\langle\delta\hat{N}\rangle}$, (the same order as $\delta\hat{\Psi}(\mathbf{r})$), and is a good choice of operator

to represent the dynamics in a number conserving treatment, since it preserves particle number by annihilating a particle orthogonal to the condensate mode, but creating a particle in the condensate mode, thus its expectation value is zero.

The expansion takes the form

$$\Phi_{\rm ex}(\mathbf{r}) = \Phi(\mathbf{r}) + \frac{1}{\sqrt{\hat{N}}}\Phi^{(1)}(\mathbf{r}) + \frac{1}{\hat{N}}\Phi^{(2)}(\mathbf{r}) + ... \tag{4.16}$$

$$\hat{\Lambda}_{\rm ex}(\mathbf{r}) = \hat{\Lambda}(\mathbf{r}) + \frac{1}{\sqrt{\hat{N}}}\hat{\Lambda}^{(1)}(\mathbf{r}) + \frac{1}{\hat{N}}\hat{\Lambda}^{(2)}(\mathbf{r}) + ... \tag{4.17}$$

We impose that the norm of $\Phi_{\rm ex}(\mathbf{r})$ be equal to one to all orders, and that the expectation value of $\hat{\Lambda}_{\rm ex}(\mathbf{x})$ is zero to all orders.

After some algebra, the equation of motion for $\hat{\Lambda}_{\rm ex}(\mathbf{r})$ may be written [39]:

$$\frac{d}{dt}\hat{\Lambda}_{\rm ex}(\mathbf{r}) = \frac{1}{\sqrt{\hat{N}}}\int_{-\infty}^{\infty} d\mathbf{r}' \sum_{j=0}^{4} \hat{R}_j(\mathbf{r},\mathbf{r}'), \tag{4.18}$$

where $\hat{R}_j(\mathbf{r},\mathbf{r}')$ are of the order $\delta\hat{\Psi}(\mathbf{r})^j$, $\delta\hat{\Psi}^\dagger(\mathbf{r})^j$ and similar products thereof.

Equations of order $\sqrt{N}$ (Gross-Pitaevskii equation)

By examining the terms in $R_0(\mathbf{r},\mathbf{r}')$ and approximating $\hat{a}^\dagger_{\rm ex}\hat{a}_{\rm ex}$ and $\hat{a}^\dagger_{\rm ex}\hat{a}_{\rm ex} - 1$ by N, we obtain:

$$i\hbar\frac{d}{dt}\hat{\Lambda}_{\rm ex} = \sqrt{\hat{N}}\int_{-\infty}^{\infty} d\mathbf{r}'\langle\mathbf{r}|\hat{Q}_{\rm ex}|\mathbf{r}'\rangle\left[-\frac{\hbar^2}{2m}\nabla^2 + V_{\rm ext}(\mathbf{r}') + g_{\rm 3D}\hat{N}|\Phi_{\rm ex}(\mathbf{r}')|^2 - i\hbar\frac{\partial}{\partial t}\right]\Phi_{\rm ex}(\mathbf{r}'), \tag{4.19}$$

where $\hat{Q}_{\rm ex} = \hat{I} - |\Phi_{\rm ex}\rangle\langle\Phi_{\rm ex}|$. Since this is the approximation to order $\sqrt{N}$, we replace $|\Phi_{\rm ex}\rangle$ by $|\Phi\rangle$ and $\hat{Q} = \hat{I} - |\Phi\rangle\langle\Phi|$.

By taking the expectation value of Eq. (4.19) we obtain:

$$\int_{-\infty}^{\infty} d\mathbf{r}'\langle\mathbf{r}|\hat{Q}|\mathbf{r}'\rangle\left[-\frac{\hbar^2}{2m}\nabla^2 + V_{\rm ext}(\mathbf{r}') + g_{\rm 3D}N|\Phi(\mathbf{r}')|^2 - i\hbar\frac{\partial}{\partial t}\right]\Phi(\mathbf{r}') = 0. \tag{4.20}$$

and thus the 3D GPE:

$$\xi(t)\Phi(\mathbf{r}) = \left[-\frac{\hbar^2}{2m}\nabla^2 + V_{\rm ext}(\mathbf{r}) + g_{\rm 3D}N|\Phi(\mathbf{r})|^2\right]\Phi(\mathbf{r}) - i\hbar\frac{\partial}{\partial t}\Phi(\mathbf{r}) \tag{4.21}$$

where $\xi(t)$ is an arbitrary function of time, which doesn't affect the dynamics. Substituting Eq. (4.20) into Eq. (4.19), we find that $\Lambda(\mathbf{r})$ (the lowest order approximation to $\Lambda_{\rm ex}(\mathbf{r})$) is constant in time.

Equations of order $\sqrt{\delta N}$

To order $\sqrt{N}$, the dynamics is described by the GPE, and no non-condensate dynamics are predicted. In order to obtain non-trivial equations governing the number of non-condensed particles, we must therefore consider terms in Eq. (4.18) up to order $\sqrt{\delta N}$.

We obtain no further corrections to the GPE in $\Phi^{(1)}(\mathbf{r})$ but obtain Bogoliubov type equations in $\hat{\Lambda}(\mathbf{r})$ [13,39]:

$$i\hbar\frac{d}{dt}\hat{\Lambda}(\mathbf{r}) = \left[H_1(\mathbf{r}) + gN|\Phi(\mathbf{r})|^2 - \xi(t)\right]\Lambda(\mathbf{r}) + g_{3D}N\int_{-\infty}^{\infty} d\mathbf{r}'\langle\mathbf{r}|\hat{Q}|\mathbf{r}'\rangle|\Phi(\mathbf{r}')|^2\hat{\Lambda}(\mathbf{r}') + g_{3D}N\int_{-\infty}^{\infty} d\mathbf{r}'\langle\mathbf{r}|\hat{Q}|\mathbf{r}'\rangle\Phi^2(\mathbf{r}')\hat{\Lambda}^\dagger(\mathbf{r}'), \tag{4.22}$$

where $\Phi(\mathbf{r})$ is the wave function whose dynamics are governed by the GPE [Eq. (4.24)].

The number of non-condensed particles is given approximately by [13]:

$$\langle\delta\hat{N}\rangle \approx \int_{-\infty}^{\infty} d\mathbf{r}\langle\hat{\Lambda}^\dagger(\mathbf{r})\hat{\Lambda}(\mathbf{r})\rangle \tag{4.23}$$

Note that particle number is not conserved to order $\sqrt{N}$; the number of non-condensate particles is allowed to grow indefinitely, but the number of condensed particles is fixed. For a treatment that does conserve particle number, one must consider equations of order $\sqrt{\delta N/N}$ (see Ref. [39]). In this treatment, the expansion is in functions of the number of condensed particles, rather than the total number of particles. Corrections to the GPE are obtained in $\Phi^{(2)}(\mathbf{r})$, such that the number dynamics are consistent with the Bogoliubov equation in $\hat{\Lambda}^{(1)}(\mathbf{r})$.

Equation (4.22) is equivalent to the standard Bogoliubov-de Gennes equations up to the projection operators $\hat{Q}$. This similarity suggests that for chaotic motion in the GPE (i.e., where the linear instabilities grow rapidly) we expect the number of non-condensate particles also to grow rapidly. We bear this in mind when in chapter 8 we investigate chaotic motion of BEC solitons.

The dynamics of the number of non-condensate particles can be calculated numerically for some arbitrary initial conditions of $\Phi(\mathbf{r})$ and the components of $\Lambda(\mathbf{r})$ by integrating Eq. (4.22) numerically. However, this method requires

a meaningful initial condition for the condensate and non-condensate modes that can be compared to experiment. When the system is assumed to be in the ground state (i.e., the system is in equilibrium and the condensate is in a stationary state) then the initial condition of $\Lambda(\mathbf{r})$ can be found by solving Eq. (4.22) for time-independent Λ. In this thesis we simulate the GPE when the condensate is not in the ground state initially; in particular we consider systems of interacting solitons. In order to keep track of the non-condensate particles in these systems, one must consider the process of formation of such solitons from a ground state. In this thesis we predict behaviour of the non-condensate particles by considering the linear stability of the GPE solutions. We leave the treatment of soliton formation and explicit calculation of non-condensate particle number for future study.

4.3 Cigar-shaped Bose-Einstein condensates

In order to produce 1D objects such as solitons, it is clear that the dynamical system must be 1D (or, at least, quasi 1D). Quasi 1D (cigar-shaped) BECs are produced when a tight radial trapping potential is applied to the condensate, such that the dynamics of the BEC in the radial direction are suppressed (although atom-atom scattering is still 3D). The dynamics of such a system may be modelled theoretically by the 3D Gross-Pitaevskii equation with a suitable potential. However, exact solutions of this equation are not readily obtained, so intensive numerical simulations are required. Instead of integrating the 3D GPE, we may gain more insight by reducing the 3D GPE to an equation with one spatial dimension.

4.3.1 One-dimensional Gross-Pitaevskii equation

The simplest, but least sophisticated, reduction to one dimension involves averaging over radial dimensions by assuming an approximate separation of the wavefunction into radial and axial factors before integrating over the radial dimensions.

We begin with the 3D GPE:

$$i\hbar\frac{\partial}{\partial t}\Phi(\mathbf{r}) = \left[-\frac{\hbar^2}{2m}\nabla^2 + V_{\text{ext}}(\mathbf{r}) + g_{3\text{D}}N|\Phi(\mathbf{r})|^2\right]\Phi(\mathbf{r}) \tag{4.24}$$

where

$$V_{\text{ext}}(\mathbf{r}) = \frac{m}{2}\left[\omega_x^2x^2 + \omega_r^2(y^2+z^2)\right], \tag{4.25}$$

and $\Phi(\mathbf{r})$ has unit norm.

We assume the wavefunction may be factorised as $\Phi(\mathbf{r}) = \psi(x)\chi(y)\chi(z)$. The radial solution $\chi(y)\chi(z)$ may be assumed to be Gaussian if the radial potential is sufficiently tight that the harmonic potential energy dominates over the interaction energy in the radial directions [49, 50], i.e.,

$$\chi(\zeta) := \left(\frac{1}{\sigma^2\pi}\right)^{1/4}\exp\left(\frac{-\zeta^2}{2\sigma^2}\right), \tag{4.26}$$

with $\sigma^2 = \hbar/m\omega_r$. We project Eq. (4.24) using the radial bra integral $\int_{-\infty}^{\infty} dydz\chi^*(y)\chi^*(z)$. This essentially averages the wavefunction over the radial degrees of freedom. Eq. (4.24) then becomes:

$$i\hbar\frac{\partial}{\partial t}\psi(x) = \left[-\frac{\hbar^2}{2m}\frac{\partial^2}{\partial x^2} + \frac{m\omega_x^2x^2}{2} + g_{1\text{D}}N|\psi(x)|^2 + \hbar\omega_r\right]\psi(x), \tag{4.27}$$

where

$$g_{1\text{D}} = g_{3\text{D}}\int_{-\infty}^{\infty} dydz|\chi(y)\chi(z)|^4 = 2\hbar\omega_r a. \tag{4.28}$$

The constant term, $\hbar\omega_r$, emerges from integrating out the radial kinetic energy and external radial potential part of the Hamiltonian. Reassigning the zero of energy allows us to drop this constant term from the Hamiltonian [Eq. (4.27)].

4.3.2 Reductions with 3D effects

The 1D GPE with no external potential coincides with the NLS (see section 2.3.4), which is convenient due to its integrability and the existence of well known analytic solutions. However, more sophisticated reductions to 1D of the 3D GPE exist, which do not ignore the time dependence of the radial modes and the coupling between the axial and radial motion.

Khaykovich and Malomed [51] assumed that the wavefunction may be factorised into a slowly varying factor dependent on the axial coordinate only and a quickly

varying factor dependent on the radial and axial coordinates. They then substituted this ansatz into the 3D GPE [Eq. (4.24)] with no axial potential. They neglected the time and spatial derivatives of the radial equation and expanded the transverse chemical potential in powers of the density to obtain the following 1D nonlinear Schrödinger equation with a quintic term.

$$i\hbar\frac{\partial\psi}{\partial t} = -\frac{\hbar^2}{2m}\frac{\partial^2\psi}{\partial x^2} + g_1|\psi|^2\psi - g_2|\psi|^4\psi, \tag{4.29}$$

where $g_1 := 2N\hbar\omega_r a$ and $g_2 := 24\ln\left(\frac{4}{3}\right)N^2\hbar\omega_r a^2$. Note that we are interested in the case where $g_1 < 0$, so both nonlinearities are self-focussing. The derivation of this equation admits the inclusion of an axial potential, which we will set to be harmonic:

$$i\hbar\frac{\partial\psi}{\partial t} = -\frac{\hbar^2}{2m}\frac{\partial^2\psi}{\partial x^2} + \frac{m\omega_x^2 x^2}{2}\psi + g_1|\psi|^2\psi - g_2|\psi|^4\psi. \tag{4.30}$$

Salasnich *et al.* [49] performed a reduction by assuming that the wavefunction may be factorised into a slowly varying factor in the axial coordinate and a quickly varying factor in the radial direction with additional axial dependence. They then performed a variational calculation to obtain the following 1D non-polynomial nonlinear Schrödinger equation:

$$\begin{aligned} i\hbar\frac{\partial\psi}{\partial t} = &-\frac{\hbar^2}{2m}\frac{\partial^2\psi}{\partial x^2} + \frac{m\omega_x^2 x^2}{2}\psi - \frac{2\hbar^2 Na}{ma_r}\frac{|\psi|^2}{\sqrt{1+2aN|\psi|^2}}\psi \\ &+ \frac{\hbar\omega_r}{2}\left(\frac{1}{\sqrt{1+2aN|\psi|^2}} + \sqrt{1+2aN|\psi|^2}\right)\psi, \end{aligned} \tag{4.31}$$

where $a_r := (\hbar/m\omega_r)$. This equation reduces to the 1D GPE [Eq. (4.27)] when $aN|\psi|^2 \ll 1$. Expanding this equation up to the quintic term gives Eq. (4.30), but with $g_2 = \hbar\omega_r a^2 N^2/2$.

Kamchatnov and Shchesnovich [50] performed a reduction which does not assume that the axial motion is slow. This approach gives three coupled equations in functions of the axial displacement: one in the axial wavefunction, one in the mean condensate radius, and one in the radial velocity potential. These equations reduces to Eq. (4.31) and Eq. (4.27) in the limiting case when the radially-averaged density is small everywhere in the axial direction [50].

4.3.3 Scalings

We may make some scalings to produce dimensionless equations. It is possible to scale out g_{1D}, in what we call soliton units, or to scale out ω_x, in what we call harmonic oscillator units. Throughout most of this thesis we will use soliton units, but will make use of harmonic oscillator units when convenient.

Soliton units

Introducing the dimensionless variables

$$\tilde{x} := \frac{m|g_{1D}|N}{\hbar^2}x \tag{4.32}$$

and

$$\tilde{t} := \frac{m|g_{1D}|^2N^2}{\hbar^3}t, \tag{4.33}$$

Eq. (4.27) then becomes:

$$\frac{\partial}{\partial\tilde{t}}\tilde{\psi}(\tilde{x}) = \frac{1}{2}\frac{\partial^2}{\partial\tilde{x}^2}\tilde{\psi}(\tilde{x}) + \frac{\tilde{\omega}^2}{2}\tilde{x}^2\tilde{\psi}(\tilde{x}) - |\tilde{\psi}(\tilde{x})|^2\tilde{\psi}(\tilde{x}). \tag{4.34}$$

We have assumed the s-wave scattering length a in g_{1D} to be negative, and set

$$\tilde{\omega} := \frac{\omega_x\hbar^3}{m|g_{1D}|^2N^2} \tag{4.35}$$

and

$$\tilde{\psi}(\tilde{x}) := \frac{\hbar}{\sqrt{mgN}}\psi(x), \tag{4.36}$$

such that $\tilde{\psi}(\tilde{x})$ is normalised to one with respect to $\tilde{x}$. Throughout the rest of this thesis the tildes have been dropped for notational convenience.

Equation (4.30) may be scaled c.f. the 1D GPE to:

$$i\frac{\partial\psi}{\partial t} = -\frac{1}{2}\frac{\partial^2\psi}{\partial x^2} + \frac{\tilde{\omega}^2}{2}x^2\psi + \tilde{g}_1|\psi|^2\psi - \tilde{g}_2|\psi|^4\psi, \tag{4.37}$$

where $\tilde{g}_1 = -1$ and $\tilde{g}_2 = 24\ln(4/3)m\omega_r a^2/\hbar$, and the wavefunction has norm one. Interestingly, g_2 may not be scaled out analogously to g_1 without rescaling the kinetic energy or changing the normalisation condition. Consequently, the value of g_2 has a qualitative effect on the form of the solution which cannot be determined by scaling considerations. Equation (4.31) may be scaled similarly, although we will not be using this equation further in this thesis.

Harmonic units

Introducing the dimensionless variables

$$\tilde{x} := \sqrt{\frac{m\omega_x}{\hbar}}x \tag{4.38}$$

and

$$\tilde{t} := \omega_x t, \tag{4.39}$$

Eq. (4.27) then becomes:

$$i\frac{\partial}{\partial\tilde{t}}\tilde{\psi}(\tilde{x}) = -\frac{1}{2}\frac{\partial^2}{\partial\tilde{x}^2}\tilde{\psi}(\tilde{x}) + \frac{1}{2}\tilde{x}^2\tilde{\psi}(\tilde{x}) - k|\tilde{\psi}(\tilde{x})|^2\tilde{\psi}(\tilde{x}). \tag{4.40}$$

We have set

$$k := -2aN\frac{\omega_r}{\omega_x}\sqrt{\frac{m\omega_x}{\hbar}} \tag{4.41}$$

and

$$\tilde{\psi}(\tilde{x}) := \left(\frac{\hbar}{m\omega_x}\right)^{\frac{1}{4}}\psi(x), \tag{4.42}$$

such that $\tilde{\psi}(\tilde{x})$ is normalised to one with respect to $\tilde{x}$.

Throughout the rest of this thesis the tildes have been dropped for notational convenience. Unlike the soliton units, the harmonic oscilator units are not defined in a homogeneous system (where $\omega_x = 0$), but have the advantage that they remain defined as a goes through zero. Again, Eqs. (4.30) and (4.31) may be scaled similarly.

Chapter 4 Summary

- Bose particles may be easily described by the second quantisation formalism.
- A Bose-Einstein condensate forms if a system of identical bose particles is cooled.
- The field operator of a BEC may be split into condensate and non-condensate parts.
- The field equations may be expanded in terms of a small parameter in a number-conserving formalism.
- The Gross-Pitaevskii equation is the lowest order equation of motion.
- Higher order considerations reveal modified Bogoliubov-de Gennes equations to describe the noncondensate modes, and corrections to the GPE.
- The 3D GPE may reduce to a 1D GPE when the radial potential is tight.

Part II

Solitons in harmonically trapped Bose-Einstein condensates

Chapter 5

Introduction

In chapter 4 we showed that dilute atomic Bose-Einstein condensates (BECs) in a cigar-shaped trapping potential are governed (rather approximately) by the 1D Gross-Pitaevskii equation (1D GPE) [Eq. (4.34)]. We saw in chapter 3 that Eq. (4.34) has N-soliton solutions in the homogeneous case, i.e., when the axial harmonic trap angular frequency, ω, is zero. In this section we discuss the effects of introducing a non-zero value of ω on the solutions to Eq. (4.34).

5.1 Motivating experiments

The existence of soliton solutions of the homogeneous 1D GPE has motivated the search for solitons in BEC in experiments that are close to this regime, i.e., with attractively interacting atoms trapped in 1D geometries.

The first experiment in such a setup, was performed by Khaykovich *et al.* in a condensate of lithium-7 [52]. A Feshbach resonance was exploited in order to tune the atomic interactions from repulsive to attractive with a scattering length of approximately 0.21 nm. The condensate was released into a 1D waveguide, which was effectively a tight radial trap of frequency 710 Hz with a weak inverted parabolic axial potential: $m\omega^2 x^2/2$ with (imaginary) angular frequency $\omega = 2\pi i \times 78$ Hz. A single solitary-wave of around 6000 atoms was observed, which propagated 1.1mm over the course of the experiment.

The other two BEC bright soliton experiments performed to date were by Strecker *et al.* [17, 54], and by Cornish *et al.* [53]. The experiment by Strecker

et al. was on a condensate of lithium-7 in a tight radial trap of frequency of 800 Hz with weak radial harmonic confinement with frequency of approximately 4 Hz. By ramping down the scattering length to around -3 Bohr radii, a train of solitons was formed, which performed oscillations at the axial trap frequency. Each soliton contained about 5000 atoms.

The third observation of solitons by Cornish *et al.* was on a condensate of rubidium-85 [53]. The consensate was trapped in a radial trap with a frequency of 17.3 Hz and an axial frequency of 6.8 Hz. Clearly, this geometry can only be loosely described as one dimensional. By suddenly switching the scattering length from positive to negative, collapse was induced in the condensate. The remnants of the condensate left after the collapse formed solitons, the number and size of which depended on the final scattering length and the number of atoms in the condensate. The solitons seemed to repeatedly collide in the centre of the trap.

5.2 Previous theoretical work

All of the experiments described above used an axial trapping potential. The addition of a (non-inverted) axial harmonic potential, as used in the experiments by Strecker *et al.* [17,54] and Cornish *et al.* [53], acts to break the integrability of the 1D GPE, meaning that we no longer have exact soliton solutions. Note, however, if the parabolic potential is inverted, as used by Khaykovich *et al.* [52], the 1D equation again becomes Lax integrable, and an exact N-soliton solution is possible [55]. In the experiment by Strecker *et al.*, soliton-like behaviour (where the solitary-waves collide and reform up to shifts in phase and position) was not observed, but rather, trains of solitary-waves were observed which never collide.

The dynamics of solitary-wave trains both in BEC and nonlinear optics have been the topic of extensive modeling using a variational method [56], numerical simulations [57–62], a Toda lattice approach, [63], a particle model [31] (quite distinct to that presented in this thesis) formulated by consideration of the interference of two overlapping solitons, analysis using the inverse-scattering transform [64] and by using a perturbative approach [65–67]. These treatments

model regimes where the solitary-waves are never well separated, where it has been found that the solitary-waves do not collide with each other and re-form, but interact with each other by attractive and repulsive forces, depending on their relative phase.

As opposed to solitary-wave trains, we investigate whether soliton-like behaviour, i.e., colliding and reforming of distinct, localized wave packets up to shifts in phase and position, is possible in the 1D GPE with a harmonic potential. Much of this work can be found in our publications [1, 2]. Soliton-like behaviour has been seen in similar nonlinear optical settings [32–34, 68], which motivates our work further. This may model the system in the experiment by Cornish *et al.* [53].

5.3 Motivation and overview

Solitary waves in the 1D GPE with harmonic potential (representing the axial trapping potential) cannot be true solitons in the sense defined by the inverse scattering transform, since they do not become infinitely separated as time tends to infinity. However, they still may retain their soliton character in the sense of colliding and re-forming up to phase-shifts. In chapters 7 and 8, we investigate the extent to which the soliton nature of the solution is preserved by extending the particle model developed in chapter 3 by the introduction of a harmonic potential, and comparing the results with simulations of the GPE dynamics.

5.3.1 Non-integrability

We find that the particle model gives good agreement with the GPE simulations in a large number of parameter regimes - the solitons collide and re-emerge up to position shifts predicted by the particle model. This is interesting because the 1D GPE with harmonic potential is thought not to be integrable. In fact, in chapter 8 we find regimes where the particle dynamics are chaotic. This suggests that the GPE solution is also chaotic, which supports the assertion that the 1D GPE with harmonic trap is likely to be non-integrable.

5.3.2 Chaotic dynamics

As suggested in chapter 1, the chaotic dynamics to be discussed in chapter 8 are interesting for a number of other reasons: they provide an easy-to-characterise example of chaos in a wave mechanical system; they provide an example of chaotic behaviour arising from a quantum mechanical system; and they provide an example where the field equations of motion have instabilities, which are predicted to imply depletion of the condensate.

Chaos in wave mechanics

As described in chapter 1, solitons provide a good opportunity for studying chaos in a wave mechanical system. Chaos in wave mechanical systems is often hard to visualise due to the infinite-dimensional nature of the phase space. However, since we can describe the positions and momenta of the solitons by a particle model [Eq. (3.13)], it is clear that chaotic dynamics in this particle model imply chaotic dynamics of this $2N$ subspace of the wave mechanical phase-space (where N is the number of solitons). This is helpful, not only for defining and visualising chaos, but also for predicting chaos, since previous work [12, 23] provides a useful guide to when the dynamics of a system of particles will be chaotic; for example, the three body problem is often chaotic [12].

Quantum chaos

In chapter 1 we explained that the manner in which chaos arises in macroscopic (classical systems) from quantum systems is a topic of interest. We also noted that in quantum mechanics, the Heisenberg equations of motion can be nonlinear, and thus exhibit chaotic behaviour. In chapter 4 we showed that the GPE is a macroscopic description arising from the Heisenberg equations of motion for the field operator. The results in chapter 8 give an example of how chaotic dynamics can arise from Heisenberg equations, and hint at how classical chaos can emerge from quantum constituents.

Instabilities and depletion

In chapter 4 we showed that the non-condensate particle number dynamics can be predicted by modified Bogoliubov-de Gennes equations. The similarity with the Bogoliubov-de-Gennes equations suggest that linear instabilities in the GPE may be an indication of depletion of the condensate [13, 14]. Chaotic regimes in chapter 8 are linearly unstable, which we confirm by analysis of divergence of nearby trajectories.

Chapter 5 Summary

- Bright solitons are solution to the homogeneous GPE with attractive non-linearity.
- Previous experimental and theoretical work on solitary-waves in BEC motivates studies of solitary-waves in a harmonic trap.
- We wish to probe the soliton character of the solitary waves in a harmonic trap.
- We will also investigate quantum chaos and chaos in wave mechanical systems.
- Chaotic soliton trajectories may indicate linear instabilities in the field equations.

Chapter 6

Solitary waves

6.1 Overview

In this chapter we consider the generalisation of the single solitary wave solution [Eq. (3.2) with $j = 1$] to the case where the 1D Gross-Pitaevskii equation (GPE) has a harmonic axial trapping potential. We first give an overview of previous work on stationary states in the nonlinear Schrödinger equation with various potentials, and then numerically determine the first stationary state of the 1D GPE with a harmonic axial potential. We then show that for any stationary solution, there exist corresponding solutions with the same density profile, which oscillate with the trap frequency but remain otherwise unchanged. Hence, a single bright solitary wave in a harmonic trap experiences an overall simple harmonic motion without any manifestation of internal dynamics in the solitary wave's density profile. The density profile and phase behaviour of a single solitary wave can therefore be found simply by considering the form of a stationary solitary wave and then inferring the behaviour of the oscillating version. We present this solution and explore the limits of tight and loose harmonic trapping. We then present a general method to find the motion of a single solitary-wave in an arbitrary trapping potential.

6.2 Stationary solutions

Stationary solutions of the nonlinear Schrödinger equation with attractive nonlinearity have been found for a number of interesting cases. With a box potential, the equation has stationary solutions which are elliptical functions [69], as it does with a double square well [70]. When the potential is harmonic, no such neat analytical solutions have been found, and solutions must be found by a mixture of analytical considerations and numerical methods [71–74].

6.2.1 Imaginary time propagation

We find a stationary solitary-wave solution to the harmonic 1D GPE numerically by the following method: The stationary solitary wave will be a solution to the eigenvalue problem:

$$-\frac{1}{2}\frac{\partial^2}{\partial x^2}\psi(x) + \frac{\omega^2 x^2}{2}\psi(x) - |\psi(x)|^2\psi(x) = \mu\psi(x), \tag{6.1}$$

and will have the form: $\psi(x) = u(x)\exp\{-i\,[\mu t + S(0)]\}$, where $u(x)$ is a real valued function and the real-valued number $S(0)$ is an initial phase. We expect the single stationary solitary wave solution to be the metastable "ground" state of the system [75–77], which may be determined numerically, for example by propagating Eq. (4.34) in imaginary time for an arbitrary initial condition different from the trivial zero solution [78, 79].

When the trapping potential is weak, the solution tends to a stationary soliton [see Eq. (3.2)]. The other limit is when the trap is tight, and the solution tends to a Gaussian, or coherent state. Scaling considerations imply that the limit where the harmonic trap frequency tends to infinity is equivalent to the limit where the nonlinear term in the 1D GPE tends to zero.

The numerically determined density $u(x)^2$ for a parameter regime consistent with the ^{7}Li experiments of Strecker *et al.* [17] is shown in Fig. 6.1, and is compared to a bright solitary wave solution of the homogeneous 1D GPE, and to the ground state of the 1D linear Schrödinger equation with harmonic potential. As expected, the solution of the 1D GPE with a harmonic potential is slightly compressed spatially compared to the bright solitary wave solution of the homogeneous GPE. These two solutions, however, are quite similar (and

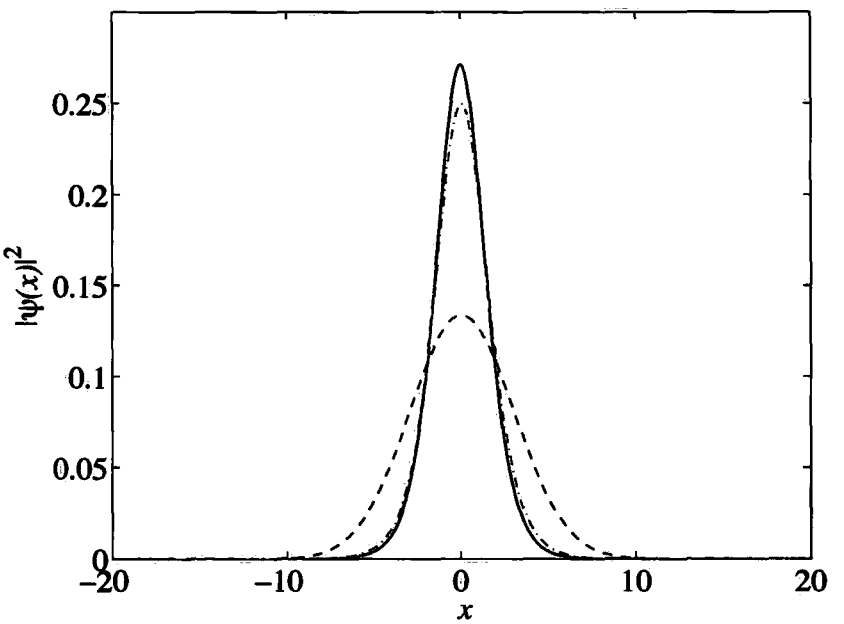

Figure 6.1: Ground state solution for harmonically trapped solitary wave of 5000 particles (solid line). Corresponding solitary wave solution to the homogeneous equation (dot-dashed line), which is used as an ansatz in the particle model. The ground state of the linear Schrödinger equation (dashed line) is given for comparison. The parameters of the system are taken to be similar to those of a recent experiment [17] the axial trapping frequency is $10/2\pi$ Hz, the radial trap frequency is $800/2\pi$ Hz, atomic mass and scattering length of ^{7}Li. Position, x, is measured in units of $\hbar^2/m|g_{1D}|N$. A unit of x is hence equal to 7.19×10^{-6} m.

can be made more similar as ω is progressively reduced), and are quite distinct from the Gaussian solution produced by the linear Schrödinger equation. Therefore it seems that we are interested in the limit of soliton-like behaviour rather than linear behaviour. Figure 6.2 shows how the eigenvalue interpolates between the two limits corresponding to weak and tight harmonic traps compared with the nonlinearity. The red dot-dashed gives the chemical potential for a soliton ansatz (the black solid line neglects the harmonic term in the chemical potential, showing that in the limit of large k, its contribution is negligible). The stationary eigenvalue of parameters of experiments of Strecker *et al.* [17] (given by the diamond in Fig. 6.2) is $4.21\hbar\omega_x$, consistent with the use of the soliton limit. We will exploit this soliton form of the wavefunction later in the thesis. The green dashed line gives the Gaussian ansatz, which is exact when the parameter $k = 0$. Clearly this is far from the regime that we consider. For competeness we include negative values of k in Fig. 6.2, and the Thomas Fermi expression for chemical potential (blue dotted line).

6.3 Harmonically oscillating solutions

6.3.1 Exact result

Here we show that an arbitrary solution to the 1D GPE with harmonic potential

$$\psi(x,t) = u(x,t)\exp\left[i\phi(x,t)\right] \tag{6.2}$$

can be converted to an oscillating solution with a modified phase:

$$\psi(x,t) = u(x-\langle x\rangle,t)\exp\left\{i\left[\phi(x,t)+\langle\dot{x}\rangle x - S(t)\right]\right\}. \tag{6.3}$$

We note in passing that this result holds for any nonlinear Schrödinger equation with the nonlinearity given by some function of $|\psi(x)|^2$ only.

If $\psi(x,t) = u(x,t)\exp\left[i\phi(x,t)\right]$ is a particular solution to the 1D GPE, where $u(x,t)$ and $\phi(x,t)$ are real-valued functions, the following coupled equations describe their behaviour:

$$\frac{\partial u}{\partial t} = -\frac{1}{2}\left[2\frac{\partial u}{\partial x}\frac{\partial \phi}{\partial x} + \frac{\partial^2 \phi}{\partial x^2}u\right], \tag{6.4}$$

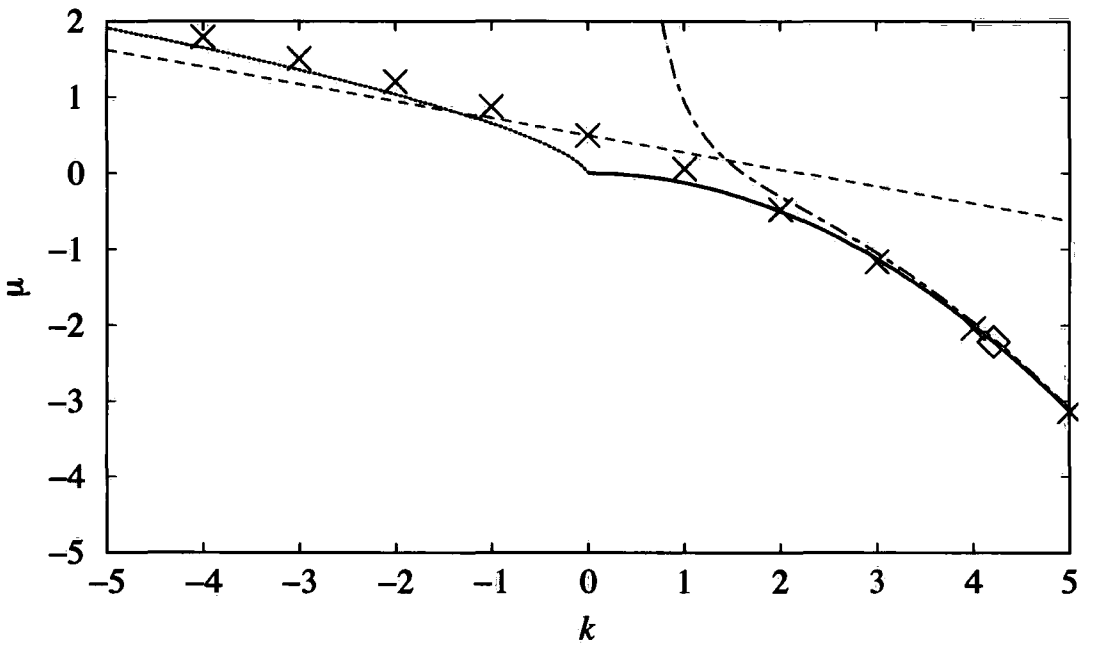

Figure 6.2: Chemical potential in units of $\hbar\omega_x$. The parameter $k = -2aN\frac{\omega_r}{\omega_x}\sqrt{\frac{m\omega_x}{\hbar}}$. The crosses give the chemical potential calculated from numerical solutions of Eq. (6.1), the black full line gives the chemical potential for a soliton in the homogeneous GPE (the harmonic term is neglected), and the red dot-dashed line gives the chemical potential of a soliton ansatz in the GPE with the harmonic potential term included, the green line gives the chemical potential of a Gaussian ansatz in the GPE, the blue dotted line gives the Thomas-Fermi chemical potential (where the kinetic energy is neglected). The diamond gives the chemical potential from numerical solution of Eq. (6.1) for parameters close to those of a recent experiment [17].

$$-\frac{\partial\phi}{\partial t} = \frac{1}{2}\left(\frac{\partial\phi}{\partial x}\right)^2 + \frac{1}{u}H(u,x)u, \tag{6.5}$$

where

$$H(u,x)u = -\frac{1}{2}u_{xx} - u^2u + V(x)u. \tag{6.6}$$

Defining the functions $\bar{u}(x,t) := u(x + \langle x\rangle, t)$ and $\theta(x,t) := \phi(x + \langle x\rangle)$, where $\langle x\rangle = x_0\cos(\omega t) + (p_0/\omega)\sin(\omega t)$, for initial conditions x_0 and p_0, and defining the coordinate $\xi = x - \langle x\rangle$ the following relations follow trivially:

$$\bar{u}(\xi,t) = u(x,t), \tag{6.7}$$

$$\theta(\xi,t) = \phi(x,t), \tag{6.8}$$

$$\frac{\partial u(x,t)}{\partial x} = \frac{\partial\bar{u}(\xi,t)}{\partial\xi}, \tag{6.9}$$

$$\frac{\partial u(x,t)}{\partial t} = -\dot{\langle x\rangle}\frac{\partial\bar{u}(\xi,t)}{\partial\xi} + \frac{\partial\bar{u}(\xi,t)}{\partial t}. \tag{6.10}$$

Also, the relationship between the partial derivatives of $\theta(\xi,t)$ and $\phi(x,t)$ is the same as that between $\bar{u}(\xi,t)$ and $u(x,t)$. From now on it is assumed that $\bar{u}$, θ and their derivatives are functions of ξ and t.

Eqs. (6.4) and (6.5) become:

$$\frac{\partial\bar{u}}{\partial t} = -\frac{1}{2}\left[2\frac{\partial\bar{u}}{\partial t}\left(\frac{\partial\theta}{\partial\xi} - \dot{\langle x\rangle}\right) + \frac{\partial^2\theta}{\partial\xi^2}\bar{u}\right] \tag{6.11}$$

and

$$\frac{\partial\theta}{\partial\xi}\dot{\langle x\rangle} - \frac{\partial\theta}{\partial t} = \frac{1}{2}\left(\frac{\partial\theta}{\partial\xi}\right)^2 + \frac{1}{\bar{u}}H(\xi)\bar{u} + \frac{\omega^2}{2}\langle x\rangle^2 + \omega^2\xi\langle x\rangle. \tag{6.12}$$

By choosing $\bar{\phi}(\xi,t)$ such that

$$\frac{\partial\bar{\phi}}{\partial\xi} = \frac{\partial\theta}{\partial\xi} - \dot{\langle x\rangle}, \tag{6.13}$$

and

$$\frac{\partial\bar{\phi}}{\partial t} = \frac{\partial\theta}{\partial t} - \xi\ddot{\langle x\rangle} + \frac{\partial S(t)}{\partial t}, \tag{6.14}$$

where

$$S(t) = \left(p_0^2 - \frac{x_0^2\omega^2}{2}\right)\frac{\sin(2\omega t)}{2\omega} + \frac{x_0p_0}{2}\cos(2\omega t) - \frac{x_0p_0}{2} + S(0), \tag{6.15}$$

we can relabel ξ as x, and find that $\bar{\phi}(x,t)$ and $\bar{u}(x,t)$ are solutions of Eqs. (6.4) and (6.5). Hence, $\bar{u}(x,t)$ has the profile of $u(x,t)$, but undergoes additional global harmonic oscillations at the trap frequency, and the result is proved.

Note that the solution Eq. (6.2) may be any solution to the GPE. We are interested in the case where it is the stationary single soliton solution. In this case, $u(x)$ and μ are those determined numerically in Sec. 6.2.1; and Eq. (6.3) will give the general single soliton solution.

We showed in section 6.2.1 that we are interested in the limit where the stationary solitary-wave density is close to that of the single soliton solution to the NLS [see Eq. (3.2)]. If we use the absolute value of this solution as an ansatz in Eqs. (6.1) and (6.2), we arrive at an approximation to the oscillating solution:

$$\psi(x,t) = 2\eta \mathrm{sech}\left[2\eta(x - \langle x\rangle)\right] \exp\left\{i\left[2\eta^2 t + \langle \dot{x}\rangle x - S(t)\right]\right\}, \tag{6.16}$$

where $S(t)$ is given by Eq. (6.15). Note that Eq. (6.16) reduces to the single soliton solution [Eq. (3.2)] of the NLS as $\omega \to 0$, as expected. In the opposite limit when the trap is tight, the oscillating solutions are oscillating Gaussians, commonly known as coherent states [80].

6.3.2 Approximate method for general potential

A more general method of deriving the motion of a single solitary wave was formulated by Scharf and Bishop [34]. Here a solution to the homogeneous GPE is used as an ansatz for the GPE with any external potential. This method has the advantage that it can be used with other than harmonic potentials. Here we show that for a harmonic potential it confirms the expected result of simple harmonic motion.

In chapter 2, we showed that the homogeneous 1D GPE has an infinite number of conserved quantities [Eq. (2.46) to (2.47)]. The first three are conservation of norm, momentum and energy, associated with the symmetries of the system with respect to phase, displacement and time respectively. In the 1D GPE with a harmonic potential, the symmetry of the system with respect to displacement is broken, but not so the symmetries with respect to phase and time; hence, the norm $\mathcal{N}$, and energy $\mathcal{E}$ are still conserved. The single solitary wave solution of the homogeneous case:

$$\psi(x) = 2\eta \mathrm{sech}\left[2\eta(x - q)\right] e^{i\dot{q}(x-q)} e^{i(2\eta^2 + \dot{q}^2/2)t} e^{i\alpha_{0j}}. \tag{6.17}$$

is used as an ansatz for the harmonic case. Evaluating the norm and energy

functionals with this ansatz yields:

$$\mathcal{N} = \int_{-\infty}^{\infty} dx |\psi(x)|^2 = 4\eta, \tag{6.18}$$

$$\begin{aligned}\mathcal{E} = &\int_{-\infty}^{\infty} dx \left[\frac{1}{2}\left|\frac{\partial\psi(x)}{\partial x}\right|^2 + |\psi(x)|^2\frac{\omega^2 x^2}{2} - \frac{1}{2}|\psi(x)|^4\right] \\ =&2\eta\dot{q}^2 - \frac{16}{5}\eta^3 + \frac{\omega^2}{2}\left(4\eta q^2 + \frac{\pi^2}{12\eta}\right).\end{aligned} \tag{6.19}$$

The conservation of the norm $\mathcal{N}$, leads to η =constant, and the conservation of the energy $\mathcal{E}$, leads to an equation of motion for the peak of the solitary wave, q:

$$\ddot{q} = -\omega^2 q. \tag{6.20}$$

Chapter 6 Summary

- Stationary states of the harmonic 1D Gross-Pitaevskii equation may be analysed numerically.
- Oscillating solitary-waves may be decomposed into absolute-value and phase.
- The absolute-value of an oscillating single solitary wave in a harmonic trap is identical to that of a stationary state, but with additional overall oscillations at the trap frequency.
- The phase of a single solitary wave can be described exactly given its "stationary eigenvalue", which must be determined numerically.
- We are interested in the regime where the absolute-value and "stationary eigenvalue" are close to those of a soliton in the nonlinear Schrödinger equation.
- The motion of a soliton in a general potential may be determined by consideration of constants of motion.

Chapter 7

Are harmonically trapped solitary matter waves solitons?

7.1 Overview

As discussed in chapter 5, the presence of an (axial) harmonic trap breaks the integrability of the 1D GPE. Consequently, there can be no soliton solutions in the strict sense (see chapter 2). It is possible, however, that the solutions can behave like solitons in a practical sense, i.e., they emerge from collisions with each other in the manner of classical particles.

As the harmonic trap strength is increased such that it dominates over the nonlinear term, the oscillating solitary waves become coherent states which pass through each other unscathed, due to the (approximate) linearity of the equations of motion in this limit. Similarly, in the limit that the wave-packets collide so fast that the kinetic energy term dominates and the equations of motion are again approximately linear, the solitary waves will also pass through each other unscathed. In both these quasi-linear limits we expect no interaction between the solitary waves. We expect there to be some analogue of these regimes in the (homogeneous) nonlinear Schrödinger equation (NLS). For colliding NLS solitons in the limits of fast collisions and of vanishing nonlinearity, the position shift [Eq. (3.3)] tend to zero, consistent with our expectations. Hence, in the limits of fast collisions and of tight harmonic trapping (small nonlinearity), the solitary waves interact in the same way as in the NLS (i.e., with vanishing

position shift).

Note that when modelling BEC dynamics, an upper limit to the colliding solitary waves' relative velocity is imposed for physical reasons, because the contact-interaction potential between atoms, used to derive the GPE, assumes low energy inter-atomic collisions, and may not be applicable to condensates with high relative approach speeds [81, 82].

In the limits where the solitary waves collide with slower relative speeds in weaker traps such that the equations of motion are no longer approximately linear, we expect the wave-packets to interact nonlinearly in a soliton-like manner. In this chapter we develop the particle model introduced in chapter 3 to determine the extent to which solitary waves in the 1D GPE with a harmonic potential retain their soliton character. We explore the case of two harmonically trapped solitary waves, and present results comparing the trajectories in the particle model with simulations of the wave dynamics in the GPE. These results allow us to determine the range of initial conditions for which the particle model is a good description of the system. As we will see, the soliton character of the solitary waves is very strong; so for reasons of simplicity we will henceforth refer to the solitary waves as solitons. Recall from chapter 3 that for the particle model to be applicable, the difference in size of the solitons must be small compared with the (dimensionless) relative approach speed: $2|\eta_1 - \eta_2| \ll |v_1 - v_2|$. Fortunately, recent experiments [17, 53] show that solitons are generated with similar sizes, such that their velocities may easily fall within our model's range of validity.

7.2 Particle model

Recall from chapter 3 that solitons colliding in the homogeneous GPE may be modelled as classical particles interacting with a force that produces the position shifts of the emerging solitons. In chapter 6, we showed that harmonically-trapped single solitons in physical regimes are close to those in the homogeneous GPE. Hence, we may characterise the harmonically trapped solitons by the parameters q_j and η_j from the homogeneous solution [Eq. (3.2)]. We also showed in chapter 6 that single solitons in a harmonic trap oscillate harmonically. The

following Hamiltonian:

$$H = \sum_{j=1}^{N_s} \left(\frac{p_j^2}{2\eta_j} + \frac{\eta_j \omega^2 q_j^2}{2} \right) \tag{7.1}$$

reproduces the harmonic motion of the solitons, keeping the interpretation of η_j as effective masses (see Sec. 6.3). We assume that the soliton-soliton interactions are not affected by the introduction of the (relatively loose) harmonic trap and construct the full Hamiltonian by adding in the contributions from the interaction potentials:

$$\begin{aligned} H = & \sum_{j=1}^{N_s} \left(\frac{p_j^2}{2\eta_j} + \frac{\eta_j \omega^2 q_j^2}{2} \right) \\ & - \sum_{1 \le j < k \le N_s} 2\eta_j \eta_k (\eta_j + \eta_k) \operatorname{sech}^2 \left[\frac{2\eta_j \eta_k}{\eta_j + \eta_k} (q_j - q_k) \right], \end{aligned} \tag{7.2}$$

where N_s is the number of solitons. This approach is expected to be valid for regimes when the timescale of the soliton-soliton collisions is much less than the period of the harmonic trap, such that the effects of the harmonic trap are negligible during the collisions. The limits of this approach are further explored in Sec. 7.3.2.

In the case of two solitons ($N_s = 2$), it is useful to define the following independent coordinates: the centre-of-mass position $Q := (\eta_1 q_1 + \eta_2 q_2)/(\eta_1 + \eta_2)$ and the relative position $q := q_1 - q_2$. The Hamiltonian [Eq. (7.2)] then takes the form:

$$\begin{aligned} H = & \frac{P^2}{2(\eta_1 + \eta_2)} + \frac{\omega^2}{2}(\eta_1 + \eta_2) Q^2 \\ & + \frac{\eta_1 + \eta_2}{2\eta_1 \eta_2} p^2 + \frac{\omega^2}{2} \frac{\eta_1 \eta_2}{\eta_1 + \eta_2} q^2 \\ & - 2\eta_1 \eta_2 (\eta_1 + \eta_2) \operatorname{sech}^2 \left(\frac{2\eta_1 \eta_2}{\eta_1 + \eta_2} q \right), \end{aligned} \tag{7.3}$$

where $P = p_1 + p_2$ is the momentum canonically conjugate to Q, and $p = (\eta_2 p_1 - \eta_1 p_2)/(\eta_1 + \eta_2)$ the momentum conjugate to q. The Hamiltonian is now clearly separable into two parts: the centre-of-mass energy

$$\Lambda = \frac{P^2}{2(\eta_1 + \eta_2)} + \frac{\omega^2}{2}(\eta_1 + \eta_2) Q^2, \tag{7.4}$$

and the interaction energy

$$\epsilon = \frac{\eta_1+\eta_2}{2\eta_1\eta_2}p^2 + \frac{\omega^2}{2}\frac{\eta_1\eta_2}{\eta_1+\eta_2}q^2 - 2\eta_1\eta_2(\eta_1+\eta_2)\mathrm{sech}^2\left(\frac{2\eta_1\eta_2}{\eta_1+\eta_2}q\right). \tag{7.5}$$

There are thus two functionally independent constants of the motion, Λ and ϵ, as many as there are degrees of freedom. Hence, the particle model for two solitons is integrable and the dynamics must be completely regular [12, 23].

7.2.1 Poincaré sections

In chapter 2, we gave a procedure for taking a Poincaré section through the phase space. Here we employ this Poincaré section to our particle model of two solitons to illustrate the regular behaviour of the system.

In terms of q_1, p_1 and p_2, when $q_2 = 0$, the constants of the motion can be written:

$$\Lambda = \frac{(p_1+p_2)^2}{2(\eta_1+\eta_2)} + \frac{\omega^2}{2}(\eta_1+\eta_2)\left[\frac{\eta_1 q_1}{\eta_1+\eta_2}\right]^2 \tag{7.6}$$

$$\epsilon = \frac{\eta_1+\eta_2}{2(\eta_1\eta_2)}\left[\frac{\eta_1 p_1 - \eta_2 p_2}{\eta_1+\eta_2}\right]^2 + \frac{\omega^2}{2}\frac{\eta_1\eta_2}{\eta_1+\eta_2}q_1^2 + V(q_1) \tag{7.7}$$

where

$$V(q_1) := -2\eta_1\eta_2(\eta_1+\eta_2)\mathrm{sech}^2\left(\frac{2\eta_1\eta_2}{\eta_1+\eta_2}q_1\right). \tag{7.8}$$

Hence,

$$p_2^2 = 2\eta_2\left[H - \eta_1\frac{\omega^2}{2}q_1^2 - \frac{p_1^2}{2\eta_1} - V(q_1)\right] \tag{7.9}$$

where $H = \Lambda + \epsilon$ is the total energy. We are interested in the case where $p_2 < 0$, so we take the negative root:

$$p_2 = -\sqrt{2\eta_2\left[H - \eta_1\frac{\omega^2}{2}q_1^2 - \frac{p_1^2}{2\eta_1} - V(q_1)\right]}. \tag{7.10}$$

Substituting into (7.6):

$$\Lambda = \frac{p_1^2}{2\eta_1}\frac{\eta_1-\eta_2}{\eta_1+\eta_2} + \frac{\omega^2}{2}q_1^2\eta_1\frac{\eta_1=\eta_2}{\eta 1+\eta 2} - \frac{p_1}{\eta_1+\eta_2}\sqrt{2\eta_2\left[H - \eta_1\frac{\omega^2}{2}q_1^2 - \frac{p_1^2}{2\eta_1} - V(q_1)\right]}. \tag{7.11}$$

This expression can be used to plot Poincaré sections of p_1 vs q_1 numerically. Alternatively, it can be inverted explicitly to obtain

$$p_1 = \pm\sqrt{2\eta_1^2\left(-b \pm \sqrt{b^2 - \frac{\Lambda^2 - \Lambda\omega^2\eta_1 q_1^2}{\eta_1^2}}\right)} \tag{7.12}$$

where

$$b := \frac{\omega^2 \eta_1 q_1^2}{(\eta_1+\eta_2)^2}\left[\eta_1^2 + 2\eta_2^2 - \eta_1\eta_2\right] = \frac{\Lambda(\eta_1-\eta_2)}{\eta_1(\eta_1+\eta_2)} - \frac{2\eta_2}{\eta_1+\eta_2}(H - V(q_1)). \quad (7.13)$$

In the case where the solitons have identical effective masses ($\eta_1 = \eta_2 := \eta$), the Hamiltonian [Eq. (7.3)] reduces to

$$H = \frac{P^2}{4\eta} + \eta\omega^2 Q^2 + \frac{p^2}{\eta} + \frac{\eta\omega^2 q^2}{4} - 4\eta^3 \mathrm{sech}^2(\eta q). \quad (7.14)$$

Figure 7.1 shows four Poincaré sections for the two particle system; sections of p_1 versus q_1 are shown for different surfaces of different total energy [12, 23]. These Poincaré sections demonstrate the regular behaviour of the integrable two particle system, as all trajectories lie on invariant tori in the phase space of the system. There are two distinct regimes observable in these Poincaré sections. In the lower regions of the sections, the centre-of-mass energy, Λ, is large and positive; in this case the interaction energy, ϵ, has a large negative contribution from the interaction term, and the solitons interact strongly. As will be seen in section 7.3.2, in this regime there is rapid energy exchange between the solitons, such that the soliton with lower amplitude oscillations is driven by the other soliton, which itself becomes damped. In the upper regions of the sections, Λ is less positive, and hence ϵ is less negative, so the energy exchange between the solitons occurs over a longer time period.

7.3 Simulation using the Gross-Pitaevskii equation

To test the validity of our particle model, we compare the results with simulations of the 1D GPE dynamics. The particle model neglects the phase degrees of freedom of the system. In order for the particle model to work well, the collision time must be much smaller than the harmonic trap period. In this case, the phase of the system should affect the solitons' density profile during the collisions only. However, if the trap has a considerable effect on the collision, the phase dynamics become important (as we will see later in this section).

For two solitons of equal size, it is possible to get an understanding of the phase behaviour of the GPE solution, by symmetry considerations. From the analysis

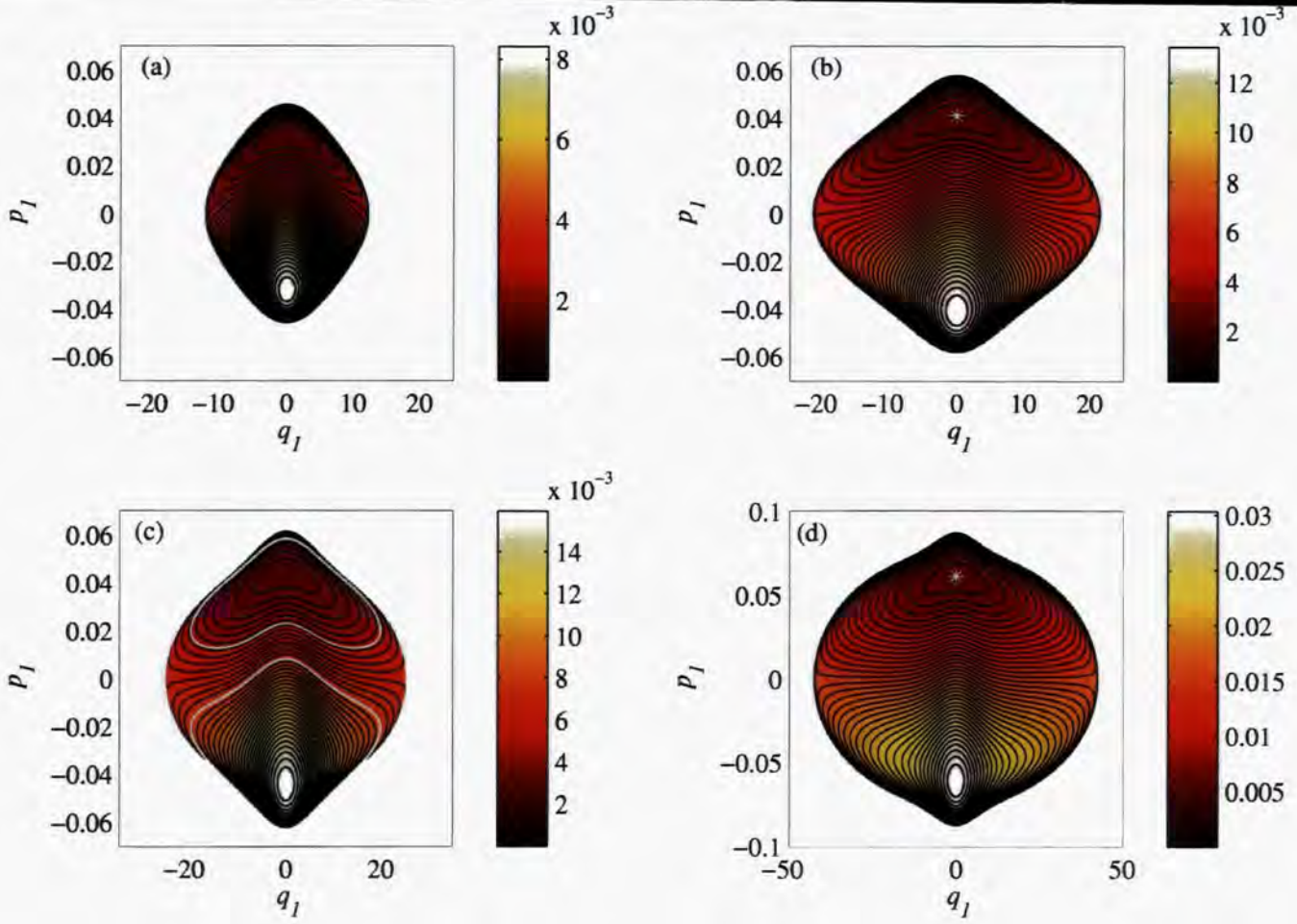

Figure 7.1: Poincaré sections for the two-soliton system corresponding to the momentum p_1 and position q_1 of one soliton, while the other soliton has coordinates $q_2 = 0$, $p_2 < 0$. q_1 and q_2 are measured in units of $\hbar^2/m|g_{1D}|N$, and p_1 and p_2 in units of $|g_{1D}|N/\hbar\eta$. The value of centre-of-mass energy, Λ, is given by the colour scale. (a) Total energy $H = 5 \times 10^{-4}$; (b) $H \approx 5.6 \times 10^{-3}$, the star corresponds to the trajectory in figure 7.2; (c) $H \approx 8.1 \times 10^{-3}$, the upper trajectory highlighted in white corresponds to that in figure 7.3, the lower to that in figure 7.4; (d) $H \approx 2.2 \times 10^{-2}$, the star corresponds to the trajectory in figure 7.5. The figures correspond to regimes where the solitons have equal effective masses, the axial trapping frequency is 1.59 Hz, and the other parameters (radial trap frequency of 127.32 Hz, atomic species mass and scattering length of ^{7}Li, and 5000 particles per soliton) are comparable to those of the recent experiment [17].

in section 6.3, we can see that an overall centre of mass motion may be added to any solution of the harmonic 1D GPE without effecting the density profile. A consequence of this is that to analyse an arbitrary system of two solitons of equal mass, only the symmetric cases with the soliton positions $q_1 = -q_2$, and momenta $p_1 = -p_2$ need be considered. Now, assuming that two solitons with equal size repeatedly collide and reemerge in a harmonic trap (see Fig. 7.2 for numerical evidence), if parity is conserved, we can show that the solitons collide repeatedly with the same relative phase in a system with no centre of mass motion, and hence also in the general case.

7.3.1 Conservation of parity

Let us consider a general parity operator $\hat{P}(\phi)$, such that $\hat{P}(\phi)\psi(x,t) = e^{i\phi}\psi(-x,t) := \chi(x,t)$. We want to know whether, if $\chi(x,t_0) = \psi(x,t_0)$, it continues to be the case that $\chi(x,t) = \psi(x,t)$ for all t.

Noting that $\hat{P}(\phi)|\psi(x,t)|^2\psi(x,t) = e^{i\phi}|\psi(-x,t)|^2\psi(-x,t) = |\hat{P}(\phi)\psi(x,t)|^2[\hat{P}(\phi)\psi(x,t)]$ we deduce from the 1D Gross-Pitaevskii equation [Eq. (4.34)] that

$$\begin{aligned} i\frac{\partial}{\partial t}\chi(x,t) =& i\hat{P}(\phi)\frac{\partial}{\partial t}\psi(x,t) \\ =& \hat{P}(\phi)\left\{\left[-\frac{1}{2}\frac{\partial^2}{\partial x^2} + \frac{\omega^2 x^2}{2} - |\psi(x,t)|^2\right]\psi(x,t)\right\} \\ =& \left[-\frac{1}{2}\frac{\partial^2}{\partial x^2} + \frac{\omega^2 x^2}{2} - |\chi(x,t)|^2\right]\chi(x,t). \end{aligned} \tag{7.15}$$

Hence, we see that the time-evolutions of $\psi(x,t)$ and $\hat{P}(\phi)\psi(x,t) = \chi(x,t)$ are governed by the same differential equation. If we also choose an initial condition such that $\psi(x,t_0) = \chi(x,t_0)$, it must therefore follow that $\chi(x,t) = \psi(x,t)$ for all t. In other words, parity is conserved in the sense that an initially symmetric wave function will have that symmetry preserved throughout its subsequent dynamical evolution.

In this thesis, the most important consequence of this result is that a system of two identical solitons with equal and opposite velocities will repeatedly collide with exactly the same collisional form (e.g., in phase or π out of phase) at the exact centre of the trapping potential. Using the results of section 6.3, it follows that an equivalent result holds upon the addition of a centre of mass oscillation.

A consequence of the phase-preservation for repeated collisions is that the condensate is stabilised against collapse when the solitons collide π out of phase [83]. Hence the condensate will be stabilised for all times if a suitable initial condition is applied such that collisions are out of phase.

7.3.2 Comparison between GPE and particle evolutions

In the Poincaré sections of Fig. 7.1, we highlighted a number of trajectories in white. These trajectories are plotted in position space as a function of time, overlaying density plots of corresponding 1D GPE solutions, in Figs. 7.2–7.5. Two solitons with equal norms in a harmonic trap have the same collisional form for all subsequent collisions; i.e., two solitons initially colliding with a phase difference ϕ_{coll}, will have this phase difference for all subsequent collisions. This property allows results of GPE simulations with repeated in-phase and π out-of-phase collisions to be compared for any trajectory in the two-particle model. Regimes with phase differences between zero and π are not considered here, but will generally be expected to display behaviour intermediate between that of the zero and π cases.

As shown in Fig. 3.1, the phase difference between the solitons has an observable effect on the solitons' form during collisons, although as the solitons tend asymptotically apart, the solitons' density dynamics are insensitive to this. Figure 7.6 shows how rapidly the solitons' trajectories in the wave and particle model converge. The convergence is more rapid when the solitons collide in-phase than when they collide π out of phase. When we formulated the particle model with a harmonic trap, we assumed the collision time to be much shorter than the period of the harmonic trap. We attribute the discrepancy between the particle and GPE dynamics in Figs. 7.2–7.5 to the non-zero collision time.

As expected, the agreement is generally better for in-phase collisions than for π out-of-phase collisions. In a harmonic trap, subsequent to a collision, two solitons can only move a finite distance apart (i.e., *not* asymptotically far) before moving together and colliding once more. Because repeated collisions preserve the collisional phase difference, the resulting discrepancy between the particle and GPE dynamics rapidly builds up. However, when the solitons collide with

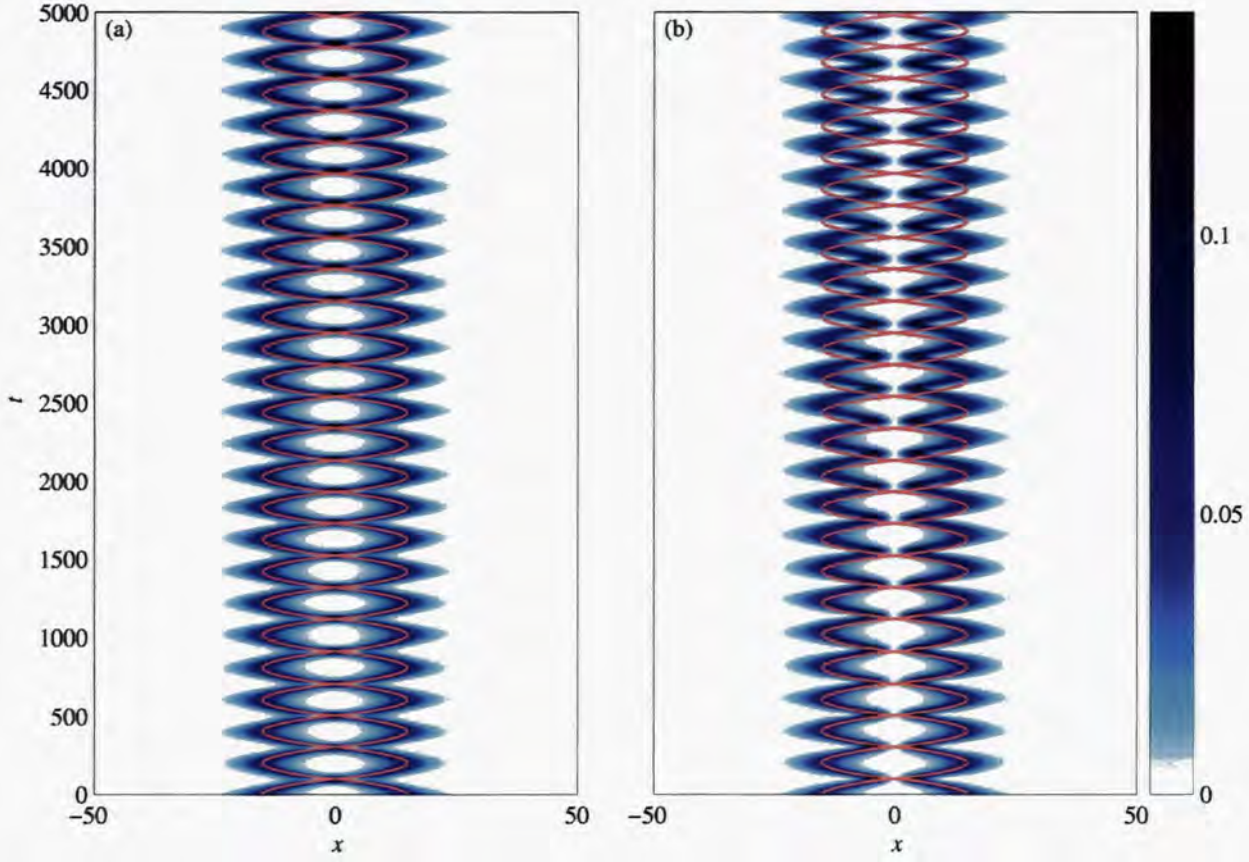

Figure 7.2: Trajectories in the particle model (red lines) plotted over density distributions predicted by 1D GPE dynamics, corresponding to the trajectory marked on figure 7.1(b). The relative phase of the solitons in the wave dynamics is zero in figure (a), and π in figure (b). x is measured in units of $\hbar^2/m|g_{1D}|N$ and t in units of $\hbar^3/m|g_{1D}|^2N^2$. The figures correspond to regimes where the solitons have equal effective masses, the axial trapping frequency is 1.59 Hz, and the other parameters (radial trap frequency of 127.32 Hz, atomic species mass and scattering length of ^{7}Li, and 5000 particles per soliton) are comparable to those in a recent experiment [17]. The unit of x is then equal to 3.6 μm, and the unit of t to 1.4 ms.

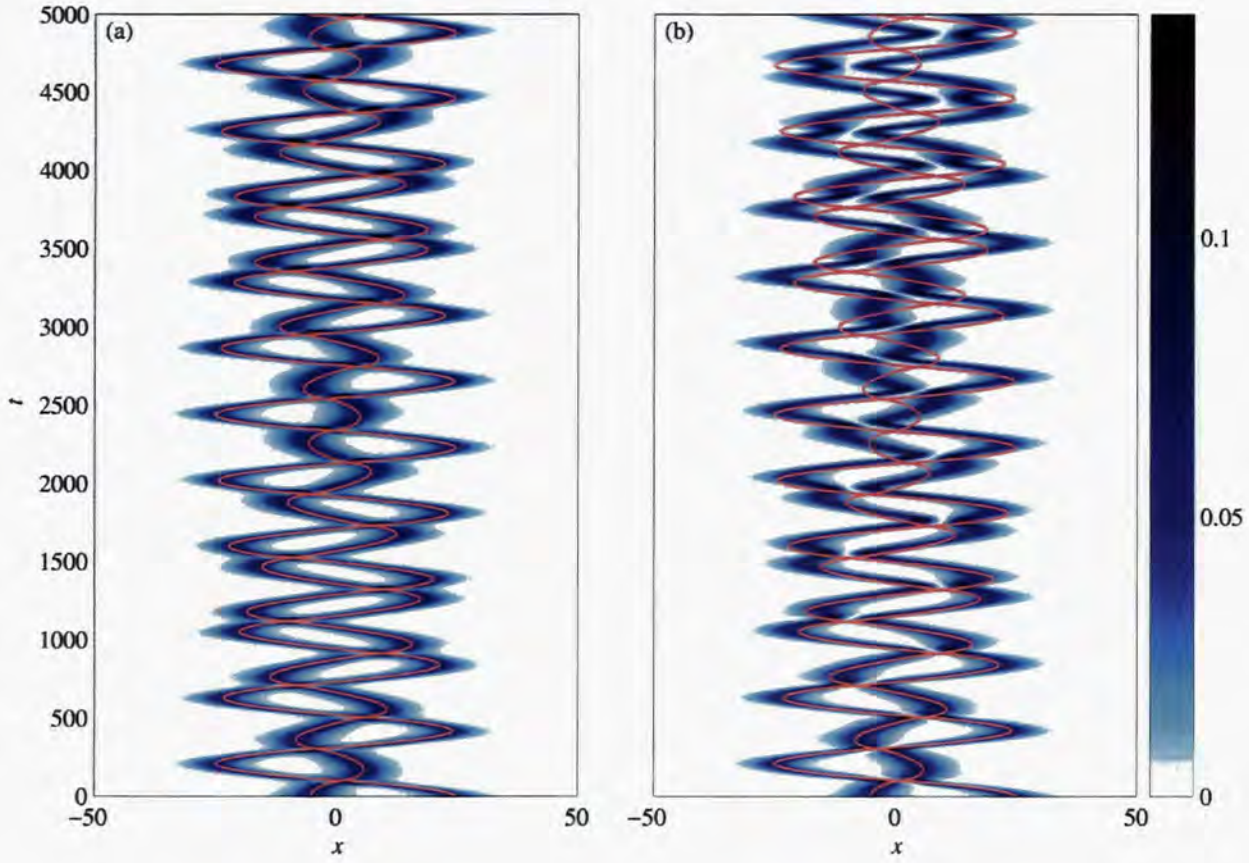

Figure 7.3: Trajectories in the particle model (red lines) plotted over density distributions predicted by 1D GPE dynamics. The trajectories correspond to those given in figure 7.2, but with additional centre-of-mass displacements. The trajectories also correspond to the upper trajectory marked on figure 7.1(c). The relative phase of the solitons in the wave dynamics is zero in figure (a), and π in figure (b). x is measured in units of $\hbar^2/m|g_{1D}|N$ and t in units of $\hbar^3/m|g_{1D}|^2N^2$. The solitons have equal effective masses, the axial trapping frequency is 1.59 Hz, and the other parameters (radial trap frequency of 127.32 Hz, atomic species mass and scattering length of ^{7}Li, and 5000 particles per soliton) are comparable to those in a recent experiment [17]. The unit of x is then equal to 3.6 μm, and the unit of t to 1.4 ms.

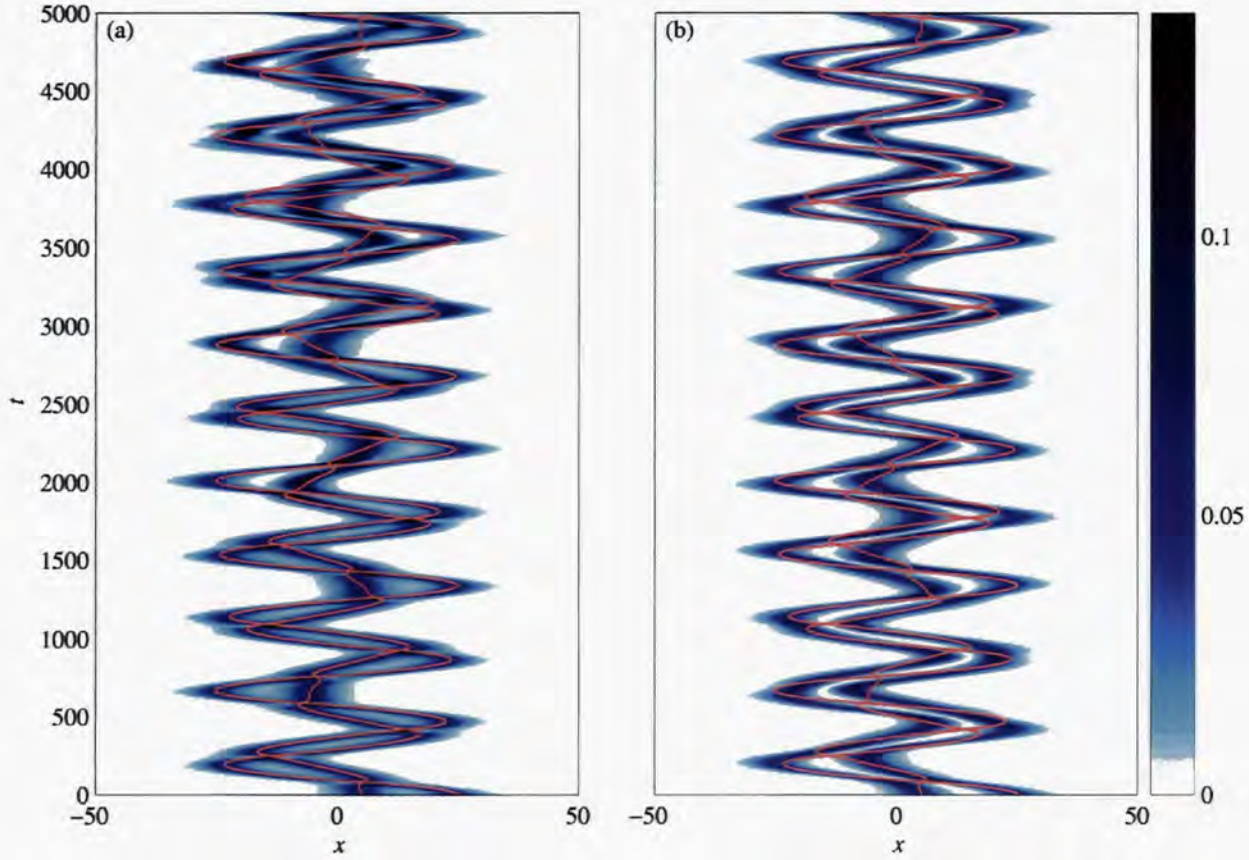

Figure 7.4: Trajectories in the particle model (red lines) plotted over density distributions predicted by 1D GPE dynamics, corresponding to the lower trajectory marked on figure 7.1(c). The relative phase of the solitons in the wave dynamics is zero in figure (a), and π in figure (b). x is measured in units of $\hbar^2/m|g_{1D}|N$ and t in units of $\hbar^3/m|g_{1D}|^2N^2$. The solitons have equal effective masses, the axial trapping frequency is 1.59 Hz, and the other parameters (radial trap frequency of 127.32 Hz, atomic species mass and scattering length of ^{7}Li, and 5000 particles per soliton) are comparable to those in a recent experiment [17]. The unit of x is then equal to 3.6 μm, and the unit of t to 1.4 ms.

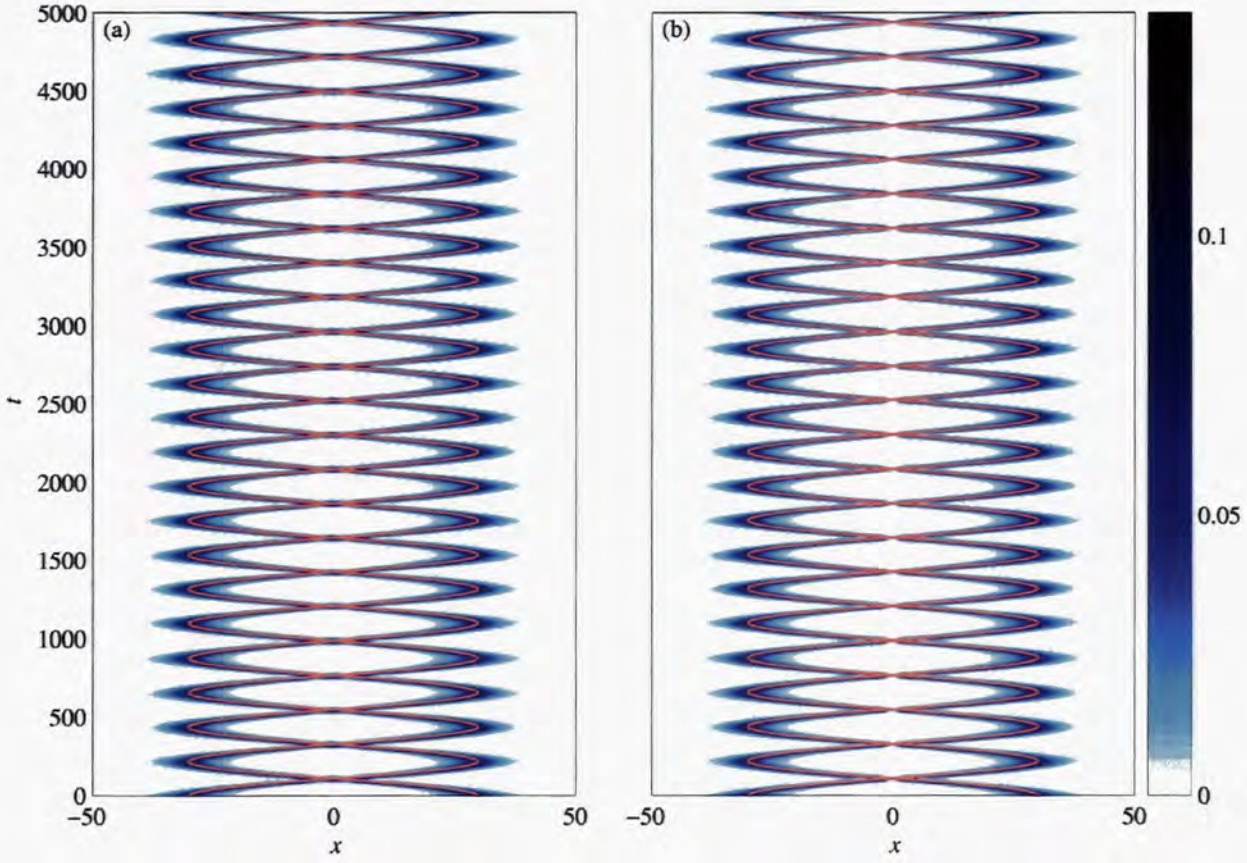

Figure 7.5: Trajectories in the particle model (red lines) plotted over density distributions predicted by 1D GPE dynamics, corresponding to the trajectory marked on figure 7.1(d). The relative phase of the solitons in the wave dynamics is zero in figure (a), and π in figure (b). x is measured in units of $\hbar^2/m|g_{1D}|N$ and t in units of $\hbar^3/m|g_{1D}|^2N^2$. The solitons have equal effective masses, the axial trapping frequency is 1.59 Hz, and the other parameters (radial trap frequency of 127.32 Hz, atomic species mass and scattering length of ^{7}Li, and 5000 particles per soliton) are comparable to those in a recent experiment [17]. The unit of x is then equal to 3.6 μm, and the unit of t to 1.4 ms.

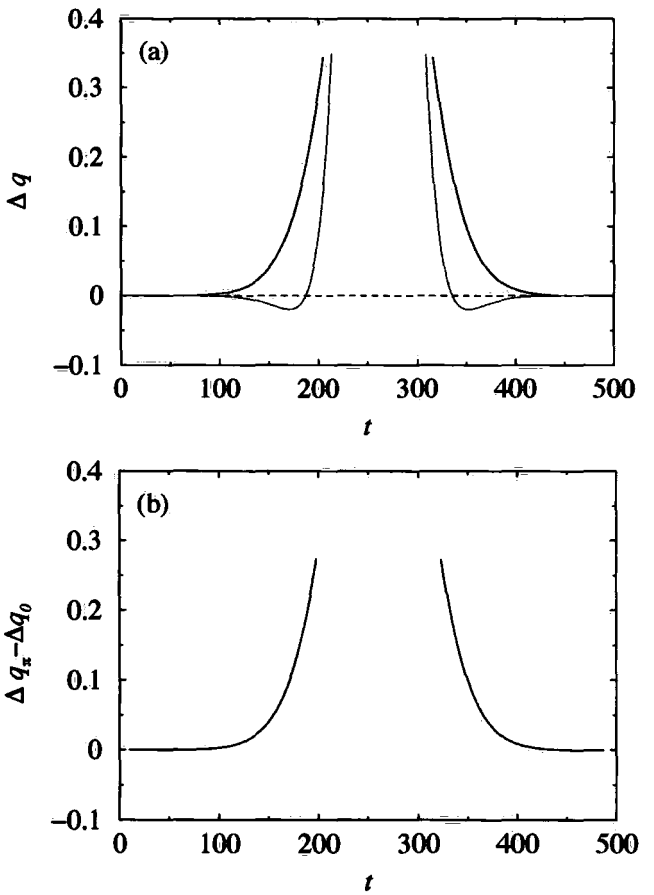

Figure 7.6: (a) Difference between soliton peak trajectory from wave simulation and particle model. The trajectories are those of the left-hand soliton in figure 3.1 going into and re-emerging from a collision in the case of $\Delta\phi = \pi$ (dark line) and $\Delta\phi = 0$ (light [red] line). Zero is indicated by the dotted line. The difference Δq is equal to the particle trajectory q_1 minus the position of the peak of the left-hand soliton, or equivalently the position of the peak of the right-hand soliton minus the particle trajectory q_2. Position is measured in units of $\hbar^2/m|g_{1D}|N$ and t in units of $\hbar^3/m|g_{1D}|^2N^2$. (b) Difference between the curves in figure (a). Note that the separation between the trajectories in the particle model and GPE dynamics is always larger in the π-phase case.

sufficient velocity [Fig. 7.5], the collision time is short enough compared to the trap period for both zero and π cases to give good agreement between the particle model and the GPE dynamics.

All the simulations discussed in this chapter are for solitons of equal effective masses $\eta_1 = \eta_2$. These regimes are consistent with those of a recent experiment [53]. For unequal effective masses, the particle dynamics are still regular (since Eq. (7.3) is separable). Recall from chapter 3 that the particle model is valid for unequal effective masses provided that the relative velocities are sufficiently large. Regimes outside this range are an area of future study. The phase behaviour of two solitons of unequal masses cannot be easily predicted by parity considerations, and are another area of future study.

The dynamics in the particle model are completely regular for two solitons, and the corresponding GPE dynamics are also regular. Hence small perturbations to the GPE dynamics should only produce small deviations from the unperturbed trajectory. From the treatment in chapter 4, we can predict that thermal and quantum fluctuations will consequently have only a small effect on the dynamics, and on the condensate population. Full integrations of the Bogoliubov-de Gennes equations, or other finite temperature treatments, to confirm this insensitivity, are an avenue for future work.

Chapter 7 Summary

- Solitons collide elastically.
- A model was formulated treating each bright soliton as a classical particle.
- This model agrees well with simulations of the wave dynamics in the cases where the collision time is short compared with the trap period.

Chapter 8

Three harmonically trapped solitons: chaos and regularity

The presence of chaos in quantum systems is a topic of intense theoretical and experimental interest [23]. A signature of classical chaos is the ergodic filling of regions in phase space. Applying this criterion in the search for chaos in wave-mechanical systems, e.g. the linear Schrödinger equation in quantum mechanics, the uncertainty relations dictate that trajectories are smeared out. Chaos is impossible to observe when dispersion dominates over the exponential divergence of neighboring trajectories. Non-dispersive waves such as solitary waves or solitons are therefore of particular interest in the study of chaotic dynamics. In this case, particle-like chaotic behaviour may be well-defined in wave-mechanical systems.

As we saw in Chapter 7, when modelled as a system of classical particles, the two soliton solution to the harmonic 1D Gross-Pitaevskii equation is integrable, and hence all trajectories are regular. However, the three body problem historically has been a ground of non-integrable behaviour (e.g., the three-body gravitational system e.g., Earth, Moon and Sun [12]), and the three-particle Hamiltonian is not obviously separable in the manner in which was the two-particle Hamiltonian; hence, a particle model of the three soliton system is a good candidate in a search for chaos.

8.1 Three solitons

Particle model

Whereas for two solitons the particle model dynamics are always regular (see Sec. 7.2), in the case of three solitons ($N_s = 3$), the situation is quite different. A useful coordinate system for the three soliton system is to be found in the normal coordinates of the system for small displacements of the particles from the origin: the centre-of-mass position

$$Z_T := \frac{\eta_1 q_1 + \eta_2 q_2 + \eta_3 q_3}{\eta_1 + \eta_2 + \eta_3}, \tag{8.1}$$

$$z_c := \frac{\eta_1(\eta_2 + 2\eta_3)q_1 + \eta_2(\eta_3 - \eta_1)q_2 - \eta_3(\eta_2 + 2\eta_1)q_3}{\eta_1\eta_2 + \eta_2\eta_3 + 4\eta_1\eta_3}, \tag{8.2}$$

(corresponding to the "stretch" mode), and

$$z_r := q_1 - 2q_2 + q_3, \tag{8.3}$$

(corresponding to the "asymmetric stretch"). The stretch modes are similar to those used to describe vibrational dynamics in a tri-atomic molecule [84]; as the system is constrained to 1D, however, there is no analogue of the molecular bending mode. Using these coordinates, the three-particle Hamiltonian [Eq. (7.2)] takes the form:

$$\begin{aligned} H =& \frac{1}{2}\left[\frac{W_T^2}{\eta_1+\eta_2+\eta_3} + w_c^2\frac{\eta_1+\eta_2+\eta_3}{\eta_1\eta_2+\eta_2\eta_3+4\eta_1\eta_3} + w_r^2\frac{\eta_1\eta_2+\eta_2\eta_3+4\eta_1\eta_3}{\eta_1\eta_2\eta_3}\right] \\ &+ \frac{\omega^2}{2}\left[Z_T^2(\eta_1+\eta_2+\eta_3) + z_c^2\frac{\eta_1\eta_2+\eta_2\eta_3+4\eta_1\eta_3}{\eta_1+\eta_2+\eta_3} + z_r^2\frac{\eta_1\eta_2\eta_3}{\eta_1\eta_2+\eta_2\eta_3+4\eta_1\eta_3}\right] \\ &- 2\eta_1\eta_2(\eta_1+\eta_2)\mathrm{sech}^2\left[\frac{2\eta_1\eta_2}{\eta_1+\eta_2}\left(\frac{\eta_2\eta_3+2\eta_1\eta_3}{\eta_1\eta_2+\eta_2\eta_3+4\eta_1\eta_2}\right)z_r + z_c\right] \\ &- 2\eta_1\eta_3(\eta_1+\eta_3)\mathrm{sech}^2\left[\frac{2\eta_1\eta_3}{\eta_1+\eta_3}\left(\frac{\eta_2\eta_3-2\eta_1\eta_2}{\eta_1\eta_2+\eta_2\eta_3+4\eta_1\eta_2}\right)z_r + 2z_c\right] \\ &- 2\eta_2\eta_3(\eta_2+\eta_3)\mathrm{sech}^2\left[\frac{2\eta_2\eta_3}{\eta_2+\eta_3}\left(\frac{-(\eta_1\eta_2+2\eta_1\eta_3)}{\eta_1\eta_2+\eta_2\eta_3+4\eta_1\eta_2}\right)z_r + z_c\right], \end{aligned} \tag{8.4}$$

where $W_T = p_1 + p_2 + p_3$, $w_c = [(\eta_2 + 2\eta_3)p_1 + (\eta_3 - \eta_1)p_2 - (\eta_2 + 2\eta_1)p_3]/(\eta_1 + \eta_2 + \eta_3)$, and $w_r = (\eta_2\eta_3 p_1 - 2\eta_1\eta_3 p_2 + \eta_1\eta_2 p_3)/(\eta_1\eta_2 + \eta_2\eta_3 + 4\eta_1\eta_3)$ are the momenta canonically conjugate to the coordinates Z_T, z_c, and z_r, respectively.

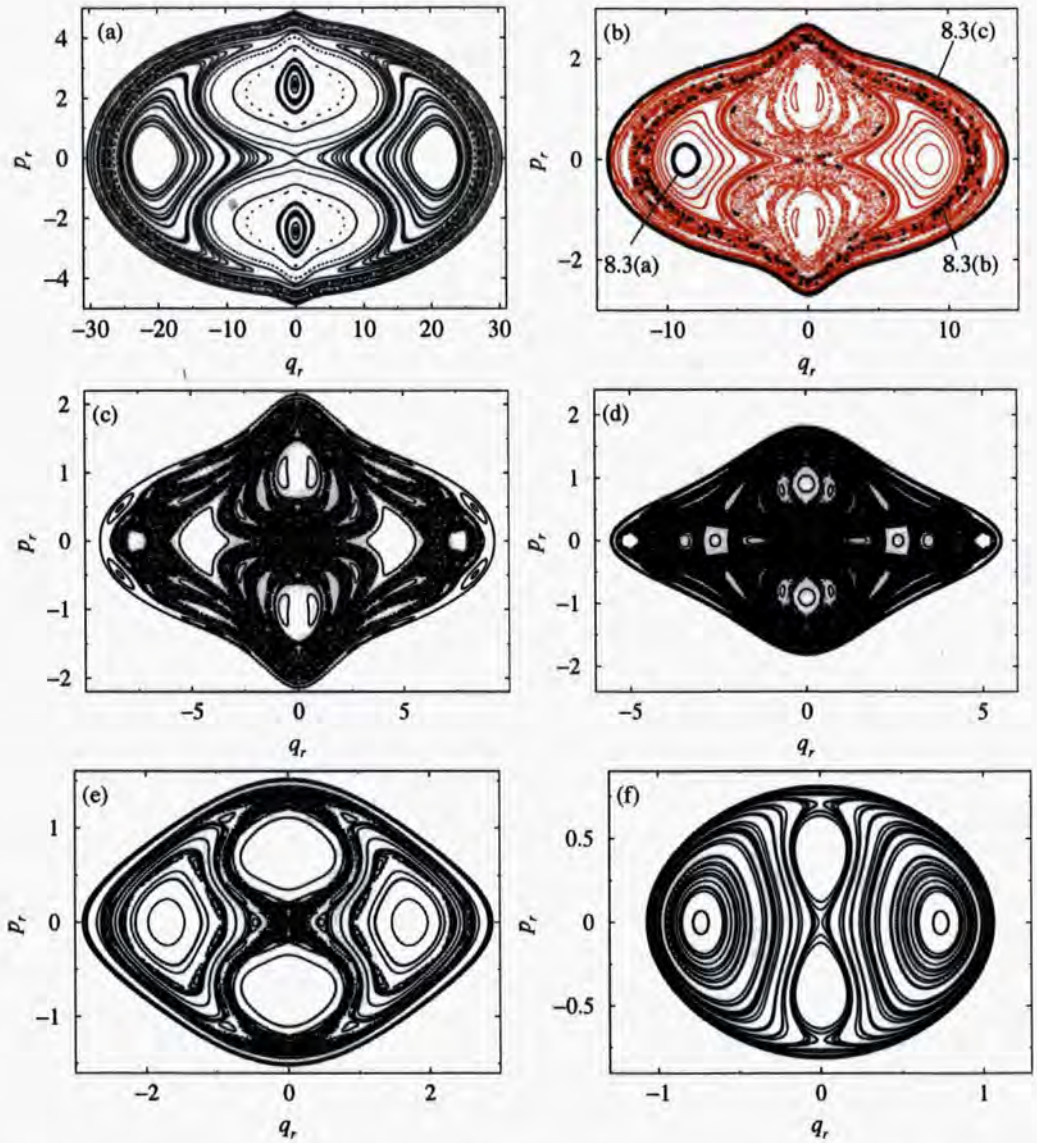

Figure 8.1: Poincaré section of the three-soliton system with (a) $\tilde{H} = 60$; (b) $\tilde{H} = 10$, regions corresponding to trajectories in figures 8.3(a) to 8.3(c) are labeled, and highlighted using larger, darker points; (c) Poincaré section of the system with $\tilde{H} = 2$; (d) $\tilde{H} = -2$; (e) $\tilde{H} = -5$; (f) $\tilde{H} = -10$. The section corresponds to the momentum p_r and position q_r of the "asymmetric stretch" mode when the "stretch" mode coordinates $q_c = 0$, $p_c < 0$. q_c and q_r are measured in units of $\eta\hbar^2/m|g_{1D}|N$, and p_c and p_r are measured in units of $|g_{1D}|N/\hbar\eta$. The figures correspond to the regime where the solitons have equal effective masses, the axial trapping frequency is 1.59 Hz, and the other parameters (radial trap frequency of 127.32 Hz, atomic species mass and scattering length of ^{7}Li, and 5000 particles per soliton) correspond to a recent experiment [17].

It is apparent in Eq. (8.4) that the Hamiltonian, as in the two-particle case, is decoupled into a centre-of-mass component, and a component describing the stretch modes (which are coupled to each other).

In the case of identical effective masses, the coordinates Z_T, z_c and z_r simplify substantially. It turns out to be convenient to consider slightly different coordinates, however, as this produces a simpler final form for the Hamiltonian describing the stretch mode dynamics. We therefore define $Q_T = \eta Z_T = \eta(q_1 + q_2 + q_3)/3$, $q_c = \eta z_c = \eta(q_1 - q_3)/2$ and $q_r = \eta z_r = \eta(q_1 + q_3 - 2q_2)$. We rescale the time to $\tilde{t} = \eta^2 t$, and then introduce the momenta $p_c = w_c/\eta^2 = (p_1 - p_3)/\eta^2$ and $p_r = w_r/\eta^2 = (p_1 - 2p_2 + p_3)/6\eta^2$. Using these dynamical variables, the resultant Hamiltonian (the reduced system Hamiltonian), with the centre-of-mass degrees of freedom removed, becomes:

$$\begin{aligned}\tilde{H} =& 3p_r^2 + \frac{\omega^2}{2\eta^4}\frac{q_r^2}{12} + \frac{p_c^2}{4} + \frac{\omega^2}{2\eta^4}q_c^2 - 4\mathrm{sech}^2(2q_c) \\ & - 4\mathrm{sech}^2(q_c + \frac{q_r}{2}) - 4\mathrm{sech}^2(q_c - \frac{q_r}{2}).\end{aligned} \tag{8.5}$$

This Hamiltonian, describing the two remaining degrees of freedom, is not separable, and it is necessary to integrate the corresponding Hamilton's equations of motion numerically to analyse the system's behaviour. As they represent a slice through the phase space of a system, Poincaré sections provide a good illustration of regions of regular and chaotic dynamics. In regions of regular behaviour, any trajectory will lie on a torus in phase-space, and will thus trace a closed curve in the Poincaré section; in regions of chaotic behaviour, a trajectory will go through every point in that region of phase space, and thus fill an area on the Poincaré section (a so-called ergodic sea) [12, 23]. We choose to show sections corresponding to the momentum p_r and position q_r of the "asymmetric stretch" mode when the "stretch" mode coordinate takes the value $q_c = 0$, and when its canonically conjugate momentum $p_c < 0$. Other sections can be expected to be equally illustrative of the qualitative behaviour.

Figure 8.1 shows nine Poincaré sections for nine different reduced system energies $\tilde{H}$. The behaviour is regular at large positive values of $\tilde{H}$ [Fig. 8.1 (a)], but as $\tilde{H}$ is reduced, chaotic behaviour emerges, characterised by ergodic regions in between regular tori. For small (negative) $\tilde{H}$ the system is mostly an ergodic sea, with islands of stability [Fig. 8.1 (c)]; but as $\tilde{H}$ is made more negative, the chaotic regions begin to subside, and the behaviour becomes increasingly

regular again.

Consideration of the form of the reduced-system Hamiltonian [Eq. (8.5)] shows that without the interaction the system is integrable, as it becomes a decoupled pair of harmonic oscillators. When $\tilde{H}$ is large and positive, the interaction part of the Hamiltonian (which is always negative) should give a relatively small contribution to the Hamiltonian, compared to the integrable part of the Hamiltonian (which is always positive). When $\tilde{H}$ is reduced, this is no longer the case, and chaotic dynamics are manifest. However, in regimes where the coordinates and momenta are close to zero, i.e., $\tilde{H}$ approaches its lower bound of -12, the interaction potential becomes approximately harmonic. The Hamiltonian $\tilde{H}$ takes the following seperable form:

$$\tilde{H} = 3p_r^2 + \left(\frac{\omega^2}{24\eta^4} + 2\right) q_r^2 + \frac{p_c^2}{4} + \left(\frac{\omega^2}{2\eta^4} + 24\right) q_c^2, \tag{8.6}$$

i.e., it again describes a pair of decoupled harmonic oscillators. We consequently expect the phase-space structure to be qualitatively similar in the opposing limits of $\tilde{H}$ very large and positive, and $\tilde{H}$ large and negative. From Figs. 8.1(a) and 8.1(f), we do indeed observe this to be the case.

We highlight some chaotic and regular trajectories on Fig. 8.1(b). These correspond to the trajectories in Fig. 8.3. The Lyapunov exponents associated with the trajectories of Figs. 8.3(a) and 8.3(b) can be estimated by reference to Fig. 8.2. In the limit as $t \to \infty$, the gradient of these curves gives the Lyapunov exponent. This limit is not easy to infer from the figure due to the rapid variations in gradients therein. However, it is clear that the chaotic region is characterised by significantly more rapid divergence of trajectories than is the regular region. As stated in chapter 5 the linear instabilities indicated by such behaviour may be used to predict depletion of the condensate.

Comparison with GPE simulations

Figure 8.3 shows a comparison of trajectories in the particle model with results from integrations of the 1D GPE [Eq. (4.34)] for the three-soliton system, where the solitons all have equal effective masses. As with the two-soliton case (Sec. 7.3.2), the trajectories in the particle model gradually acquire a shift with respect to the trajectories traced out by the GPE wavefunction peaks. In Figs.

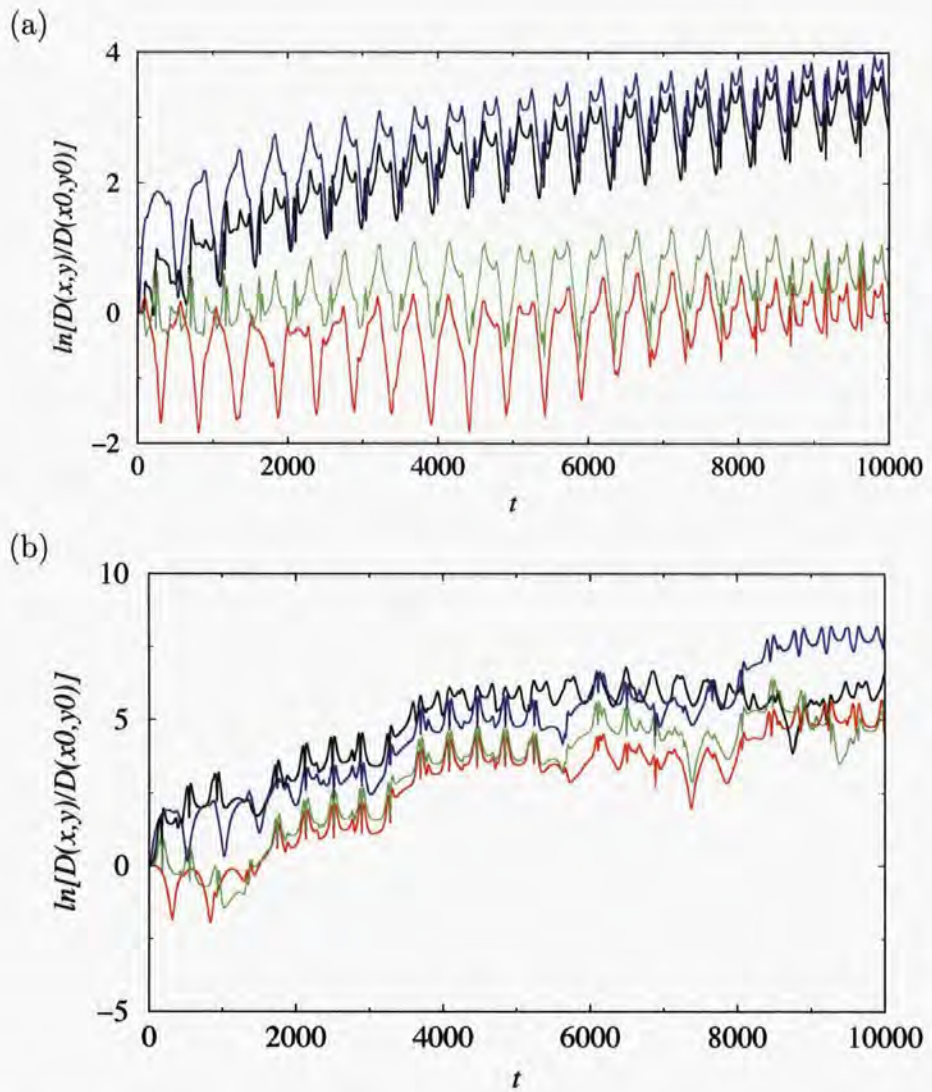

Figure 8.2: Divergence, D, of displaced trajectories from trajectories corresponding to (a) the regular trajectory of Fig. 8.3(a) and (b) the chaotic trajectory of Fig. 8.3(b). The four lines give the divergences for initial displacements in four orthogonal directions of the (four-dimensional) phase space. The gradients of these logarithmic plots in the limit $t \to \infty$ give the four Lyupunov exponents for each trajectory. The curves which diverge the fastest give the leading exponents.

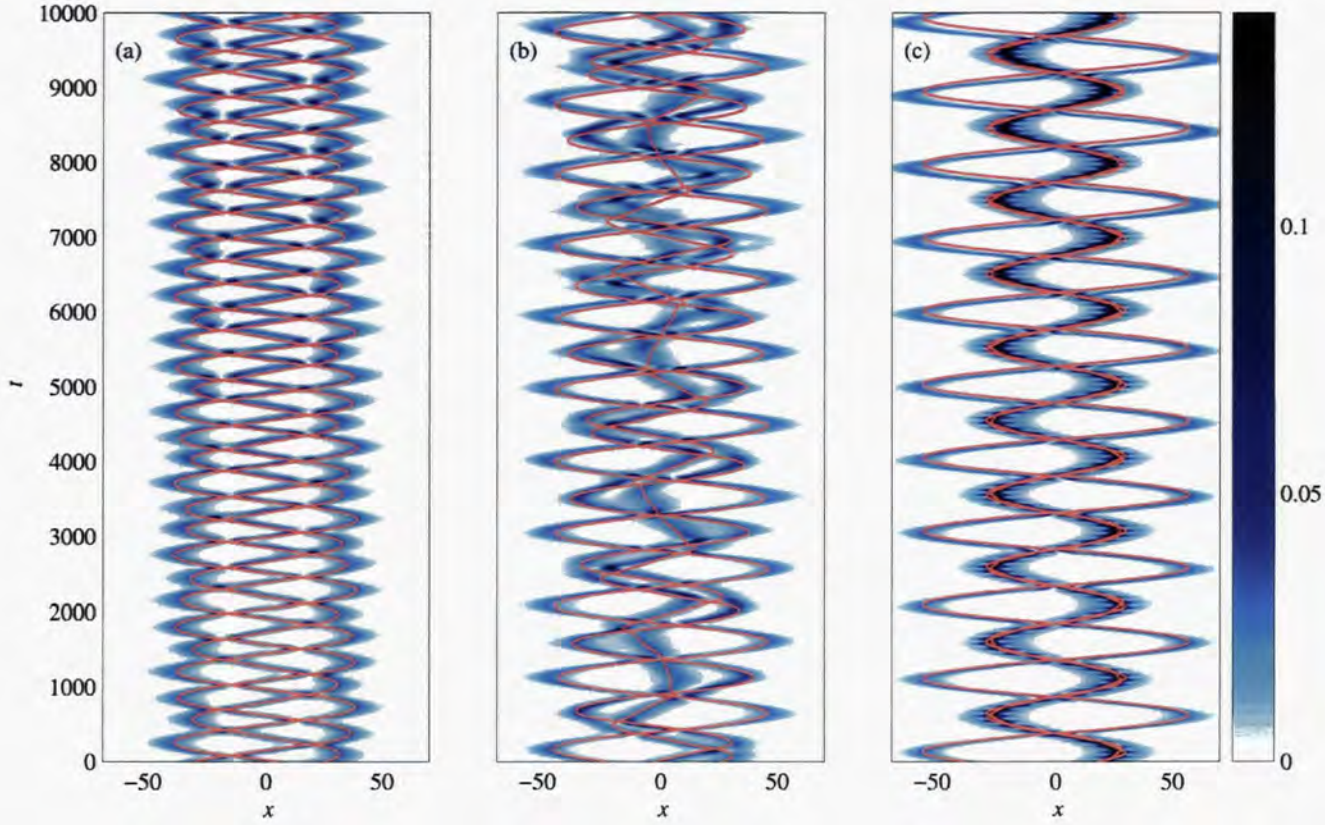

Figure 8.3: Trajectories in the particle model (red lines) plotted over density distributions predicted by 1D GPE dynamics, corresponding to a regular orbit. The parameters of the system are those of 8.1(b): $\tilde{H}$=10, the solitons have equal effective masses, the axial trapping frequency is 1.59 Hz, and other parameters (radial trap frequency of 127.32 Hz, atomic mass and scattering length of ^{7}Li, and 5000 particles per soliton) correspond to the recent experiment [17]. The unit of x is then equal to 2.4 μm, and the unit of t to 0.6 ms.

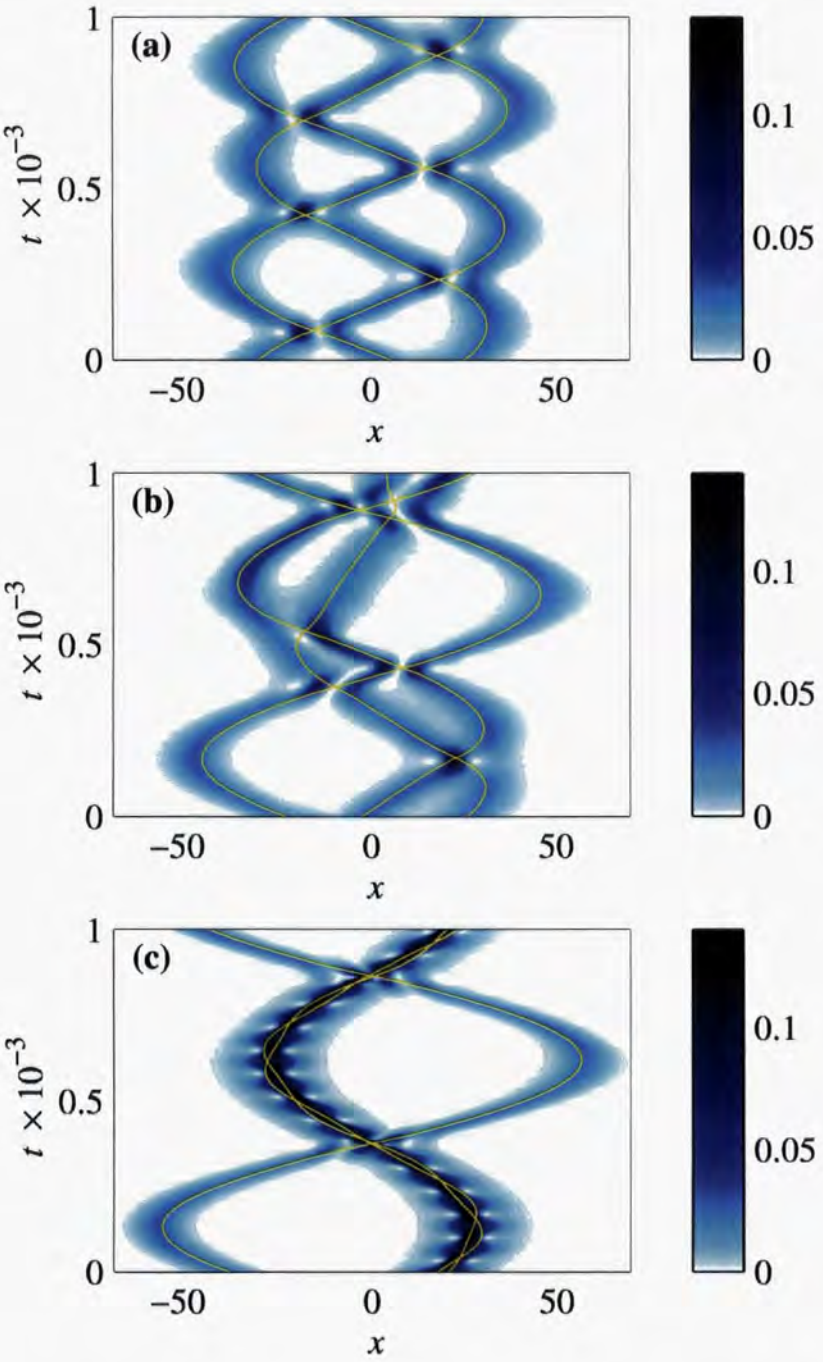

Figure 8.4: Details of the trajectories in figure 8.3 (a) to (c). The yellow lines correspond to the red lines in those figures. The unit of x is then equal to 2.4 μm, and a unit of t to 0.6 ms.

8.3(a) and 8.3(b) the overall shift indicates that subsequent collisions tend to take place sooner in the particle model than is predicted by the GPE evolution; interestingly, in Fig. 8.3(c) we observe the opposite, however. As before, these shifts are caused by an accumulation of small errors, due to the fact that within a harmonic confining potential the individual solitons do not move asymptotically far from each other subsequent to collisions. In Fig. 8.3(c) there is the added complication that two of the solitons appear to have formed a "bound state." Figure 8.4 shows these trajectories in more detail.

The comparisons illustrate the good agreement between the particle model and the 1D GPE in the regimes in which the particle model is valid, i.e., when solitons are well separated between collisions [Fig. 8.3(a) and 8.3(b)], even when the motion is chaotic [Fig. 8.3(b)]. When two of the solitons are not well separated [Fig. 8.3(c)], the 1D GPE simulation shows that a "bound state" is formed, which looks like a single "higher-order" soliton with an excited breathing mode [64]. The particle model does not predict well the behaviour within the "bound state", but does give a good prediction of the centre-of-mass motion of the "bound state" and its interactions with the other soliton; it is likely that the behaviour of the density of the "bound state" is strongly coupled to the phase behaviour within the "bound state." As in the two soliton case (Sec. 7.3.2), errors gradually accumulate in the particle model which lead to an overall "time shift" in the overall collision dynamics. It should be noted, however, that apart from this shift qualitative agreement with the dynamics predicted by the GPE remains quite good right up until the limits of our numerical calculations ($t = 10000$ corresponding to 6 seconds for the experimental parameters in [17]).

The particle model exhibits good agreement with the 1D GPE in the regime of large separation of the solitons before and after collisions, even when the particle motion is chaotic. This confirms the surprising robustness of bright matter-wave solitons, as observed experimentally [17, 52–54]. There is a good degree of agreement even when "bound states" are modeled (states not in a regime of large separation).

In chapter 5, we gave reasons why chaotic regimes of the GPE are interesting. For systems of three harmonically trapped solitons we have identified such regimes, the chaotic trajectories in Fig. 8.3(b), for example. These regions may also be a useful predictor of regimes of condensate instability. Regimes where

the condensate dynamics are unstable will be sensitive to quantum and thermal fluctuations, which can be explored with a fuller treatment of the condensate and non-condensate atoms [13], or other finite temperature treatments. The GPE trajectories and the number of condensate particles are both predicted to be unstable to fluctuations. This is a possible avenue for future study. Systems of unequal effective masses should be qualitatively similar to those of equal masses, but these too are an area for future study.

Experimental demonstration of such chaotic dynamics in a wave mechanical system requires a relatively straightforward adaption of recent experiments on bright matter wave solitons [17, 52–54]. For example, a system of three solitons can be created reproducibly by careful choice of the initial conditions; as explained in chapter 5 when a collapse is induced in a condensate by suddenly switching the scattering length from positive to negative, the number of solitons in the remaining condensate depends on the total particle number and final scattering length [53]. Manipulation of the optical trapping potential during the solitons' creation will allow the solitons' initial velocities to be chosen. Chaotic regions of phase space may be probed by measuring the sensitivity of the subsequent evolution of the density distribution to the initial condition. Desctructive time-of-flight measurements could be used to measure the position of the solitons at particular times, so many repeated measurements must be taken to plot each trajectory of the solitons in phase space.

Chapter 8 Summary

- Solitons present a paradigm for wave chaos due to their classical particle character.
- The three body problem is a fertile ground for chaotic behaviour.
- The particle model for three solitons is regular in the limits of low and high reduced energy.
- In between these limits, ergodic regions appear in the phase space of the system, where the trajectories are chaotic.
- The Lyupunov exponents for regular and chaotic were inferred from log-log plots of the divergence of the trajectories versus time.
- The particle model is a good model for the Gross-Pitaevskii dynamics in both regular and chaotic regimes. This is evident from comparisons of numerical simulations of the particle and Gross-Pitaevskii dynamics.

Part III

Three-dimensional effects in cigar-shaped Bose-Einstein condensates

Chapter 9

Introduction

In realistic models for cigar shaped BECs beyond the 1D Gross-Pitaevskii equation (GPE), the integrability of the nonlinear wave equation is broken by residual 3D effects. Whereas in integrable systems, solitons collide elastically, this is not necessarily true in non-integrable systems. Indeed, numerical simulations by Parker *et al.* have shown that in the 3D GPE, solitary-wave collisions are inelastic; specifically, there is particle exchange between the solitary waves accompanied by changes in their outgoing velocities [85]. Parker *et al.* have found numerical evidence that the total number of particles exchanged has sinusoidal dependence on the phase difference between the solitary waves when the solitary waves collide with large relative velocity.

Homogeneous three dimensional trapped Bose-Einstein condensates with attractive interatomic interactions are prone to collapse [75]. This collapse can be mitigated by trapping the condensate in an external potential [53, 75, 86]. However, collapse still occurs if the condensate particle density becomes too large. In 1D (cigar-shaped) regimes, the critical number of atoms can be expressed as $N_{\max} = ka_r/|a|$, where a is the scattering length, and $a_r = \sqrt{\hbar/m\omega_r}$ is the radial harmonic length. Here, k is some constant which depends on the ratio of the axial to the radial potential [86]. The optimal number of particles occurs in radial trap geometries [86], but the detailed effects of trap geometry on the collapse parameter, k, are still a topic for investigation. In the 1D GPE, scaling considerations imply that solitary-wave solutions occur for any number of particles. Clearly, when 3D effects are taken into account, solitary-waves

can only exist for a limited number of particles up to $N_{\max}$. These effects are investigated in experiment [53] and theoretical models [49,51].

Parker *et al.* in 3D GPE simulations show that in-phase collisions between solitary waves, during which the particle density becomes large, can cause collapse of the solitary wave solution if the relative velocity is relatively small [53,83,85]. If the solitary waves collide with small relative velocity but sufficiently out of phase, collapse does not occur, and the particle exchange depends on the tangent of the solitary waves' relative phase.

In chapter 4 we reviewed several reductions of the 3D GPE to 1D equations which accounted for some radial motion [49,50]. Khaykovich and Malomed performed simulations of solitary wave collisions using the nonlinear Schrödinger equation with a quintic term [Eq. (4.30)] [51], which displayed the same quantative behaviour as Parker's simulations, i.e., the solitary waves collided inelastically, and the solution collapsed for large particle densities. Salasnich *et al.* [49] performed simulations of the non-polynomial Schrödinger equation [Eq. (4.31)], also seeing collapse of the condensate for large particle densities. However, Salasnich *et al.* claimed to observe that when solitary waves did emerge from the collisions, such collisions were elastic.

Other non-integrable equations [87–90] show that integrability breaking in solitary wave equations can produce inelastic collisions where particles are exchanged between solitary-waves depending on their relative phase.

The numerical simulations provide fascinating results for which we would like to provide a mechanism or explanation. The phase dependent particle exchange between solitary waves is suggestive of Josephson dynamics. However there are important differences between solitary-wave collisions and Josephson junctions; most notably, Josephson current is due to a linear superposition of modes whereas solitary-wave particle exchange is a consequence of the nonlinear collisional dynamics of the solitary waves.

To get a fundamental understanding of the solitary-wave collapse and to find a way to model collisions in non-integrable systems we use a variational approach to derive equations of motion for the parameters of solitary-wave solutions. In this part of the thesis we show how the variational approach provides many insights into solitary-wave dynamics, and then use this to find the solitary-wave

dynamics generated by Eq. (4.30).

Chapter 9 Summary

- Three dimensional BECs are prone to collapse.
- The collapse is dependent on the trapping strength, trapping geometry and the atomic species' scattering length.
- Solitary-wave collisions in 3D systems are inelastic, with particle exchange dependent on the relative phase of the solitary-waves.
- For in-phase collisions, the particle can exceed a critical amount such that collapse of the condensate occurs.
- We will study these 3D effects by using a variational approach with a nonlinear Schrödinger equation with quintic nonlinearity.

Chapter 10

A variational analysis of integrability-breaking

The variational approach involves using a Lagrange density for a system suspected to support solitary wave solutions and using a variational ansatz with appropriate parameters corresponding to single or multiple solitary waves. The Lagrange density can then be integrated over space to yield a Lagrangian which is a function of the solitary wave parameters. If the solitary-wave ansatz is well motivated, computation of the Euler-Lagrange equations will produce the approximate solitary-wave dynamics. This approach may be useful to predict the collapse dynamics of single and multiple solitons, and the positional dynamics and particle exchange between solitons caused by three-dimensional effects.

As well as yielding approximate solutions to the classical wave equation, the variational approach may have other uses. For example, the Lagrangian may be phenomenologically quantised in order to capture some of the quantum effects of solitons [35].

10.1 Three-dimensional effects

In chapter 4 we showed several reductions from the 3D Gross-Pitaevskii equation (GPE) to 1D equations [49–51] which still captured some of the effects of the 3D behaviour (essentially through breaking integrability). References [49, 51] presented numerical simulations of soliton-soliton collisions. In order to gain

a deeper understanding of the collisions, and go further than these numerical simulations, we use a variational approach to derive the soliton dynamics.

We showed in chapter 4 that Eq. (4.30) may be scaled such that either g_1 or ω may be scaled out. For this treatment, we keep both g_1 and ω as free parameters, such that we retain the freedom to scale out whichever suits our purposes best.

Equation (4.37) may be derived from the following Lagrange density:

$$\mathcal{L}_{\mathrm{KM}} = \frac{i}{2}\left(\psi\psi_t^* - \psi^*\psi_t\right) + \frac{1}{2}|\psi_x|^2 + \frac{\omega^2}{2}|\psi|^2 + \frac{g_1}{2}|\psi|^4 - \frac{g_2}{3}|\psi|^6, \tag{10.1}$$

where we have dropped the tildes from g_1 and g_2. Note that this is minus the definition given in some treatments.

10.1.1 One soliton

In chapter 4, consideration of the scalings Eq. (4.30) shows that two limits exist: $\omega \gg g_1$, and $g_1 \gg \omega$. g_2 may not be scaled. In the case $g_1 \gg \omega$, we use a soliton ansatz, and consider the effect on the solution of ramping up g_2. In the opposite limit, $\omega \gg g_1$, we consider a Gaussian ansatz and again consider the effect of ramping up g_2.

Soliton ansatz

Motivated by the single-soliton solution [Eq. (3.2)] of the 1D GPE [Eq. (3.1)], we employ the following varational ansatz:

$$\psi(x; A, B, q, \phi_1, \phi_2) = B\mathrm{sech}A(x-q)\exp\left[i\phi_1(x-q) + i\phi_2\right], \tag{10.2}$$

and impose that the action

$$S = \int\int_{-\infty}^{\infty} \mathcal{L}_{\mathrm{KM}} dx dt \tag{10.3}$$

be stationary for all variations in the variables A, q, ϕ_1 and ϕ_2. The Lagrangian becomes:

$$L = 2\frac{B^2}{A}\left(\dot{\phi}_2 - \dot{q}\phi_1\right) + \phi_1^2\frac{B^2}{A} + \frac{B^2 A}{3} + \frac{2B^4}{3A}g_1 - \frac{16}{45}g_2\frac{B^6}{A} + B^2\frac{\omega^2}{2}\left(\frac{2q^2}{A} + \frac{\pi^2}{6A^3}\right), \tag{10.4}$$

and the Euler-Lagrange equations yield the dynamics of the solitary-wave parameters:

The Euler-Lagrange equation for ϕ_2 implies:

$$\frac{2B^2}{A} = \text{const.}, \tag{10.5}$$

i.e., the norm is conserved. Note that constraining the norm of ψ to one implies $A = 2B^2$.

The normalisation condition, along with the Euler-Lagrange equations for A and B, implies:

$$A\left(\frac{1}{2} - \frac{g_2}{8}\frac{16}{15}\right) + \frac{g_1}{4} = -\frac{\omega^2}{18A^3}. \tag{10.6}$$

When $\omega = 0$, this reduces to:

$$B^2 = A/2 = \frac{-g_1}{4 - 16g_2/15}. \tag{10.7}$$

This shows that A and B are conserved individually, and that when $\omega = 0$, $g_2 = 24\ln(4/3)m\omega_r a^2 N^2/\hbar < 3.75$, or else A and B become undefined. As g_2 approaches this limit, the soliton becomes increasingly narrow and peaked. This is qualitatively consistent with the analytical solution [51], and essentially predicts the collapse of the solution as $N \to N_{\max} = \sqrt{3.75\hbar/24\ln(4/3)m\omega_r a^2} = ka_r/a$, where a_r is the harmonic length. The collapse parameter $k = \sqrt{3.75/24\ln(4/3)} \approx 0.74$ compares with the exact result of Khaykovich and Malomed of $k = \sqrt{3/192\ln(4/3)}\pi \approx 0.73$ [51]. This compares with values in the literature of about $k = 0.675$ for numerical experiments with the 3D GPE [83]. When ω is finite, for large enough A, the term in ω in Eq. (10.6) can be neglected, and the collapse condition is the same as in the homogeneous case. By taking parameters close to the recent experiment of Strecker *et al.* [17], we find $N_{\max} \approx 15672$. With the value of $N = 5000$ particles per soliton which was observed in the Strecker experiment, and that we have generally been using in this thesis, $g_2 = 0.382$, which is well below the collapse limit.

The Euler-Lagrange equations for q and ϕ_1 give the trajectory of the soliton:

$$\dot{q} = \phi_1, \tag{10.8}$$

and

$$\ddot{q} = -\omega^2 q. \tag{10.9}$$

This is the oscillatory behaviour as expected.

Clearly, when $\omega = 0$

$$\dot{q} = \phi_1 = \text{const.}, \tag{10.10}$$

and the solitons move at constant speed.

The Euler-Lagrange equations collectively imply the phase behaviour:

$$\phi_2 = \left[\frac{1}{2}\dot{q}^2 + \frac{\omega^2}{2} + \left(\frac{2}{3} + \frac{8g_2}{45}\right)\frac{g_1^2}{(4 - 16g_2/15)^2} - \frac{g_1^2}{12 - 16g_2/5}\right] t + \phi_0. \tag{10.11}$$

Note that when g_2 is zero, we recover the 1D GPE solution [Eq. (6.16)].

Coherent state ansatz

We now proceed with a coherent state ansatz, useful when the effects of g_1 are small compared with those of ω:

$$\psi(x; A, B, q, \phi_1, \phi_2) = B \exp\left[-A^2(x-q)^2\right] \exp\left[i\phi_1(x-q) + i\phi_2\right]. \tag{10.12}$$

The Lagrangian then becomes:

$$L = \frac{B^2}{A}\sqrt{\frac{\pi}{2}}\left(\dot{\phi}_2 - \phi_1\dot{q} + \frac{\phi_1^2}{2} + \omega^2 2q^2\right) + \frac{\omega^2}{2}\frac{B^2}{A^3} + AB^2\frac{\sqrt{2\pi}}{4} + g_1\frac{B^4}{4A} + g_2\frac{B^6}{3\sqrt{6}A}. \tag{10.13}$$

The Euler-Lagrange equation for ϕ_2 again implies a relationship between the height and width of our ansatz:

$$\frac{B^2}{A} = \text{const.} \tag{10.14}$$

Our normalisation condition implies that in this instance, the constant is equal to $\sqrt{2/\pi}$.

The Euler-Lagrange equations for q and ϕ_1 are the same as for the soliton ansatz:

$$\dot{q} = \phi_1, \tag{10.15}$$

$$\ddot{q} = -\omega^2 q. \tag{10.16}$$

The Euler-Lagrange equations for B^2 and A^{-1} give the equation:

$$-\frac{\omega^2}{2}\frac{2\sqrt{2\pi}}{8A^3} + \frac{\sqrt{2\pi}A}{2} - g_2\frac{4A}{\sqrt{63\pi}} + g_1\frac{\sqrt{2}}{2\sqrt{\pi}}\left(1 - \frac{A^2}{2}\right) = 0 \tag{10.17}$$

We are interested in the limit where $g_1 = 0$,

$$A^4 = \frac{\omega^2\sqrt{2\pi}}{8\left(\sqrt{2\pi}/2 - 4g_2/3\sqrt{6\pi}\right)}. \tag{10.18}$$

This reduces to the expression for a coherent state when g_2 is zero. The inclusion of g_2 reveals a collapse condition in this regime. This collapse parameter is larger than that for a soliton ansatz by approximately a factor of two, showing that Gaussian-shaped solutions are more stable against collapse than sech-shaped solutions. This result is consistent with the result in Ref. [86] that ramping up the axial trap from zero increases the critical particle number until the trap geometry is spherical. Note that Eq. (4.30) is not valid when the axial trap is of comparable strength to the radial trap such that the motion in both directions is of the same speed, however, it is still valid for cases where the axial trap is weaker than the radial trap but more significant than the cubic nonlinearity.

The Euler-Lagrange equations also imply the phase behaviour:

$$\dot{\phi}_2 = \frac{\dot{q}^2}{2} - \frac{\omega^2}{2}q^2 - \frac{1}{A^2}\frac{\omega^2}{8} + \frac{A^2}{2} + g_1\frac{A}{\pi} + g_2\frac{2A^2}{\sqrt{3\pi}\pi}. \tag{10.19}$$

This reduces to the expression for a coherent state when g_1 and g_2 are zero. The only effect of the nonlinearities on the phase is additions to the chemical potential term (linear in time).

10.1.2 Two solitons

Khaykovich and Malomed [51] examine a formal superposition of two solitary-wave solutions to Eq. (4.30) and conjecture that the asymmetry in such a solution is connected to the asymmetric collisions between two solitary-waves. In order to investigate the inelastic collisions of two solitons in more detail, we would like to do a variational calculation with the full two soliton solution to the homogeneous 1D GPE (which is given explicitly in Ref. [31]), or by a formal superposition of two single solitons. Both of these approaches involve integrals in the Lagrangian that have proved difficult to evaluate analytically. The problem may be simplified since it may not be necessary to evaluate the whole Lagrangian in the case of two solitons, but only the terms in g_2, since we may be able to infer the form of the rest of the Lagrangian from the known

behaviour of the solution of the 1D GPE. We leave these problems as avenues for future work.

Chapter 10 Summary

- Three dimensional effects can be investigated by examining a nonlinear Schrödinger equation with a quintic term.
- We can examine the properties of the solutions by using a variational approach.
- When the trap is weak compared with the cubic nonlinear term, a soliton single ansatz predicts a collapse of the condensate when the soliton comprises a large number of particles.
- When the trap is strong compared with the cubic nonlinear term, a Gaussian ansatz predicts collapse for a large number of particles (different from the result for a soliton ansatz).
- The interpolating behaviour between strong and weak trap is an area for future study.
- The collisional behaviour of two solitary waves is another area for future study.

Chapter 11

Conclusions and future work

In this thesis we have investigated the consequences of non-integrability on the solitary waves in trapped Bose-Einstein condensates caused by an axial harmonic trap, and non-integrability caused by three dimensional effects.

To analyse the soliton-like nature of the solitary-waves in an axial harmonic trap, we adapted a particle analogy for the solitary-waves, first used in a nonlinear optics context in Refs. [32–34]. Exact soliton solutions exist in strictly one-dimensional systems in the absence of an external trapping potential. These solitons behave in a particle-like manner, and we showed the particle analogy to be a good model also when a harmonic trapping potential is present up to a gradual shift in the trajectories when the harmonic trap period is short compared with the collision time of the solitons. We showed that the collision time of the solitons is dependent on the relative phase of the solitons as they collide. The gradual shift in trajectories may, in fact, be a useful indicator of the relative phase of solitons in interferometry experiments.

In the case of two solitons, we showed that the particle model is integrable, and the dynamics are completely regular. In the case of a system of two solitary waves of equal norm, we showed that, due to the conservation of parity and the seperability of the centre-of-mass motion in harmonically trapped systems, the solitons retain their phase difference for repeated collisions. This phase preservation can be used to find regimes where there is agreement between the wave and particle models. This also implies that soliton-like regimes may be found in 3D geometries where solitary waves can be made to repeatedly collide

out of phase, stabilising the condensate against collapse [83].

The extension to three particles supports both regular and chaotic regimes. The trajectory shift observed for two solitons carries over to the case of three solitons. This shift aside, the agreement between the particle model and the wave dynamics remains good, even in chaotic regimes. We predict that these chaotic regimes will be an indicator of rapid depletion of the condensate due to quantum transitions of the condensate particles into non-condensate modes. To produce a firm theoretical prediction of such depletion, one must integrate the modified Bogoliubov-de Gennes equations. Such an integration requires knowledge of the initial condition of the system of condensate and non-condensate atoms in order to arrive at a physically meaningful result. Hence, an avenue for future work is to simulate the soliton formation from an initial equilibrium condition whilst keeping track of the condensate and non-condensate particles before continuing to integrate the dynamics of condensate and noncondensate particles.

Another interesting avenue for future work is to investigate the soliton dynamics when the axial trap is not harmonic. Laser trapping of atoms provides Gaussian traps; in these traps the particle model is thought not to be seperable even for two solitons. Thus chaotic regimes of two solitons may be possible.

To analyse the residual effects of the three dimensional nature of the solitary waves, we used a nonlinear Schrödinger equation with an additional quintic term derived by Khaykovich and Malomed [51]. We performed variational calculations, and confirmed the collapse of a soliton when the number of particles contained therein is increased past a critical number. When the nonlinear term is decreased relative and/ or the axial trap frequency is increased, the solution is close to a Gaussian, but collapse still occurs. Future work could be done to find the interpolating behaviour between these two regimes.

We propose additional further work in which the variational treatment is extended to two solitons. This approach could provide a theoretical model for particle exchange between the solitons and conditions for collapse during soliton collisions.

Appendix A

Numerical method for integrating the Gross-Pitaevskii equation

The results of integrating the Gross-Pitaevskii equation have been obtained numerically in this thesis by using a Crank Nicolson method [91] with a Numerov approximation [92] of the spatial derivative. The Numerov method gives a greater numerical accuracy than the basic Crank Nicolson method for a given spacial step size, and is consequently less prone to numerical errors. In this appendix, we outline the basic Crank Nicolson method before describing the incorporation of the Numerov approximation.

A.1 Crank Nicolson Method

We define the nonlinear operator $H(x)$ by its action on the wavefunction $\psi(x,t)$:

$$H(x)\left[\psi(x,t)\right] := \left[-\frac{1}{2}\frac{\partial^2\psi}{\partial^2 x} + V(x,t) - |\psi(x,t)|^2\right]\psi(x,t), \tag{A.1}$$

The equation

$$i\frac{\partial}{\partial t}\psi(x,t) = H(x)\left[\psi(x,t)\right] \tag{A.2}$$

has the approximate solution

$$\psi(x,t+\Delta t) = \exp(-iH(x)\Delta t)\left[\psi(x,t)\right] \tag{A.3}$$

when $\Psi(x,t)$ varies slowly enough over Δt such that $H(x)$ may be treated like a linear operator.

We may approximate the time operator using Cayley's form [91]:

$$\exp(-iH(x)\Delta t) = \frac{1 - iH(x)\Delta t/2}{1 + iH(x)\Delta t/2} + O(\Delta t^3). \tag{A.4}$$

The numerical evolution is hence described by

$$[1 + iH(x)\Delta t/2]\,\psi(x, t + \Delta t) = [1 - iH(x)\Delta t/2]\,\psi(x,t). \tag{A.5}$$

To describe the wave equation numerically, we must treat the wavefunction as a vector $\vec{\psi}(t)$ with N entries $\psi(x_n, t)$, indexed by N space steps of size Δx. The operator, $H(x)$, can be approximated up to $O(\Delta x^3)$ by

$$H(x_n)\,[\psi(x_n,t)] = \left[-\frac{1}{2}\delta_x^2 + V(x_n,t) - |\psi(x_n,t)|^2\right]\psi(x_n,t), \tag{A.6}$$

where δ_x^2 is the central difference operator defined by

$$\delta_x^2\psi(x,t) := \frac{\psi(x + \Delta x, t) + \psi(x - \Delta x, t) - 2\psi(x,t)}{\Delta x^2}. \tag{A.7}$$

If $V(x)$ gets sufficiently large at the edges of our spacial grid that the wavefunction is negligibly small there, we may ignore the boundary conditions. The evolution equation [Eq. (A.5)] becomes a matrix equation:

$$[1 + iH(t + \Delta t)\Delta t/2]\,\vec{\psi}(t + \Delta t) = [1 - iH(t)\Delta t/2]\,\vec{\psi}(t), \tag{A.8}$$

where $H(t)$ is the (time-dependent) matrix:

$$H_{\text{matrix}}(t) = \begin{pmatrix} f(x_1,t) & -1 & 0 & 0 & \cdots & 0 \\ -1 & f(x_2,t) & -1 & 0 & \cdots & 0 \\ 0 & & \ddots & & & \vdots \\ \vdots & & & \ddots & & 0 \\ 0 & \cdots & 0 & -1 & f(x_{N-1},t) & -1 \\ 0 & \cdots & 0 & 0 & -1 & f(x_N,t) \end{pmatrix},$$

and $f(x_n,t) = 2 + V(x_n) - \psi(x_n,t)$. The difference equation [Eq. (A.8)] can now be integrated numerically by using the well known algorithm for a tri-diagonal matrix equation [91]. Because the equation is nonlinear, the tri-diagonal matrix on the left hand side of Eq. (A.8) is a function of $\vec{\psi}(t+\Delta t)$ (the desired solution). Consequently, the previous value of $\vec{\psi}(t)$ must be used, and the process iterated until the solution converges. It is found [93] that only one iteration is required in practice.

A.2 Numerov Method

The Crank Nicolson method is accurate up to $O(x^3)$. However, by using the Numerov approximation of the spatial derivative, we obtain a method accurate up to $O(x^6)$.

By making Taylor expansions of $\psi(x+\Delta x)$ and $\psi(x-\Delta x)$ around x we can obtain the following expression

$$\psi(x+\Delta x)+\psi(x-\Delta x)-2\psi(x)=\psi^{(2)}(x)(\Delta x)^2+\frac{1}{12}\psi^{(4)}(x)(\Delta x)^4+O(\Delta x^6). \tag{A.9}$$

Taking a centred difference expression for the fourth derivative:

$$\psi^{(4)}(x)=\delta_x^2\psi^{(2)}(x)+O(\Delta x^3), \tag{A.10}$$

equation (A.9) becomes

$$(\Delta x)^2\delta_x^2\psi(x)=(\Delta x)^2\psi^{(2)}(x)+\delta_x^2\psi^{(2)}(x)\frac{(\Delta x)^4}{12}+O(\Delta x^6). \tag{A.11}$$

We arrive at an expression for the second derivative of our wave function up to accuracy $O(\Delta x^6)$:

$$(1+\frac{1}{12}(\Delta x)^2\delta_x^2)\frac{\partial^2\psi(x,t)}{\partial x^2}\approx\delta_x^2\psi(x,t). \tag{A.12}$$

By defining the operator $M_x:=(1+(\Delta x)^2\delta_x^2/12)$, which, in matrix form, is given by:

$$M=\frac{1}{12}\begin{pmatrix}10 & 1 & 0 & 0 & \cdots & 0\\ 1 & 10 & 1 & 0 & \cdots & 0\\ 0 & & \ddots & & & \vdots\\ \vdots & & & \ddots & & 0\\ 0 & \cdots & 0 & 1 & 10 & 1\\ 0 & \cdots & 0 & 0 & 1 & 10\end{pmatrix},$$

we obtain

$$\frac{\partial^2\psi(x,t)}{\partial x^2}=M_x^{-1}\delta_x^2\psi(x,t). \tag{A.13}$$

The evolution equation [Eq. (A.5)] becomes

$$\left[1-\frac{i\Delta t}{2}\left(-\frac{1}{2}M_x^{-1}\delta_x^2+V(x_n)-|\psi(x_n,t+\Delta t)|^2\right)\right]\psi(x_n,t+\Delta t)$$
$$=\left[1+\frac{i\Delta t}{2}\left(-\frac{1}{2}M_x^{-1}\delta_x^2+V(x_n)-|\psi(x_n,t)|^2\right)\right]\psi(x_n,t), \tag{A.14}$$

or, equivalently:

$$\left[M_x - \frac{i\Delta t}{2}\left(-\frac{1}{2}\delta_x^2 + M_x(V(x_n) - |\psi(x_n, t+\Delta t)\|^2)\right)\right]\psi(x_n, t+\Delta t)$$
$$= \left[M_x + \frac{i\Delta t}{2}\left(-\frac{1}{2}\delta_x^2 + M_x(V(x_n) - |\psi(x_n, t)|^2)\right)\right]\psi(x_n, t), \qquad \text{(A.15)}$$

which can now be written in matrix form and integrated by a tri-diagonal matrix routine as described in section A.1. As in the simple Crank Nicolson routine, there is $\vec{\psi}(t+\Delta t)$ dependence in the tridiagonal matrix, so again the previous solution is used and the process iterated until the solution converges. Again, this is achieved with a single iteration.

$$\left[M_x - \frac{i\Delta t}{2}\left(-\frac{1}{2}\delta_x^2 + M_x(V(x_n) - |\psi(x_n, t)|^2)\right)\right]\tilde{\psi}(x_n, t+\Delta t)$$
$$= \left[M_x + \frac{i\Delta t}{2}\left(-\frac{1}{2}\delta_x^2 + M_x(V(x_n) - |\psi(x_n, t)|^2)\right)\right]\psi(x_n, t), \qquad \text{(A.16)}$$

$$\left[M_x - \frac{i\Delta t}{2}\left(-\frac{1}{2}\delta_x^2 + M_x(V(x_n) - \left|\tilde{\psi}(x_n, t+\Delta t)\right|^2)\right)\right]\psi(x_n, t+\Delta t)$$
$$= \left[M_x + \frac{i\Delta t}{2}\left(-\frac{1}{2}\delta_x^2 + M_x(V(x_n) - |\psi(x_n, t)|^2)\right)\right]\psi(x_n, t), \qquad \text{(A.17)}$$

A.3 FORTRAN code

We implemented the Crank-Nicholson Numerov method using the following FORTRAN code. This particular code evolves two solitons in a harmonic trap corresponding to Fig. 7.2(b).

We first declare variables etc.

```
PROGRAM CNmethod
IMPLICIT NONE
INTEGER, parameter ::  X=6000, T=200000*5*10
integer:: xind, tind, period, check
REAL*8 :: dx,rdt
REAL*8,DIMENSION(X):: V, density
REAL*8 :: PI,k
COMPLEX*16, DIMENSION(X) ::  Hpsi, a, b,c,a2,b2,c2, Hpsi1, Hpsi2
COMPLEX*16, DIMENSION(0:X+1) :: psi, psi1, psi2
COMPLEX*16:: dt
REAL*8 ::eta1,eta2,q1,q2,qd1,qd2
```

We then define the space and timesteps, π and the period with which we sample our wavefunction for plotting puposes.

```
dx=0.1d0 !SPACESTEP
rdt=0.0005d0 !TIMESTEP
period=1000
PI=4.0d0*ATAN(1.0d0)
```

We then define the trap constant $k = \omega^2/2$, and the soliton parameters η_i, q_i and $\dot{q}_i$.

```
k=9.99d-5
eta1=0.25d0/2.0d0
eta2=0.25D0/2.0d0
q1=-15.0d0
q2=15.0d0
qd1=0.0d0
qd2=0.0d0
```

We then define the harmonic potential and individual solitons,

```
DO xind=1,x
V(xind)=k*DBLE(xind-3000)*DBLE(xind-3000)*dx*dx
END DO
DO xind=1,X
   psi1(xind)=2.0d0*eta1*EXP(DCMPLX(0.0D0,qd1*(xind-3000)*dx))/COSH(2.0d0*eta1*(((xind-3000)*dx)-q1))
   psi2(XIND)=2.0d0*eta2*EXP(DCMPLX(0.0D0,qd2*(xind-3000)*dx+PI))/COSH(2.0d0*eta2*(((xind-3000)*dx)-q2))
END DO
```

before adding the solitons to form the initial condition. We pin the ends of the wavefunction to zero to form box boundary conditions. (This condition is unnecessary for the case of an attractive condensate in a harmonic potential, since the density should always be zero towards the edge of the range of x; but we include it for completeness.)

```
DO xind=1,x
 Psi(xind)=Psi1(xind)+Psi2(xind)
 density(xind)=ZABS(psi(xind))*ZABS(psi(xind))
END DO
psi(0)=(0.0d0,0.0d0)!PINS EDGE OF THE SOLUTION TO ZERO
psi(X+1)=(0.0d0,0.0d0)
```

We then evolve the wavefunction for T timesteps, calling the subroutines Matrixop2, RHS and Tridiag a number of times. These subroutines solve the

tridiagonal matrix equations [Eqs. (A.16) and (A.17)]; the functions of the subroutines are described below. We write out the density ψ^2 every 1000 timesteps. For this simulation the time variable is real-valued. Note, however, that the time variable is of complex type, and the code may be easily adapted to run in imaginary time for the purposes of finding a ground state (see section 6.2.1).

```
dt=DCMPLX(rdt,0.0d0)
DO tind=1,T,1

  IF (MOD(tind,period)==0) then !SELECTS TIMES TO WRITE TO FILES
    DO xind=1,X
         IF (xind>2300 .and. xind<3701)THEN
              WRITE (1904,*) REAL(density(xind))          !WRITES DENSITY
         END IF
    END DO
  END IF

   check=0
   CALL Matrixop2 (X,dt,dx,density,V,psi,a,b,c,check,a2,b2,c2)
   CALL RHS (X,a2,b2,c2,Psi,HPsi)
   CALL Tridiag (a,b,c,HPsi,Psi,X,tind)
   check=1
   CALL Matrixop2(X,dt,dx,density,V,psi,a,b,c,check,a2,b2,c2)
   CALL Tridiag (a,b,c,HPsi,Psi,X,tind)

END DO

STOP

END PROGRAM
```

The subroutine Matrixop2 defines the variables a, b and c, which are the "tridiagonals" of the tridiagonal matrix of the left and right-hand side of Eq. (A.16) on the first call, and the left-hand side of Eq. (A.17) on the second call.

```
SUBROUTINE MATRIXOP2(X,dt,dx,density,V,psi,a,b,c,check,a2,b2,c2)
INTEGER :: j, xind, X,i, check
REAL*8 :: Y(x),dx,z,redt
COMPLEX*16 :: psi(0:X+1),a(X),b(X),c(x),HPsi(X),a2(X),b2(X),c2(x)
COMPLEX *16 :: dt
REAL*8:: V(X), density(X)
69 FORMAT (F14.8,3X,F14.8,X,F14.8,3X,F14.8,3X,F14.8)
Psi(0)=0.0d0
Psi(X+1)=0.0d0
redt=real(dt)
write(250,*) redt
DO xind=1,X,1
  density(xind)=zabs(psi(xind))*zabs(psi(xind))
```

```
 y(XIND)=- density(xind)+V(xind)+0.0d0 !effective potential
ENDDO
DO xind=1,X,1

   b(xind)=DCMPLX(10.0d0/12.0d0,(redt/2.0d0)*((1/(dx**2))+(10.0d0/12.0d0)*y(xind)))
   b2(xind)=DCMPLX(10.0d0/12.0d0,(-redt/2.0d0)*((1/(dx**2))+(10.0d0/12.0d0)*y(xind)))
  if(xind>1)then
     a(xind)=DCMPLX(1.0d0/12.0d0,(redt/2.0d0)*(-(1.0d0/(2.0d0*dx**2))+(1.0d0/12.0d0)*y(xind-1)))
     a2(xind)=DCMPLX(1.0d0/12.0d0,(-redt/2.0d0)*(-(1.0d0/(2.0d0*dx**2))+(1.0d0/12.0d0)*y(xind-1)))
  endif
  if(xind<x)then
   c(xind)=DCMPLX(1.0d0/12.0d0,(redt/2.0d0)*(-(1.0d0/(2.0d0*dx**2))+(1.0d0/12.0d0)*y(xind+1)))
   c2(XIND)=DCMPLX(1.0d0/12.0d0,(-redt/2.0d0)*(-(1.0d0/(2.0d0*dx**2))+(1.0d0/12.0d0)*y(xind+1)))
  endif
   if (check==0)then
   HPsi(xind)=DCONJG(a(xind))*(Psi(xind-1)+Psi(xind+1))+DCONJG(b(xind))*Psi(xind)
   end if
END DO
END
```

The subroutine RHS computes the RHS of Eqs. (A.16) and (A.17). Since these are the same, the subroutine is called only once for each timestep.

```
SUBROUTINE RHS (X,a2,b2,c2,Psi,HPsi)
INTEGER :: X, xind
COMPLEX*16::Psi(0:X+1),a2(X),b2(X),c2(x), HPsi(X)
DO xind=1,X,1
 HPsi(xind)=(a2(xind))*(Psi(xind-1))+(b2(xind))*Psi(xind)+c2(xind)*Psi(xind+1)
ENDDO
END
```

The Tridiag subroutine takes a, b and c, and solves the tridiagonal matrix equations [Eq. (A.16) and Eq. (A.17)] for $\tilde{\psi}(x_n, t+\Delta t)$ and $\psi(x_n, t+\Delta t)$ when it is called for the first and second time respectively.

```
SUBROUTINE Tridiag(a,b,c,HPsi,Psi,X,tind)
INTEGER :: h,X,tind,check
COMPLEX*16 :: bet, gam(X)
COMPLEX*16 :: b(X), a(X),c(x), HPsi(X),Psi(0:X+1)

bet=b(1)
Psi(1)=HPsi(1)/bet
DO h=2,X
   gam(h)=c(h-1)/bet
   bet=b(h)-a(h)*gam(h)
   if (bet.eq.0.)then
      pause 'ertri'
      write (*,*)tind, check, b(h), a(h),c(h)
```

```
   end if
   Psi(h)=(HPsi(h)-a(h)*Psi(h-1))/bet
END DO
DO h=X-1,1,-1
   Psi(h)=Psi(h)-gam(h+1)*Psi(h+1)
END DO

RETURN
END
```

Appendix B

Codes for integrating particle model

B.1 Model for two solitons

This code integrates the two-soliton particle model using numerical integration from NAG routines. The regime corresponds to that in Fig. 7.2(b).

The script calls the NAG routines D02LAF,D02LXF,D02LZF.

We start by declaring variables and external routines.

```
PROGRAM PARTICLE_ANALOGY
implicit none
INTEGER NEQ,LRWORK,IFAIL
PARAMETER (NEQ=2,LRWORK=580)
INTEGER MAXSTP
DOUBLE PRECISION:: T,TEND,Y(NEQ),YP(NEQ),YDP(NEQ),RWORK(LRWORK),TNEXT,YWANT(NEQ),YPWANT(neq),ETA1,ETA2,k1
DOUBLE PRECISION:: H,TOL,THRES(NEQ),THRESP(NEQ),TINC,YOLD(NEQ)
LOGICAL START, ONESTP,HIGH
EXTERNAL D02LAF,D02LXF,FCN,D02LZF
TINC=0.10D0
H=0.0d0 !STEP SIZE
TOL=5d-15 !ERROR PARAMETER
THRES(1)=0.0d0
THRESP(1)=0.0d0
MAXSTP=0
ONESTP=.true. !.TRUE. RETURNS EVERY STEP; .FALSE AT END ONLY
HIGH=.false. !HIGH ORDER INTEGRATION
start=.true.
IFAIL=0 ! IN EVENT OF FAILURE GIVES FAILURE TYPE
PI=4.0d0*ATAN(1.0d0)
```

We initially call D02LXF and define the initial conditions and parameters of our system.

```
CALL D02LXF(NEQ,H,TOL,THRES,THRESP,MAXSTP,START,ONESTP,HIGH,RWORK,LRWORK,IFAIL)
!initial conditions
Y(1)=-15.0d0
Y(2)=15.0d0
YP(1)=0.0d0
YP(2)=0.0d0
ETA1=0.25d0/2.0d0
ETA2=0.25d0/2.0d0
T=0.0d0
TEND=5000
TNEXT=T+TINC
```

We call the NAG routines for times less than TEND. We read out the trajectories for a position vs. time plot and for the Poincaré section (Fig. 7.1).

```
20 IFAIL=-1
 CALL D02LAF(FCN,NEQ,T,TEND,Y,YP,YDP,RWORK,LRWORK,IFAIL)
40 IF (TNEXT.LE.T)THEN
    IFAIL=0
    CALL D02LZF(NEQ,T,Y,YP,NEQ,TNEXT,YWANT,YPWANT,RWORK,LRWORK,IFAIL)
    CALL FCN (NEQ,T,Y,YDP)!TEST PURPOSES

    WRITE(001,*)YWANT(1),TNEXT
    WRITE(002,*)YWANT(2),TNEXT

    IF((YOLD(2)>0.0D0 .AND. YWANT(2)<0.0D0).OR.(YOLD(2)<0.0D0 .AND. YWANT(2)>0.0D0))THEN
          WRITE(003,*) YPWANT(1)/0.055D0, YWANT(1) !TO POINCARE SECTION
    ENDIF

    YOLD(1)=YWANT(1)
    YOLD(2)=YWANT(2)
    TNEXT=TNEXT+TINC

    GO TO 40
 ENDIF

 IF (T.LT.TEND) GO TO 20

ENDPROGRAM
```

The following subroutine returns the second time derivatives of the particle positions, i.e., Newton's/Lagrange's equations of motion. It is used by the NAG routines.

```
SUBROUTINE FCN (NEQ,T,Y,YDP)
implicit none
INTEGER NEQ
DOUBLE PRECISION ::T,Y(NEQ),YDP(NEQ)
DOUBLE PRECISION :: EPSILON,K,ETA1,ETA2
DOUBLE PRECISION :: K1,K2
EPSILON=1.0d0!0.001*2.0d0
K=2.0d0*9.99d-5
ETA1=0.25d0/2.0d0
ETA2=0.25d0/2.0d0
K1=2.0D0*ETA1*ETA2/(ETA1+ETA2)
K2=-K1
YDP(1)=(-4*k*EPSILON*Y(1) -16*ETA2*(ETA1+ETA2)*K1*TANH(K1*(Y(1)-Y(2)))/(((COSH((K1*(Y(1)-Y(2)))))**2))/4
YDP(2)=(-4*K*EPSILON*Y(2) -16*ETA1*(ETA1+ETA2)*K2*TANH(K1*(Y(1)-Y(2)))/(((COSH((K1*(Y(1)-Y(2)))))**2))/4
RETURN
ENDSUBROUTINE
```

B.2 Model for three solitons

This code integrates the three-soliton particle model. It uses NAG routines D02EJF and D02EJW for integrating stiff systems, i.e., those systems with dynamics on two or more different timescales. As described in chapter 2, a trajectory is likely to be chaotic when there is a resonance between two frequencies of motion - clearly this is an indication that the system might stiff. We suspect the three-soliton particle model may be stiff, and in chapter 8 we find chaotic trajectories (using the code below). The trajectories generated by this code with these parameters are those of Fig. 8.1(b).

The code generates trajectories on the Poincaré section of reduced energy $H_r = 10$. The initial values of the coordinates q_c, q_r, and p_c are chosen randomly from a uniform distribution and rejected if, this choice does not define an initial value of p_r on the surface of constant reduced energy. The random numbers are generated using the NAG routines: G05CAF and G05CBF.

```
PROGRAM PARTICLE_ANALOGY
IMPLICIT NONE
INTEGER NEQ,IW,IFAIL
PARAMETER (NEQ=4,IW=(12+NEQ)*NEQ+50)
INTEGER STEPNO!COMMON
DOUBLE PRECISION:: T,Y(NEQ),W(IW)
DOUBLE PRECISION:: TEND,H!COMMON
DOUBLE PRECISION:: TOL
DOUBLE PRECISION :: Q1,Q2,Q3,P1,P2,P3,ENERGY,ETA,QD1,QD2,QD3,F,k,A,B,C
```

```
DOUBLE PRECISION ::YOLD,TOLD
INTEGER NOUT, TINT
PARAMETER (NOUT=6)
DOUBLE PRECISION:: X
INTEGER I, period,J
DOUBLE PRECISION:: G05CAF
EXTERNAL G05CAF
EXTERNAL G05CBF
LOGICAL START, ONESTP,HIGH

EXTERNAL FCN, PEDERV, OUT
EXTERNAL D02EJF,D02EJW

DOUBLE PRECISION:: XOLD(NEQ), XPOLD(NEQ)
COMMON /DATA1/ TOLD, YOLD(NEQ),J,I

CALL G05CBF(0) !INITIALISES RANDOMS

ENERGY=10.0d0
eta=0.25d0/3.0d0
K=((2.0d0*1.97d-5))/(eta**4)
DO I=1,24                    !RUNS FOR DIFFERENT INITIAL CONDITIONS
    10   X=G05CAF(X)
    Q1=25.0d0*X -12.5d0 !INITIAL qc
    X=G05CAF(X)
    Q2=75.0d0*X -37.5d0 !INITIAL qr
    X=G05CAF(X)
    P1=X-0.5d0 !INITIAL pc
    A=0.5D0*q2+q1
    B=2.0D0*q1
    C=-0.5D0*q2+q1
    F=P1**2/4.0d0 + K*q1**2+ k*q2**2/(12.0d0) -4.0D0/(COSH(A)**2) -4.0D0/(COSH(B)**2) -4.0D0/(COSH(C)**2)
    IF ((ENERGY-F).LT.0)THEN
       GO TO 10
    END IF

   P2=SQRT((1/3.0d0)*(Energy-F)) !INITIAL pr

   H=0.5d0 !STEP SIZE
   TOL=5d-15!ERROR PARAMETER
   IFAIL=0
   T=0.0D0
   Y(1)=Q1
   Y(2)=Q2
   Y(3)=P1
   Y(4)=P2
   YOLD(1)=Y(1)
   YOLD(2)=Y(2)
   YOLD(3)=Y(3)
   YOLD(4)=Y(4)
   T=0.0d0 !INITIAL TIME
   TEND=200 !END TIME
```

```
   CALL D02EJF(T,TEND,NEQ,Y,FCN,PEDERV,TOL,'DEFAULT',OUT,D02EJW,W,IW,IFAIL) !NAG INTEGRATION
END DO
ENDPROGRAM
```

This subroutine defines Hamilton's equations for the system. It is called by the NAG routine.

```
SUBROUTINE FCN (T,Y,F)
IMPLICIT NONE
INTEGER ::NEQ
PARAMETER (NEQ=4)
DOUBLE PRECISION ::T,Y(NEQ),F(NEQ)
DOUBLE PRECISION :: K,eta
DOUBLE PRECISION :: A,B,C,A2,A3
DOUBLE PRECISION:: M,Ci,TCROSS,MY,MPY,CY,CPY,YINT,YPINT
eta=0.25d0/3.0d0
K=((2.0d0*1.97d-5))/(eta**4)
A=0.5D0*Y(2)+Y(1)
B=2.0d0*Y(1)
C=-0.5d0*Y(2)+Y(1)

F(1)=Y(3)/2.0d0!QCDOT
F(2)=Y(4)*6.0d0!QRDOT
F(3)=-2.0d0*K*Y(1) - 8.0D0*TANH(A)/(COSH(A)**2) -16.0d0*TANH(B)/(COSH(B)**2)- 8.0D0*TANH(C)/(COSH(C)**2)!PCDOT
F(4)=-K*Y(2)/6.0d0 - 4.0D0*TANH(A)/(COSH(A)**2) + 4.0D0*TANH(C)/(COSH(C)**2)

RETURN
ENDSUBROUTINE
```

This subroutine defines the elements of the Jacobian. It is called by the NAG routine.

```
SUBROUTINE PEDERV(T,Y,PW) !JACOBEAN ELEMENTS
IMPLICIT NONE
INTEGER NEQ
PARAMETER (NEQ=4)
DOUBLE PRECISION :: T, Y(NEQ), PW(NEQ,NEQ)
DOUBLE PRECISION :: A,B,C,A2,A3,K,eta
eta=0.25d0/3.0d0
K=((2.0d0*1.97d-5))/(eta**4)
A=0.5D0*Y(2)+Y(1)
B=2.0D0*Y(1)
C=-0.5D0*Y(2)+Y(1)

PW(1,1)=0.0D0
PW(1,2)=0.0D0
PW(1,3)=0.5D0
PW(1,4)=0.0D0
```

```
PW(2,1)=0.0D0
PW(2,2)=0.0D0
PW(2,3)=0.0D0
PW(2,4)=6.0D0
PW(3,1)=-2.0d0*K -8.0D0*(-3.0D0*TANH(A)**2 +1.0D0)/(COSH(A)**2) - 32.0D0*(-3.0D0*TANH(B)**2 +1.0D0)/(COSH(B)**2)
-8.0D0*(-3.0D0*TANH(C)**2 +1.0D0)/(COSH(C)**2)
PW(3,2)=0.0d0-4.0D0*(-3.0D0*TANH(A)**2 +1.0D0)/(COSH(A)**2)+4.0D0*(-3.0D0*TANH(C)**2 +1.0D0)/(COSH(C)**2)
PW(3,3)=0.0D0
PW(3,4)=0.0D0
PW(4,1)=0.0d0-4.0D0*(-3.0D0*TANH(A)**2 +1.0D0)/(COSH(A)**2)+4.0D0*(-3.0D0*TANH(C)**2 +1.0D0)/(COSH(C)**2)
PW(4,2)=-K/6.0d0 -2.0D0*(-3.0D0*TANH(A)**2 +1.0D0)/(COSH(A)**2)-2.0D0*(-3.0D0*TANH(C)**2 +1.0D0)/(COSH(C)**2)
PW(4,3)=0.0D0
PW(4,4)=0.0D0

ENDSUBROUTINE
```

This subroutine is called by the NAG routine. The Poincaré section is computed and the time is evolved. A change of variables is made from the normal coordinates, y_i, to the single particle coordinates, x_i, so that these may be plotted if required. The single particle coordinates depend on the removed centre of mass motion. We make the choice that the centre of mass coordinate is always zero.

```
SUBROUTINE OUT(T,Y)
implicit none
INTEGER :: NEQ,I,J
PARAMETER (NEQ=4)
INTEGER :: TEST,PERIOD
DOUBLE PRECISION :: T,Y(NEQ),K,F(NEQ/2)
DOUBLE PRECISION::TOLD,YOLD,hpart,TCROSS
DOUBLE PRECISION :: X(1+NEQ/2),XP(1+NEQ/2),
double precision ::eta,qt
COMMON /DATA1/ TOLD, YOLD(NEQ),J,I
eta=0.25d0/3.0d0
K=((2.0d0*1.97d-5))/(eta**4)
PERIOD=100

QT=0.0D0!ANALYTICAL SOLUTION IS Q0*cos(sqrt(K)*t) - WE SET Q0=0

X(1)=QT +Y(1)/ETA +(Y(2)/ETA)*(1/6.0D0)!real trajectories
X(3)=2.0D0*(-Y(1)/ETA +0.5D0*X(1))
X(2)=0.5D0*(X(1)+X(3)-Y(2)/ETA)

F(1)=Y(3)/2.0d0!QC sqiggle by dt squiggle
F(2)=Y(4)*6.0d0!QR sim

XP(1)=QT +eta*F(1) +(eta*F(2))*(1/6.0D0)!real VELOCITIES
XP(3)=2.0D0*(-eta*F(1) +0.5D0*XP(1))
XP(2)=0.5D0*(XP(1)+XP(3)-eta*F(2))
```

```
      IF((YOLD(1)>0.0D0 .AND. Y(1)<0.0D0).OR.(YOLD(1)<0.0D0 .AND. Y(1)>0.0D0))THEN  !POINCARE SECTION

         IF(Y(3)<0.0D0)THEN
            WRITE(I+71000,*)  Y(2),Y(4)
         ENDIF
      ENDIF

 TOLD=T
 YOLD(1)=Y(1)
 YOLD(2)=Y(2)
 YOLD(3)=Y(3)
 YOLD(4)=Y(4)

T=T+0.0005D0
RETURN
ENDSUBROUTINE
```

Bibliography

[1] A. D. Martin, C. S. Adams, and S. A. Gardiner, Phys. Rev. A **77**, 013620 (2008).

[2] A. D. Martin, C. S. Adams, and S. A. Gardiner, Phys. Rev. Lett. **98**, 020402 (2007).

[3] A. T. Filippov, *The Versatile Soliton* (Birkhauser, Boston, 2000).

[4] D. J. Korteweg and G. deVries, Philos. Mag. Ser. 5 **39**, 422 (1895).

[5] C. S. Gardner, J. M. Greene, M. D. Kruskal, and R. M. Miura, Phys. Rev. Lett. **19**, 1095 (1967).

[6] N. J. Zabusky and M. D. Kruskal, Phys. Rev. Lett. **15**, 240 (1965).

[7] M. H. Anderson *et al.*, Science **269**, 198 (1995).

[8] K. B. Davis *et al.*, Phys. Rev. Lett. **75**, 3969 (1995).

[9] F. Dalfovo, S. Giorgini, L. P. Pitaevskii, and S. Stringari, Rev. Mod. Phys. **71**, 463 (1999).

[10] H. A. Haus and W. S. Wong, Rev. Mod. Phys. **68**, 423 (1996).

[11] G. I. Stegeman and M. Segev, Science **286**, 1518 (1999).

[12] L. E. Reichl, *The Transition to Chaos In Conservative Classical Systems: Quantum Manifestations* (Springer-Verlag, New York, 1992).

[13] Y. Castin and R. Dum, Phys. Rev. A **57**, 3008 (1998).

[14] S. A. Gardiner, J. Mod. Opt. **49**, 1971 (2002).

[15] James Anglin, private correspondence.

[16] F. K. Abdullaev, A. Gammal, A. M. Kamchatnov, and L. Tomio, Int. J. Mod Phys B **19**, 3415 (2005).

[17] K. E. Strecker, G. B. Partridge, A. G. Truscott, and R. G. Hulet, Nature **417**, 150 (2002).

[18] P. Y. P. Chen and B. A. Malomed, J. Phys. B **38**, 4221 (2005).

[19] A. V. Carpentier, H. Michinel, M. I. Rodas-Verde, and V. M. Pérez-García, Phys. Rev. A **74**, 013619 (2006).

[20] L. D. Carr and J. Brand, Phys. Rev. A **70**, 033607 (2004).

[21] V. Ahufinger, A. Mebrahtu, R. Corbaln, and A. Sanpera, New J. Phys. **9**, 4 (2007).

[22] H. Goldstein, C. Poole, and J. Safco, *Classical Mechanics* (Addison-Wesley, New York, 2002).

[23] M. C. Gutzwiller, *Chaos in Classical and Quantum Mechanics* (Springer-Verlag, New York, 1990).

[24] E. N. Lorenz, J. Atm. Sci. **20**, 130 (1963).

[25] V. E. Zakharov and A. B. Shabat, Sov. Phys. JETP **34**, 62 (1972).

[26] M. J. Ablowitz, D. J. Kaup, A. C. Newell, and H. Segur, Phys. Rev. Lett. **30**, 1262 (1973).

[27] P. G. Drazin and R. S. Johnson, *Solitons: an introduction* (Cambridge University Press, Cambridge, 1989).

[28] M. J. Ablowitz and H. Segur, *Solitons and the Inverse Scattering Transform* (SIAM, Philadelphia, 1981).

[29] L. D. Faddeev and L. Takhtajan, *Hamiltonian Methods in the Theory of Solitons* (Springer-Verlag, Berlin Heidelberg, 1987).

[30] V. E. Zakharov and A. B. Shabat, Zh. Eksp. Teor. Fiz. **61**, 118 (1971).

[31] J. P. Gordon, Opt. Lett. **8**, 596 (1983).

[32] R. Scharf, Chaos, Solitons & Fractals **5**, 2527 (1995).

[33] R. Scharf and A. Bishop, Phys. Rev. E **47**, 1375 (1993).

[34] R. Scharf and A. Bishop, Phys. Rev. A **46**, 2973 (1992).

[35] J. N. Maki and T. Kodama, Phys. Rev. Lett. **57**, 2097 (1986).

[36] C. J. Pethick and H. Smith, *Bose-Einstein Condensation in Dilute Gases* (Cambridge University Press, Cambridge, 2002).

[37] L. Pitaevskii and S. Stringari, *Bose-Einstein Condensation* (Clarendon Press, Oxford, 2003).

[38] C. W. Gardiner, Phys. Rev. A **56**, 1414 (1997).

[39] S. A. Gardiner and S. A. Morgan, Phys. Rev. A **75**, 043621 (2007).

[40] N. N. Bogoliubov, J. Phys. (USSR) **11**, 23 (1947).

[41] P. G. de Gennes, *Superconductivity of Metals and Alloys* (W. A. Benjamin, New York, 1966).

[42] P. Nozieres and D. Pines, *The Theory of Quantum Liquids (Vol. II)* (Addison-Wesley, New York, 1990).

[43] H. T. C. Stoof and M. Bijlsma, Phys. Rev. E **47**, 939 (1993).

[44] M. Rusch and K. Burnett, Phys. Rev. A **59**, 3851 (1999).

[45] S. A. Morgan, J. Phys. B **33**, 3847 (2000).

[46] S. Inouye, M. Andrews, J. Strenger, H. J. Miesner, and W. Ketterle, Nature **392**, 151 (1998).

[47] T. Köhler, K. Góral, and P. S. Julienne, Rev. Mod. Phys. **78**, 1311 (2006).

[48] O. Penrose and L. Onsager, Phys. Rev. **104**, 576 (1956).

[49] L. Salasnich, A. Parola, and L. Reatto, Phys. Rev. A **66**, 043603 (2002).

[50] A. M. Kamchatnov and V. S. Shchesnovich, Phys. Rev. A **70**, 023604 (2004).

[51] L. Khaykovich and B. A. Malomed, Phys. Rev. A **74**, 023607 (2006).

[52] L. Khaykovich *et al.*, Science **296**, 1290 (2002).

[53] S. L. Cornish, S. T. Thompson, and C. E. Wieman, Phys. Rev. Lett. **96**, 170401 (2006).

[54] K. E. Strecker, G. B. Partridge, A. G. Truscott, and R. G. Hulet, Adv. Space Res. **35**, 78 (2005).

[55] G. Chong and W. Hai, J. Phys. B **40**, 211 (2006).

[56] U. A. Khawaja, H. Stoof, R. Hulet, K. Strecker, and G. Partridge, Phys. Rev. Lett. **89**, 200404 (2002).

[57] L. Carr and J. Brand, Phys. Rev. Lett. **92**, 040401 (2004).

[58] K. Gawryluk, M. Brewczk, M. Gajda, and J. Mostowski, J. Phys. B **39**, L1 (2006).

[59] A. Hasegawa, Opt. Lett. **9**, 288 (1984).

[60] V. V. Konotop and M. Salerno, Phys. Rev. A **65**, 021602 (2002).

[61] V. Leung, A. Truscott, and K. Baldwin, Phys. Rev. A **66**, 061602 (2002).

[62] L. Salasnich, A. Parola, and L. Reatto, Phys. Rev. Lett. **91**, 080405 (2003).

[63] V. S. Gerdjikov, B. B. Baizakov, M. Salerno, and N. A. Kostov, Phys. Rev. E **73**, 046606 (2006).

[64] N.-C. Panoiu, I. V. Mel'nikov, D. Michalache, C. Etrich, and F. Lederer, Phys. Rev. E **60**, 4868 (1999).

[65] V. I. Karpman and V. V. Solov'ev, Physica 3D , 487 (1981).

[66] Y. S. Kivshar and M. S. Malomed, Rev. Mod. Phys. **61**, 763 (1989).

[67] T. Okamawari and A. Hasegawa, Phys. Rev. A **51**, 3203 (1995).

[68] P. V. Elyutin, A. V. Buryek, V. V. Gubernov, R. A. Sammut, and I. N. Towers, Phys. Rev. E **64**, 016607 (2001).

[69] L. Carr, C. W. Clark, and W. Reinhardt, Phys. Rev. A **62**, 063611 (2000).

[70] W. Li, Phys. Rev. A **74**, 063612 (2006).

[71] V. M. Pérez-García, H. Michinel, and H. Herrero, Phys. Rev. A **57**, 3837 (1998).

[72] M. Kunz, T. Kupper, V. K. Mezentsev, E. G. Shapiro, and S. Turitsyn, Physica D **128**, 273 (1999).

[73] Y. S. Kivshar, T. J. Alexander, and S. K. Turitsyn, Phys. Lett. A **278**, 225 (2001).

[74] S. A. Morgan, R. J. Ballagh, and K. Burnett, Phys. Rev. A **55**, 6 (1997).

[75] P. A. Ruprecht, M. J. Holland, K. Burnett, and M. Edwards, Phys. Rev. A **51**, 4704 (1995).

[76] Y. Kagan, G. V. Shlyapnikov, and J. M. T. Walraven, Phys. Rev. Lett. **76**, 2670 (1996).

[77] L. P. Pitaevskii, Phys. Lett. A **221**, 14 (1996).

[78] M. L. Chiofalo, S. Succi, and M. P. Tosi, Phys. Rev. E **62**, 7438 (2000).

[79] L. Lehtovaara, J. Toivanen, and J. Eloranta, J. Comput. Phys. **72**, 351 (2007).

[80] A. Galindo and P. Pascual, *Quantum Mechanics I* (Springer-Verlag, Berlin, 1989).

[81] T. Köhler and K. Burnett, Phys. Rev. A **65**, 033601 (2002).

[82] N. R. Thomas, N. Kjaergaard, P. S. Julienne, and A. C. Wilson, Phys. Rev. Lett. **93**, 173201 (2004).

[83] N. G. Parker, S. L. Cornish, C. S. Adams, and A. M. Martin, J. Phys. B **40**, 3127 (2007).

[84] J. Tennyson and S. C. Farantos, Chemical Physics **93**, 237 (1985).

[85] N. G. Parker, A. M. Martin, S. L. Cornish, and C. S. Adams, cond-mat/0603059 (unpublished).

[86] A. Gammal, T. Frederico, and L. Tomio, Phys. Rev. A **64**, 055602 (2001).

[87] S. V. Dmitriev, D. A. Semagin, A. A. Sukhorukov, and T. Shigenari, Phys. Rev. E **66**, 046609 (2002).

[88] S. V. Dmitriev, P. G. Kevrekidis, B. A. Malomed, and D. J. Frantzeskakis, Phys. Rev. E **68**, 056603 (2003).

[89] R. H. Goodman and R. Haberman, Phys. Rev. Lett. **98**, 104103 (2007).

[90] I. E. Papacharalampous, P. G. Kevrekidis, B. A. Malomed, and D. J. Frantzeskakis, Phys. Rev. E **68**, 046604 (2003).

[91] W. H. Press, S. A. Teukolsky, W. T. Vetterling, and B. P.Flannery, *Numerical Recipies in Fortran* (Cambridge University Press, Cambridge, 1992).

[92] C. A. Moyer, Am. J. Phys. **72**, 351 (2004).

[93] N. G. Parker, Ph.D. Thesis, Durham (2004).